2007/2 vol.4

ACTA GEOTECHNICA SLOVENICA

2007/2

ISSN 1854-0171

ACTA GEOTECHNICA SLOVENICA

ISSN: 1854-0171

ustanovitelji	founders

Univerza v Mariboru, Fakulteta za gradbeništvo
University of Maribor, Faculty of Civil Engineering

Univerza v Ljubljani, Fakulteta za gradbeništvo in geodezijo
University of Ljubljana, Faculty of Civil and Geodetic Engineering

Univerza v Ljubljani, Naravoslovnotehniška fakulteta
University of Ljubljana, Faculty of Natural Sciences and Engineering

Slovensko geotehniško društvo
Slovenian Geotechnical Society

Društvo za podzemne in geotehniške konstrukcije
Society for Underground and Geotechnical Constructions

izdajatelj	publisher

Univerza v Mariboru, Fakulteta za gradbeništvo
University of Maribor, Faculty of Civil Engineering

naklada	circulation

500 izvodov - issues

tisk	print

Tercia tisk d.o.o. Ptuj

Revija redno izhaja dvakrat letno. Članki v reviji so recenzirani s strani priznanih mednarodnih strokovnjakov. Baze podatkov v katerih je revija indeksirana: ICONDA - The international Construction database, GeoRef
Pri financiranju revije sodeluje Javna agencija za raziskovalno dejavnost republike Slovenije.

naslov uredništva	address

ACTA GEOTECHNICA SLOVENICA
Univerza v Mariboru, Fakulteta za gradbeništvo
Smetanova ulica 17
2000 Maribor
Slovenija
Telefon / Telephone: +386 (0)2 22 94 300
Faks / Fax: +386 (0)2 25 24 179
E-pošta / E-mail: ags@uni-mb.s

spletni naslov	web address

http://www.fg.uni-mb.si/journal-ags

The journal is published twice a year. Papers are peer reviewed by renowned international experts. Indexation data bases of the journal: ICONDA - The International Construction Database, GeoRef
Financially supported also by Slovenian Research Agency.

VSEBINA

CONTENTS

UVODNIK

Zaključuje se četrto leto izhajanja mednarodne revije Acta Geotechnica Slovenica. Skladno z začrtano uredniško politiko so v vsaki številki revije objavljeni štirje članki, ki obravnavajo temeljna znanja in prikazujejo inovativnosti iz praktičnih primerov, kar je za bralce še posebej zanimivo. Medtem, ko revijo v Sloveniji prejemajo vsi člani Slovenskega geotehniškega društva, ki združuje večino strokovnjakov s tega področja, lahko tuja znanstvena javnost najde povzetke člankov na spletnih straneh revije in v splošnih ter specializiranih bazah, kot sta GeoRef in Iconda. Promocija revije na mednarodnih konferencah in brezplačno pošiljanje izvodov nekaterim predsednikom geotehniških društev po svetu, izbranim univerzam, znanstvenim inštitucijam in knjižnicam je že obrodila sadove, saj se za naročilo revije zanima tudi vedno več posameznikov in inštitucij iz tujine. Veseli smo, da se krog naših avtorjev in bralcev vedno bolj širi.

V drugi številki četrtega letnika so zbrani naslednji štirje zanimivi članki:

Vladimir Vukadin v prispevku predstavlja osnovno definicijo mehkih kamnin in trdih zemljin ter njihovo značilno napetostno-deformacijsko obnašanje. Prikazano je, da se materiali z različno sestavo in genezo v pomembnih vidikih obnašajo podobno. To omogoča postavitev teoretičnega okvirja, znotraj katerega je mogoče ustrezno formulirati in postaviti konstitutiven materialni model, ki opisuje njihovo obnašanje. Ključni element za postavitev teoretičnega okvirja in konstitutivnega modela je vpeljava koncepta strukture in destrukturizacije. V zaključku članka je na kratko predstavljen konstitutivni model za mehke kamnine in trde zemljine S_BRICK, ter rezultati primerjave napovedi modela z rezultati laboratorijskih preiskav.

V članku, ki so ga pripravili Violeta J. Mircevska, Vladimir Bickovski in Mihail Garevski je opisano 3D nelinearno dinamično obnašanje kamnite pregrade. Za kamnito maso je upoštevan material, ki zadovoljuje Mohr-Coulombov kriterij porušitve. Pregrada se nahaja v strmem, ozkem kanjonu, v obliki črke 'V'. Obravnavan je koncept modela »brezmasnega kamnitega temelja«, pri čemer je določen del kamnine vključen v model.

Prispevek avtorjev Ivana in Martina Vaníčka se osredotoča na tunele v praškem metroju z različnih vidikov – geologije, konstrukcijskih sistemov in vpliva poplavljanja. Izbrano mesto za opazovanja je bil eden najbolj prizadetih delov z velikim sistemom razpok. Monitoring tega mesta, ki je temeljil na makro in mikro pristopih, ni kazal posebnega propadanja. Vseeno je bil za kontrolo v daljšem časovnem obdobju nameščen in uporabljen brezžični sistem za zbiranje in prenašanje podatkov.

Bojan Žlender in Ludvik Trauner podajata rezultate raziskav dinamičnih lastnosti polžarice iz jugozahodne lokacije Ljubljanskega barja. Izvedeni so bili ciklični triosni preizkusi. V preiskavi so bili spreminjani pogoji: začetna efektivna napetost (50, 100, 150 kPa), količnik por (2,1 do 1,2) in faktor ciklične obremenitve CSR (med 0,1 in 1). Med posameznim preizkusom so bile merjene časovne spremembe napetosti, deformacij in pornega vodnega tlaka. Parametri fizikalnih lastnosti so podani kot funkcije zgoščenosti polžarice, torej volumenske deformacije, gostote, poroznosti ali vlažnosti.

Ludvik Trauner
Glavni urednik

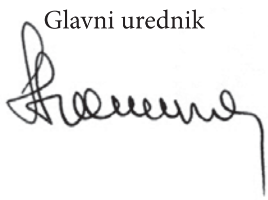

EDITORIAL

The fourth year of publication of the international journal Acta Geotechnica Slovenica is coming to an end. In accordance with the editorial policy, there have been four papers in each issue, treating fundamental knowledge and showing innovations in terms of practical examples. All of which we believe is of great interest to our readers. In Slovenia, all the members of the Slovenian Geotechnical Society, which brings together the majority of experts in the field, receive our journal. Foreign scientists can find summaries of the papers on the journal's web pages and there is also information in specialized databases such as GeoRef and Incond. The promotion of the journal at international conferences and the complimentary copies sent to the presidents of geotechnical associations worldwide, selected universities, scientific institutions and libraries have already proved a success, since more and more individuals and foreign institutions have shown an interest in subscribing to the journal. We are very pleased to report that the circle of authors and readers is getting wider.

In the second issue of the fourth year of publication we have four interesting papers:

First, in the paper by Vladimir Vukadin, we have a definition of soft rocks and hard soils together with the typical stress-strain behaviour of soft rocks and hard soils. The investigation demonstrated that materials with a different structure and origin behave in a similar way. This makes it possible to set up a theoretical framework, within which a formulation and construction of a constitutive material model can describe the behaviour. The key element to constructing a theoretical framework and a constitutive model is the introduction of the concept of structure and destructurization. Finally, a brief presentation of a constitutive model for soft rocks and hard soils, called S_BRICK, is given along with the laboratory results of the model's prediction.

Second, in the paper prepared by Violeta J. Mircevska, Vladimir Bickovski and Mihail Garevski, the 3D nonlinear dynamic behaviour of a rock-fill dam is presented. For the rocky mass a material based on the Mohr-Coulomb failure criterion is taken into consideration. The dam is situated in a steep, narrow, "V-shaped" rigid canyon. The concept of a 'massless rock foundation' is treated, for which a certain part of the rock is included in the model.

Third, the contribution of Ivan Vaníček and Martin Vaníček is focused on the tunnels of the Prague Metro, looked at from various aspects, i.e., geology, construction systems, and the influence of flooding. The section of the tunnels that was selected for monitoring is one of the most affected, and has a large system of cracked segments. The monitoring of this section, which is based on macro- and micro-approaches, showed no significant deterioration. Nevertheless, for long-term monitoring a wireless system for data collection and transfer was installed and implemented.

Finally, Bojan Žlender and Ludvik Trauner present the results of the dynamic properties of snail soil from a south-west location of the Ljubljana Marsh. They performed a series of cyclic triaxial tests, and the investigation was based on a series of tests in which the conditions varied: initial effective pressures (50, 100, 150 kPa), void ratio (2.0–1.2) and factor of cyclic loading CSR (0.1–1.0). In between the individual tests, measurements of stress, deformation and pore-water pressure were taken. The parameters of the physical properties are given in terms of the functions of the condensed snail soil, which are functions of the volume deformation, the density, the porosity or the water content.

Ludvik Trauner
Editor–in–chief

MODELIRANJE NAPETOSTNO-DEFORMACIJSKEGA OBNAŠANJA MEHKIH KAMNIN IN TRDIH ZEMLJIN

VLADIMIR VUKADIN

o avtorju

Vladimir Vukadin
IRGO-Inštitut za rudarsvo, geotehnologijo in okolje
Slovenčeva 93, 1000 Ljubljana, Slovenija
E-pošta: vlado.vukadin@irgo.si

izvleček

V prispevku je uvodoma predstavljena osnovna definicija mehkih kamnin in trdih zemljin. V nadaljevanju je nato predstavljeno značilno napetostno-deformacijsko obnašanje mehkih kamnin in zemljin, kjer bo prikazano, da se materiali z različno sestavo in genezo v pomembnih vidikih obnašajo podobno. To omogoča postavitev teoretičnega okvirja, znotraj katerega je mogoče ustrezno formulirati in postaviti konstitutiven materialni model, ki opisuje njihovo obnašanje. Ključen element za postavitev teoretičnega okvirja in konstitutivnega modela je vpeljava koncepta strukture in destrukturizacije. V zaključku je na kratko predstavljen konstitutivni model za mehke kamnine in trde zemljine S_BRICK, ter rezultati primerjave napovedi modela z rezultati laboratorijskih preiskav.

ključne besede

mehke kamnine, trde zemljine, napetosto-deformacijsko obnašanje, konstitutivni modeli, S_BRICK, BRICK, struktura, destrukturizacija

MODELING OF THE STRESS-STRAIN BEHAVIOR IN HARD SOILS AND SOFT ROCKS

VLADIMIR VUKADIN

About the author

Vladimir Vukadin
IRGO-Institute for Mining Geotechnology and Environment
Slovenčeva 93, 1000 Ljubljana, Slovenia
E-mail: vlado.vukadin@irgo.si

Abstract

The paper begins with a definition of hard soils and soft rocks (HSSR); this is followed by a short overview of the typical stress-strain behavior of HSSR. It is shown that in spite of the differences in the origin, type and strength of materials, similar stress-strain behaviors can be observed for different materials, ranging from soils to rocks. Based on this observed similarity a theoretical framework can be postulated, with which an appropriate constitutive model for HSSR can be formulated. This model includes the concepts of structure and destructurization as intrinsic material properties. A model named S_BRICK that takes into account the structure and destructurization has been developed and a comparison of this model's predictions with laboratory results is presented.

Keywords

hard soils and soft rocks, stress-strain behavior, constitutive modeling, S_BRICK, BRICK, structure, destructurization

1 INTRODUCTION

For a long time hard soils and soft rocks (HSSR) were treated as borderline cases in soil and rock mechanics; this was mostly due to the fact that their strength and stiffness properties usually exceeded the design requirements expected for soft soils. However, with the increasing number of large geotechnical projects executed in HSSR, a better understanding of their geomechanical behavior is needed so that they can be more accurately modeled.

First, a classification of HSSR will be presented; this will be followed by a description of their typical stress-strain behavior. It will be shown that regardless of their strength, these materials behave in a similar manner to soils. The main difference between HSSR and soft soils is in their structure, which is responsible for the higher strength and stiffness in HSSR.

A model called S_BRICK, which includes both structure and destructuring, will be briefly explained, and then a comparison between the S_BRICK model's predictions and the laboratory results on stiff North Sea clay will be presented. A comparison will also be carried out with a model that does not include structure. This model is called BRICK. It will be shown that the structure and its stability represent the key parameters that need to be accounted for in order to successfully model the behavior of HSSR.

2 A DEFINITION OF HARD SOILS AND SOFT ROCKS (HSSR)

From the practical point of view it is convenient to define HSSR according to their strength. There are several different classifications available, for example, ISRM [1], Bieniawski [2], BSI [3], and IAEG [4], to name just a small selection, which differ somewhat in terms of terminology and differ significantly in terms of defining the upper and lower limits of soils and rocks. IAEG [4], for instance, sets the limit for the uniaxial unconfined compressive strength (UCS), σ_c, for "weak rock" at 15 MPa, BSI [3] sets it at 5 MPa, and ISMR [1] and Bieniawski [2] set the limit for weak rock at 25 MPa. Hawkins and Pinches [5] have proposed a classification for the entire range of geological materials, i.e., soils and rocks, based on the UCS for the upper limit and the undrained triaxial strength, c_u, for the lower limit. The advantage of this classification is that it doubles each class of soil and rock and also acknowledges the continuum between soils and rocks. The classification is presented in Table 1.

Table 1. The classification of soils and rocks according to their strength [5]

	Range		Description
c_u	<20	kPa	Very soft soils
c_u	20–40	kPa	Soft soils
c_u	40–80	kPa	Firm soils
c_u	80–160	kPa	Stiff soils
c_u	160–320	kPa	Very stiff soils
c_u	320–640	kPa	Hard soils
σ_c	1.25–2.5	Mpa	Very weak rocks
σ_c	2.5–5	Mpa	Weak rocks
σ_c	5–10	Mpa	Moderately weak rocks
σ_c	10–50	Mpa	Moderately strong rocks
σ_c	50–100	Mpa	Strong rocks
σ_c	100–200	Mpa	Very strong rocks
σ_c	>200	Mpa	Extremely strong rocks

Geological materials classified as HSSR, which are written in bold in Table 1, represent an important fraction of all the geological materials in the geosphere, where most of construction takes place. They can be of different origin, ranging from igneous (decomposed and weathered granites or basalts, tuffs, etc.), to metamorphic (phyllites, weathered and decomposed gneisses and schists) to sedimentary origin (claystones, siltstones, flysh marls, etc.), and are the products of rock-forming, rock-altering and sediment-forming processes.

However, only using strength to distinguish between soils and rocks can be misleading when their engineering behavior is being considered. There are some instances when the behavior of rocks can be better described using the concepts of soil mechanics. When the frictional strength of discontinuities becomes comparable to the intact strength of the rock (Hyett and Hudson [6]), for example, at large depths, rocks can behave and fail in a plastic manner that is typical for soils. On the other hand, Picarelli and Olivares [7] describe the failure of stiff, highly fissured clay shales that fail on small-scale fissures that interconnect and form a discontinuity along which the material fails. Such phenomena are well described using the concepts of rock mechanics.

There is enough experimental evidence in the literature that demonstrates the conceptually similar stress-strain behavior of different geological material. Figure 1a, for example, shows oedometer compression and recompression curves for tests carried out on natural intact samples of three stiff clays and a marl (Burland et al. [8]), and Figure 1b shows oedometer results for tests carried out on three different clay shales (Bertuccioli and Lanzo [9]).

The compression curves of all the materials, ranging from stiff soils to marls and shales, show a similar compression behavior to that of soft soils, i.e., an initially stiff response until the normal compression line is reached, the beginning of isotropic hardening, and an increase of the state boundary surface with continuing compression, followed by a stiff response when unloading.

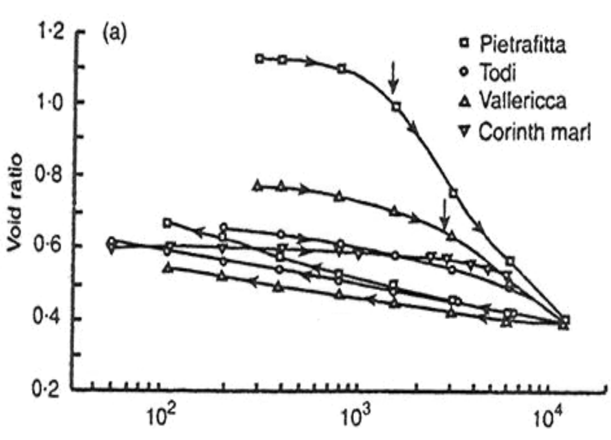

a)

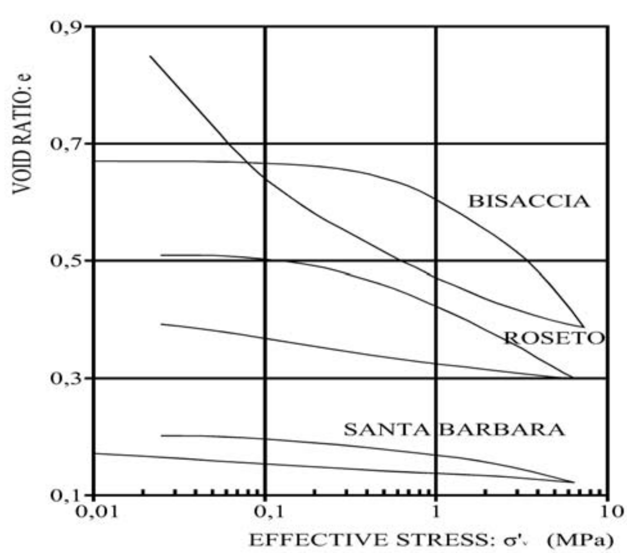

b)

Figure 1. Oedometer compression curves for a) three stiff clays and a marl [8], b) three different clay shales [9].

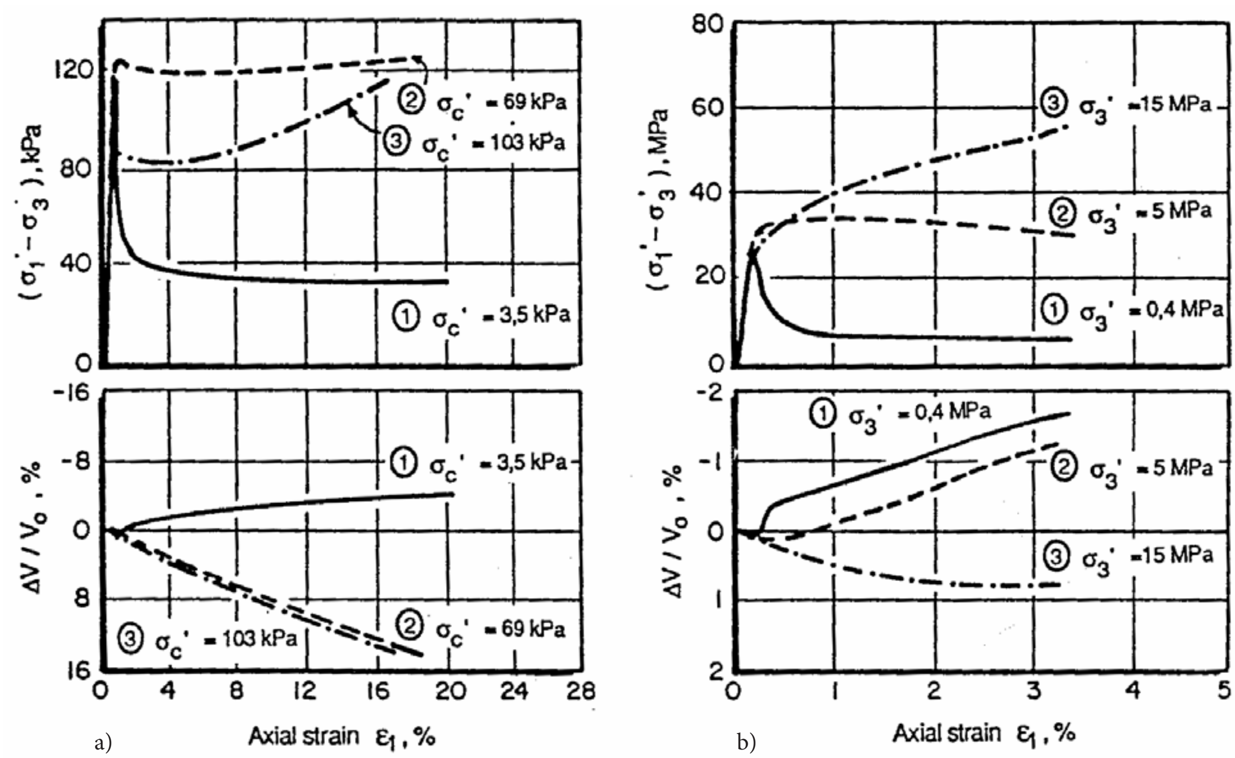

Figure 2. Isotropically consolidated drained triaxial tests on a) Saint Vallier clay (Lefebre [10]) and b) oolitic limestone (Elliot & Brown [11]).

Figure 2 shows the results of isotropically consolidated drained triaxial tests on a Saint Vallier clay (Lefebre [10]) and a oolitic limestone (Elliot & Brown [11]). The tests labeled 1 were carried out at a low confining stress; the tests labeled 2 were carried out at an intermediate confining stress; and the tests labeled 3 were carried out at a high confining stress.

For both materials, when tested at a low confining stress (1), the results show a well-defined peak and a strain-softening behavior after the peak, with a dilating volumetric response. The test carried out at a high confining stress shows stiff behavior until the yield surface is encountered, from where the deviator stress slowly increases toward the critical state line. Note that the volumetric behavior is compressive. It is also important to note that regardless of the strength difference between the clay (soft soil) and the oolitic limestone (weak to moderately weak rock) the responses are similar and can be well described using the concepts of critical state soil mechanics.

Based on similar examples in the literature, Kavvadas [12] has proposed that the concepts of soil mechanics can be applied for the modeling of HSSR as long as the following two conditions are fulfilled:

1. the materials are significantly influenced by macro-structural features (large-scale discontinuities),
2. the influence of excess pore pressure is important.

This definition of HSSR is important because it opens up the possibility for the development of a constitutive model for the entire range of geological materials, from soft soils to soft rocks, within the theoretical framework of critical state soil mechanics.

3 STRUCTURE: A KEY PARAMETER FOR THE DEVELOPMENT OF CONSTITUTIVE MODELS FOR HSSR

It has been shown that in addition to important features like nonlinearity, state and stress history, a constitutive model has to include the effects of structure and destructuring in order to describe the behavior of natural geological materials (Burland et al. [8], Leroueil and Vaugan [13], Kavvadas and Amorosi [14], Rouainia and Wood [15], Baudet [16], Cotecchia [17]). The origins of structure in natural materials are complex and can be attributed to different processes as well as physical and chemical conditions during and after sedimentation.

There are different classifications and definitions that take into account different aspects of structure. Lambe and Whitman [18] proposed that structure is a combination of *fabric* and *bonding*, where *fabric* represents the arrangement of the soil particles and *bonding* represents the chemical, physical or any other types of bonds between the particles. *Bonding* is the dominant effect in rocks, while in soils the influence of *fabric* is more important. It is obvious that according to this classification, structure is present in both natural and reconstituted geological materials, because no matter how much a material is remolded or destructured it still has some type of fabric. But from the mechanical point of view the influence of structure in reconstituted materials represents the reference state, beyond which the strength and the stiffness of natural materials cannot fall.

The influence of structure can be best observed when the behavior of a structured material is compared to the behavior of a reconstituted material. Structure is responsible for the increase of stiffness and strength in comparison to the reconstituted material, but the influence of structure is most clearly manifested in the larger state boundary surface (SBS) of the structured material. Leroueil and Vaugan [13] introduced the concept of structure-permitted space, which is shown in the *v-p* space in Figure 3, where *v* represents the specific volume and *p* represents the mean effective stress.

Figure 4 shows the state boundary surfaces for undisturbed, partly destructured and reconstituted Pappadai clay in a *p*/*q* diagram, normalized with the mean effective stress p_e^* taken at the isotropic reconstituted normal compression line using the same specific value as for intact clay (Cotecchia and Chandler [19]).

The influence of structure is clearly seen in the size of the state boundary surfaces, resulting in the higher strength of the undisturbed Pappadai clay in comparison to the partly destructured or reconstituted Pappadai clay.

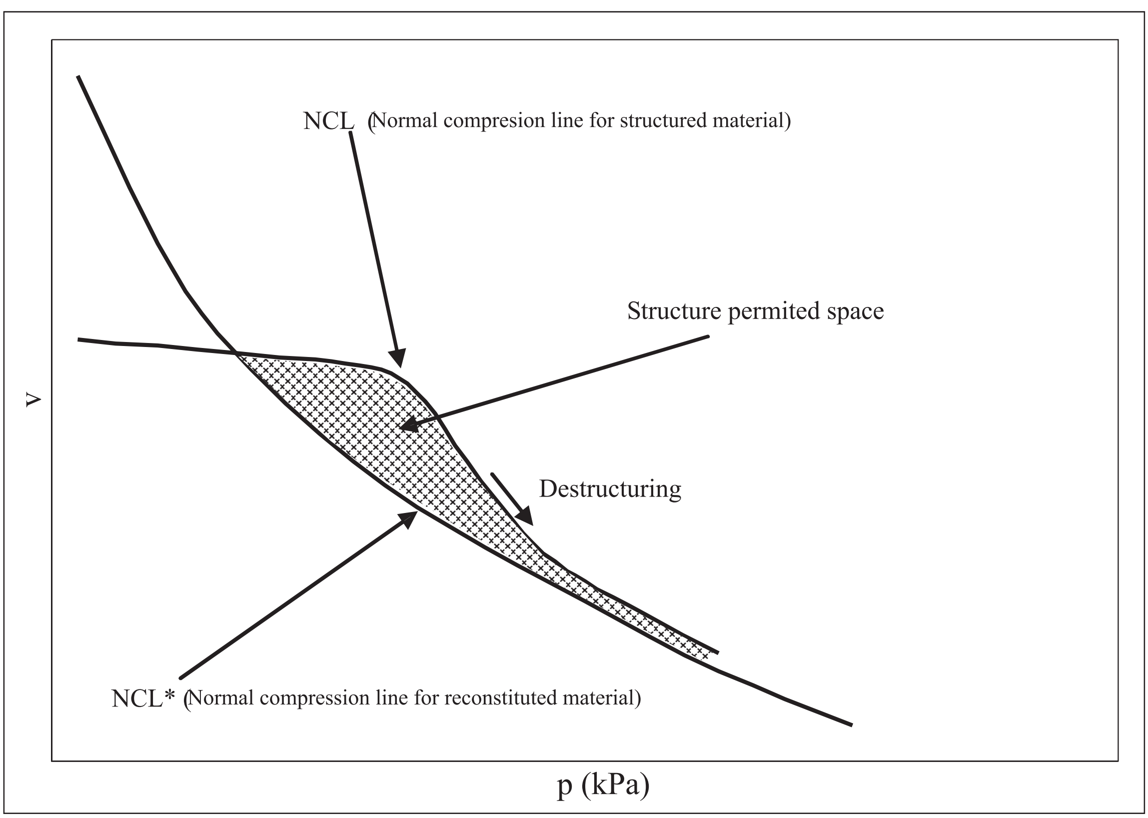

Figure 3. Structure-permitted space by Leroueil and Vaugan [13].

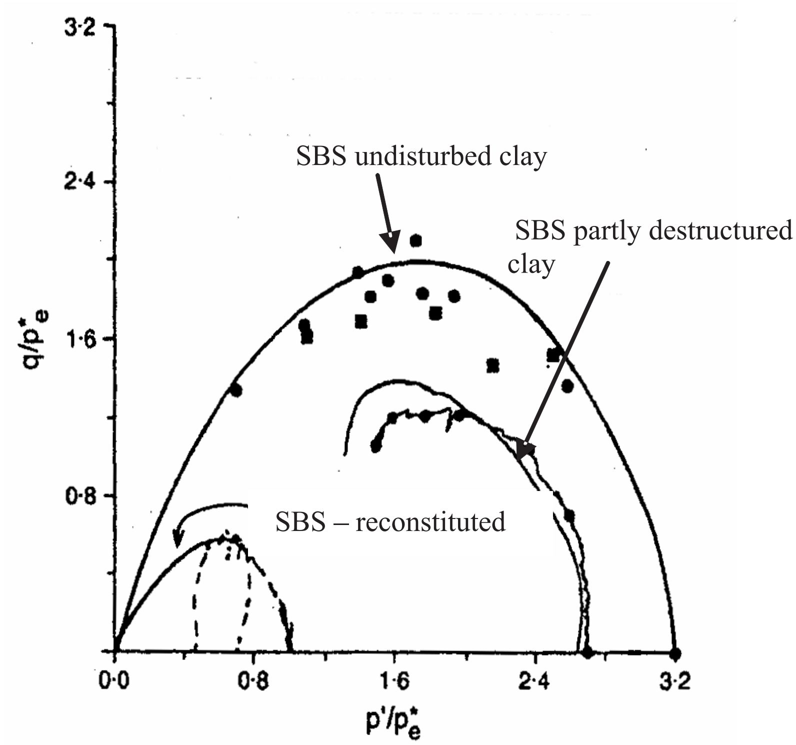

Figure 4. Influence of structure on the state boundary surface of undisturbed, partly destructured and reconstituted Pappadai clay (Cotecchia and Chandler [19]).

Besides strength, structure also influences the stiffness across the entire range of deformations, with the most pronounced influence being in the range of small and very small deformations. Rampello and Silvestri [20] studied small strain stiffness in stiff Vallerica clay in the undisturbed and reconstituted states. They investigated the dependence of the elastic stiffness (denoted G_0) on the mean effective stress and the specific volume (Figure 5). For a given value of the mean effective stress or the specific volume, natural (undisturbed) clay has a higher value of elastic stiffness across the entire range of mean effective stress or specific volume.

According to Baudet [16] Vallerica clay has a stable structure; this can also be seen from Figure 5, where no tendency to converge can be observed for the shear moduli of the undisturbed and reconstituted clays. Similar results were obtained by Jovičić et al. [21],

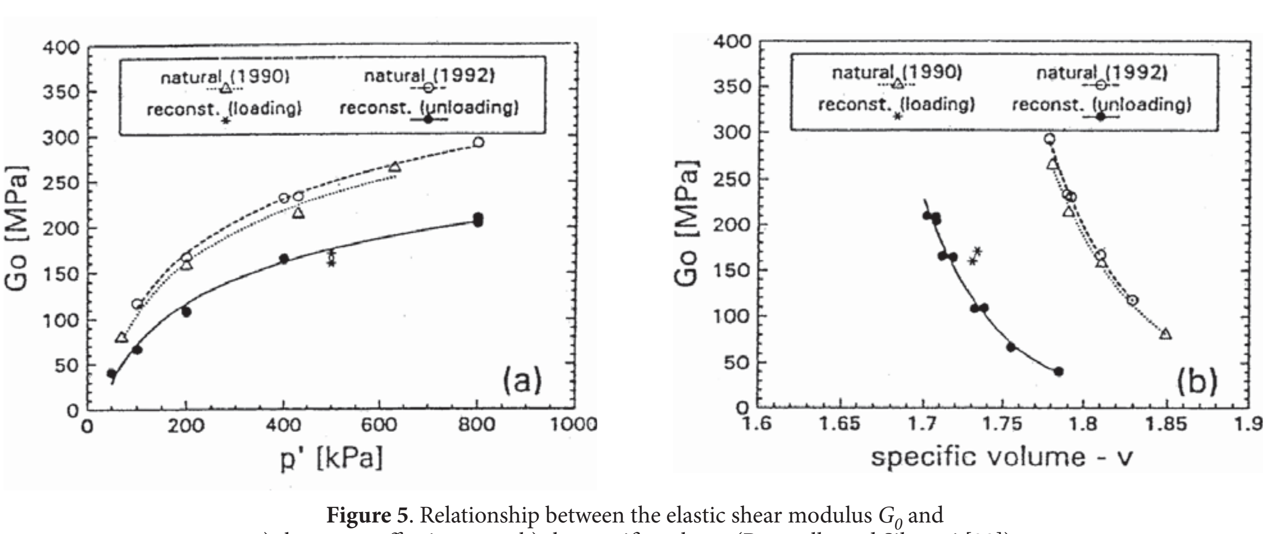

Figure 5. Relationship between the elastic shear modulus G_0 and a) the mean effective stress b) the specific volume (Rampello and Silvestri [20]).

who compared shear-stiffness degradation with strain for both reconstituted and intact stiff North Sea clays (Figure 6). They demonstrated that the influence of structure can be seen from the very small strains up to the point of failure.

A very important element of structure is its stability. We can see from Figure 3 that there is a tendency for the normal compression line of structured material to converge toward the normal compression line of the reconstituted material, which implies destructuring toward the reconstituted material. Destructuring caused by plastic straining is responsible for decreasing the state boundary surface, the strength and the stiffness.

Leroueil and Vaugan [13] have identified different yielding modes in natural materials. According to Leroueil and Vaugan [13] yielding can occur during shearing, compression and swelling, as shown in Figure 7. Similarly, destructuring can also be decoupled into shearing, compression and swelling.

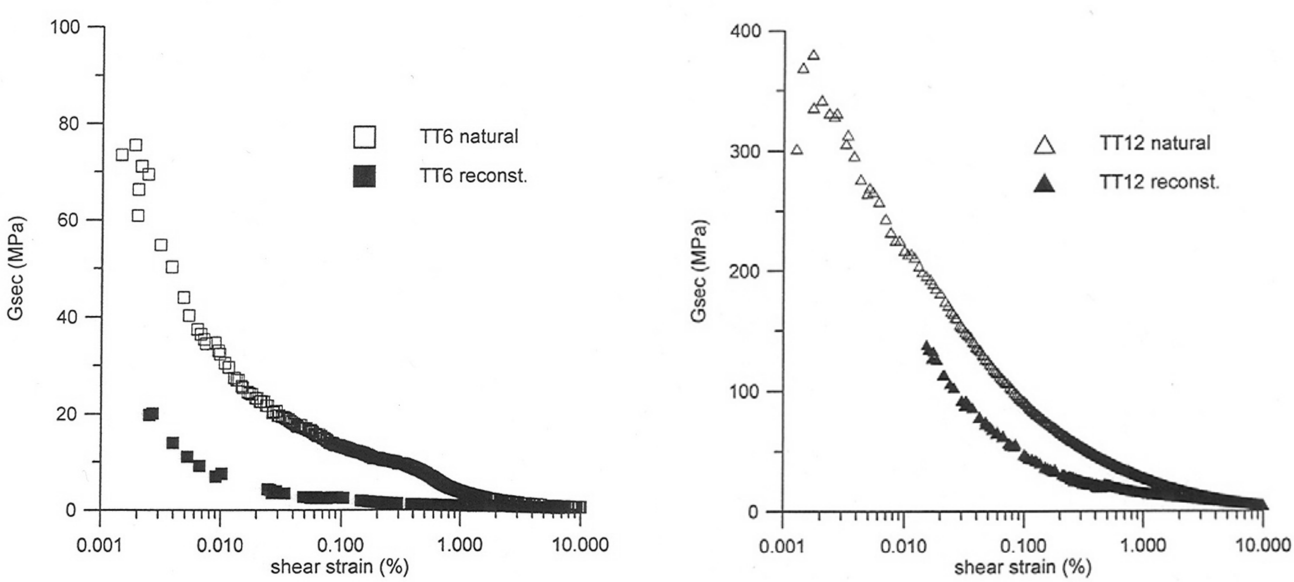

Figure 6. Comparison of shear-stiffness degradation with strain for two natural and reconstituted samples of stiff North Sea clay (Jovičić et al. [21]).

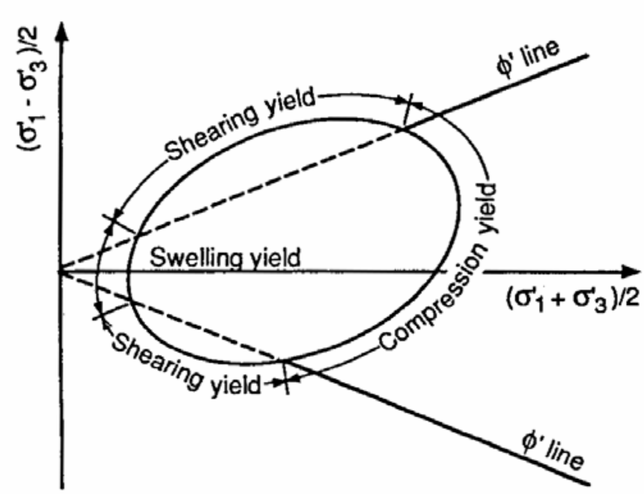

Figure 7. Different modes of yielding and destructuring by Leroueil and Vaugan [13].

Destructuring during isotropic compression and swelling is governed purely by the volumetric component of the plastic strain. In the case of a normal compression stress path, the role of the deviator component in the destructuring is still not fully understood. However, it is reasonable to suspect that because the deviator component shows no tendency toward the state boundary surface, the influence of the deviator's plastic strain is negligible. During shearing, of course, the destructuring is governed by both the volumetric and deviator components of the plastic strain. It is also important to note that during swelling the destructuring of the stress paths can occur inside the state boundary surface, which was also shown by Leroueil and Vaugan [13].

4 S_BRICK: A CONSTITUTIVE MODEL FOR HSSR

The S_BRICK constitutive model for modeling HSSR (Vukadin [22], Vukadin et al. [23]) was developed from the BRICK model (Simpson [24], [25]) and includes both structure and destructuring. The basic BRICK model already includes many important soil behaviors, such as nonlinearity, stress-path dependency, and state, and is therefore a suitable platform for further development [23].

The influence of structure is accounted for by the introduction of two new parameters: α and ω. The first parameter, α, is used to increase or decrease the size of the area beneath the *S-shaped* curve and has a direct influence on the value of the critical state angle and hence on the strength response of the model. The *S-shaped* curve for London clay published by Simpson [24] was taken as a reference shape. The second parameter, ω, represents the state parameter for structured materials and is best understood as an increase of the distance between the normal compression line and the critical state line in structured material in comparison with reconstituted material. The parameter ω represents the key parameter for modeling the stiffness increase, and the parameter α, for the strength increase due to structure [22].

The destructuring is implemented for both the structure parameters, α and ω. The rates of destructuring were made dependent on the sum of the volumetric and shear components of the plastic strains, and are of the exponential type. The destructuring implemented in S_BRICK is given by the following two expressions:

in which the symbols represent the following:

α , ω	initial values of structure parameters
α_k , ω_k	final values of structure parameters
$\alpha_t^{c,sh,sw}$, $\omega_t^{c,sh,sw}$	current values of structure parameters in compression (c), shear (sh) and swelling (sw)
ε_v^{pl} , ε_s^{pl}	volumetric and shear component of plastic strain (i=2-6)
$\delta\varepsilon_v^{pl}$, $\delta\varepsilon_s^{pl}$	increment of volumetric and shear component of plastic strain (i=2-6)
$x_1^{c,sh,sw}$, $y_1^{c,sh,sw}$	parameters that quantify influence of volumetric and deviatoric plastic strain of destructuring parameter α
$x_2^{c,sh,sw}$, $y_2^{c,sh,sw}$	parameters that quantify influence of volumetric and deviatoric plastic strain of destructuring parameter ω

all symbols are without units

The destructuring in S_BRICK is implemented separately, by introducing different parameters $x_i^{c,sh,sw}$ and $y_i^{\,c,sh,sw}$ for shearing (sh), compression (c) and swelling (sw). The decoupling of the plastic strain's influence on the volumetric and shear components and the introduction of the parameters x and y, which quantify the rate of destructuring, gives the model an additional flexibility [24]. The full implementation of structure and destructuring requires the determination of an additional 16 parameters in total. Four of them (α, α_k, ω and ω_k) represent the structure and twelve $(x_i, y_i)^{c,sh,sw}$ represent the destructuring of the structure in compression, swelling and shearing. It is reasonable to expect that not all types of destructuring are present for a dominant stress path, so it is very likely that the necessary total number of additional parameters can be as low as four. Accordingly, the destructuring is implemented in such a way that some model parameters that are not necessary or are not available can be omitted without hindering the behavior of the model. A more detailed formulation of the model is given by Vukadin [22], [23].

$$\alpha_t^{c,sh,sw} = \alpha_k + \left(\alpha - \alpha_k\right)\exp\left[-\left(x_1^{c,sh,sw}\left(\varepsilon_v^{pl} + \delta\varepsilon_v^{pl}\right) + y_1^{c,sh,sw}\left(\varepsilon_s^{pl} + \delta\varepsilon_{s_i}^{pl}\right)\right)\right] \quad 1)$$

$$\omega_t^{c,sh,sw} = \omega_k + \left(\omega - \omega_k\right)\exp\left[-\left(x_2^{c,sh,sw}\left(\varepsilon_v^{pl} + \delta\varepsilon_v^{pl}\right) + y_2^{c,sh,sw}\left(\varepsilon_s^{pl} + \delta\varepsilon_{s_i}^{pl}\right)\right)\right] \quad 2)$$

5 S_BRICK PREDICTION OF THE STRESS-STRAIN BEHAVIOR OF STIFF NORTH-SEA CLAY

Vukadin et. al [23] have presented predictions of the S_BRICK and BRICK models on a conceptual level where the advantages of S_BRICK when modeling the structure and the destructurization were demonstrated. Here, a comparison of the modeled stress-strain behavior of stiff North Sea clay with the S_BRICK and BRICK models is presented. The stress-strain behavior of North Sea clay was investigated in the laboratory by Jovičić et al. [21]. Stress-path drained triaxial tests were carried out by investigating the strength and stiffness of reconstituted and natural samples at in-situ stresses and also when swelled back to effective stresses as low as 10 kPa [21]. In addition, undrained shear strength tests were also carried out.

All together, twelve different intact samples were investigated, taken from different depths, ranging between 15 and 70 m, and with undrained shear strengths (c_u) ranging from 150 to 800 kPa. According to Table 1, North Sea clay can be classified as a very stiff soil to a very weak rock, depending on the section of clay being investigated [21]. The samples were taken from four different sections, based on an undrained profile with different stress histories and amounts of structure.

The input parameters for modeling the North Sea clay with BRICK were taken from Jovičić et al. [21], who in addition to other parameters took into account the material stress history as an input parameter. For each individual section of the clay a different history was modeled in such a way that the amount of over-consolidation was varied, iterated and then fixed for each clay section, so that the calculated and the measured undrained shear strengths coincide. It was concluded that for three clay sections, the iterated over-consolidation ratios were unrealistically high, which the authors [21] explained by the presence of structure in the clay, which was not accounted for with the BRICK model.

For the S_BRICK model most of the input parameters were the same as for the BRICK model, the only difference was that the stress history was realistically modeled and parameters that represent the structure and destructurization were included. The same as with S_BRICK, a match between the calculated and measured undrained shear strengths was sought and the structure parameters were obtained by iteration. All in all, five additional parameters were included in the model for each individual clay section. The input parameters representing the structure for the modeled clay sections are presented in Table 2.

Table 2. Input parameters for the structure and destructurisation for the modeled clay section with S_BRICK-

Parameter	α	α_k	ω	ω_k	x_2	y_2
Clay	0.85	0.85	1.2	0.6	800	900

The parameter α was determined from the critical state angle for the reconstituted clay obtained from triaxial shearing tests. The parameter ω was obtained by matching the small strain stiffness, and the parameter ω_k, by matching the strength and stiffness at the critical state after the destructurization was finished. Due to the fact that no oedometric tests were available, only a destructurization during shearing was modeled, and the parameters x_2 and y_2 were obtained with a trial-and-error process so that a best fit across the entire range of deformation could be achieved.

All the numerical tests were carried out in the following steps:

- First, a stress history was numerically reproduced, prior to sampling as one-dimensional compression and swelling.
- Second, the amount of over-consolidation for the BRICK model was determined so that the undrained shear strength of the modeled clay coincided with the laboratory results. For the S_BRICK model a realistic stress history was modeled with the inclusion of the structure parameters α and ω, so that the undrained shear strength was matched.
- Third, for both models the sampling and isotropic swelling or compression was modeled until the initial effective stress prior to shearing was reached.
- Finally, a numerical stress path was applied, which was similar to the stress path applied in the triaxial apparatus.

Two individual tests, TT6 and TT7, shown in Figures 8 and 9, were chosen as an example for a direct comparison between the observed and predicted stress-strain behaviors. Each figure shows separately the variation of the deviator stress q, the angle of the shearing resistance φ' and the volume strain e_v with the axial strain e_a. In addition, a degradation of the secant shear modulus G_s is shown against the logarithmic shear strain e_s, measured with local instrumentation. The sample TT6 was unloaded to an isotropic effective stress of 25 kPa with the OCR for BRICK equal to 406 and the OCR for S_BRICK equal to 120, while sample TT7 was unloaded to an isotropic effective stress of 50 kPa, with the OCR for BRICK equal to 203 and the OCR for S_BRICK equal to 60.

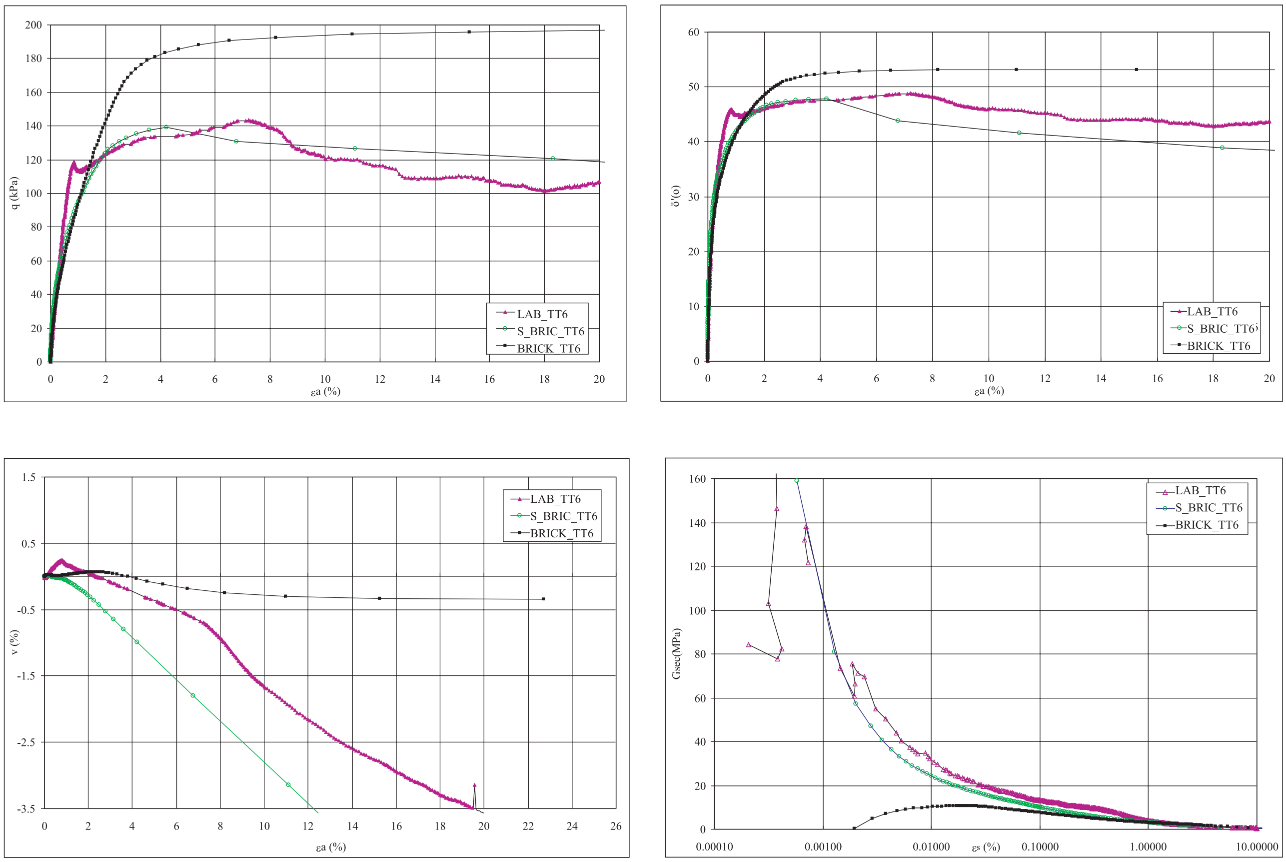

Figure 8. Comparisons of the strength, volumetric and stiffness predictions of the BRICK and S_BRICK models for sample TT6.

The numerically predicted behaviors by both models for the samples TT6 and TT7 are shown in Figures 7 and 8. It can be seen that the S_BRICK model more accurately reproduced the strength, stiffness and volumetric behavior for both samples. For sample TT6 the BRICK model overestimates the deviator stress and the mobilized frictional response and greatly underestimates the stiffness response and dilation in comparison with the S_BRICK model, whose prediction of the strength and stiffness behavior was very good. The S_BRICK model was especially good at predicting the shear-stiffness degradation from very small strain (0.001%) up to the point of failure. The S_BRICK model somewhat over predicted the amount of dilation, but its prediction was still reasonably good.

Similar results as for sample TT6 were obtained for sample TT7 (Figure 9, see next page), where the strength, stiffness and volumetric response were also significantly better predicted with the S_BRICK model. For sample TT7 it was not possible to compare the stiffness response of the model from very small strains, like for sample TT6, due to measurement difficulties, but based on the available data the S_BRICK model still accurately predicted the stiffness degradation from small strains (0.01%) up to the point of failure.

CONCLUSIONS

Hard soils and soft rocks (HSSR) represent an important part of all geological materials and are often encountered in geotechnical projects around the world. The most convenient definition for HSSR is based on their strength, as proposed by several authors [1], [2], [3], [4], to name just a small selection. A classification that seems to be the most appropriate was proposed by Hawkins and Pinches [5]; this is because it acknowledges the continuum between soils and rocks.

However, from a constitutive modeling stand point, it is more important to define the theoretical framework through which HSSR can be modeled. It was shown that

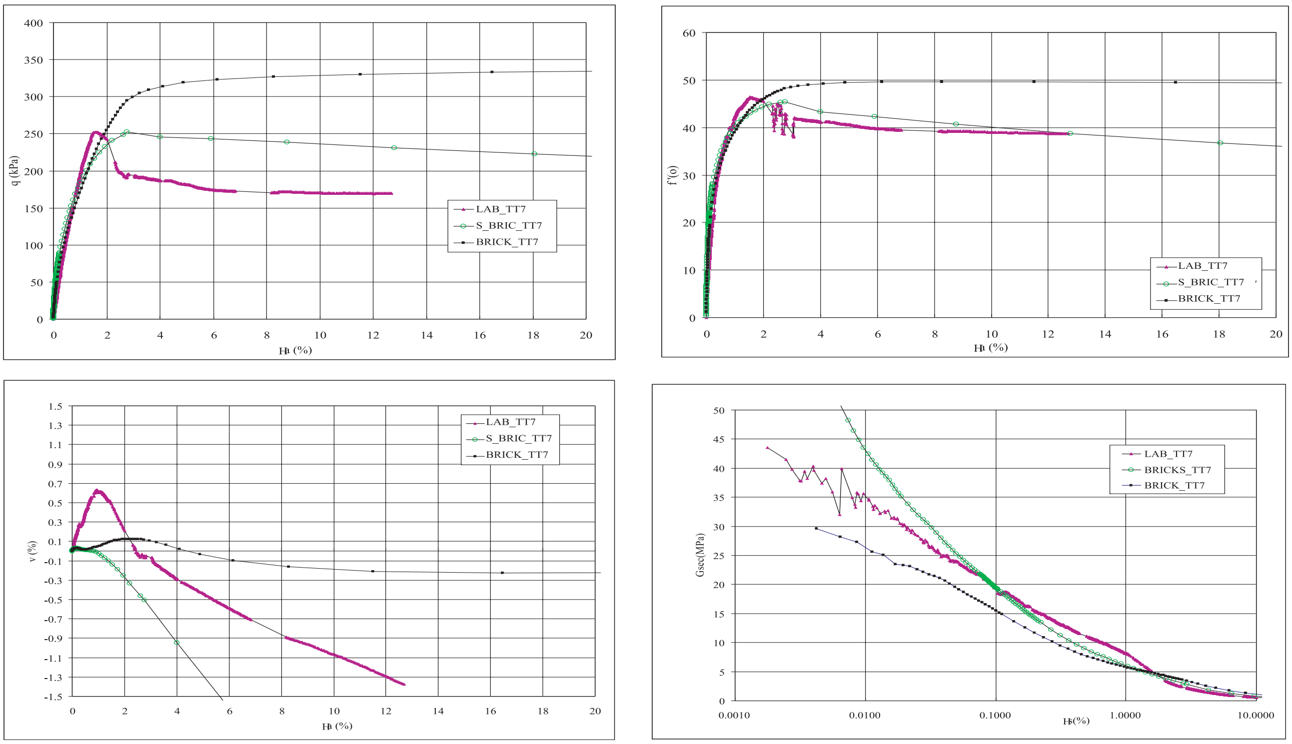

Figure 9. Comparison of the strength, volumetric and stiffness predictions of the BRICK and S_BRICK models for sample TT7.

the stress-strain behavior of most HSSR can be successfully described using the framework of critical state soil mechanics, as long as the materials are not influenced by discontinuities, and the effects of an excess pore pressure are important [12].

It has also been shown that the higher strength and stiffness encountered in HSSR in comparison to soft soils can be attributed to structure, which represents a key additional parameter in modeling. A very important element of structure is its stability under different stress paths, which also has to be taken into account.

A model for HSSR that includes structure and destructurization named S_BRICK was developed [22], [23] based on the BRICK model [24], [25]. This S_BRICK model was briefly explained here. The comparison of both models' predictions, the S_BRICK and the BRICK, was carried out on stiff North Sea clay. The predictions of the S_BRICK model were significantly better that the predictions of the BRICK model.

This comparison of the results highlighted the importance of structure and destructurization as key parameters in constitutive models as well as validating the proposition that HSSR can be successfully modeled using the framework of critical state soil mechanics.

The S_BRICK model will have to be further validated on a wider range of materials from soft soils to soft rocks in order to fully confirm its capabilities before it can be incorporated into a numerical environment and used in real boundary-value geotechnical problems.

ACKNOWLEDGEMENTS

The development of the S_BRICK model was sponsored by the SRA (Slovenian Research Agency – ARRS) as a part of a sponsored PhD study and a research project "Development and implementation of a constitutive model for Soft Rocks and Hard Soils-L2-7036". The author is grateful to dr. Vojkan Jovičić for guidance, discussions and help during the course of the PhD project and also to dr. Brian Simpson for all the help, ideas and discussions regarding the BRICK model and its further development.

REFERENCES

[1] International Society for Rock Mechanics ISRM. (1982). Suggested Methods: Rock Characterization, Testing and Monitoring. Edited by Browm, E.T. Oxford.

[2] Bieniawski, Z.T. (1973). Engineering classification of jointed rock mases. *Transactions of the South African Institution of Civil Engineers*, 15, 335-344.

[3] British Standard Institution BSI (1981). *Code of practice for site investigation*, BS 5930. HMSO, London.

[4] IAEG. (1979). Report fo the commission on engineering geological maping. *Buletin IAEG 19*, 364-371.

[5] Hawkins, A.B., and Pinches, G.M. (1992). Engineering description of mudrocks. *Quarterly Journal of Engineering Geology 25*, 17-30

[6] Hyett, A.I., and Hudson, J.A. (1990). A photoelastic investigation of the stress state close to rock joints. *Proc. Conf. on rock Joints* (ed. Barton N. and Stephansson F.), Balkema, 227-233.

[7] Picarelli, L., and Olivares, L. (1998). Ingredients for modeling the mechanical behaviour of intensly fissured clay shales. *Proc. 2nd Int. Symp. On the Geotechnics of Hard Soils and Soft Rocks*, Napoli, Balkema.

[8] Burland, J.B., Rampello, S., Georgiannou, V.N., and Calabresi, G. (1996). A laboratory study of the strength of four stiff clays. *Geotechnique 46*, 3, 491-514.

[9] Bertuccioli, P., and Lanzo, G. (1993). Mechanical properties of two Italian structurally complex clay soils. *Geotechnical Engineering of Hard Soils-Soft Rocks*, Athens, Greece, (Ed. Anagnostopoulos, A.G. et. al.), Balkema, 383-389.

[10] Lefebre, G. (1970). *Contribution a l etude de le stabilite des pentes dans les argiles cimentees*. PhD thesis, Universite Laval, Quebec.

[11] Elliot, G.M., and Brown, E.T. (1985). Yield of soft high porosity rock. *Geotechnique 35*, 4, 413-423.

[12] Kavvadas, M. (2000). General report: Modelling the soil behaviour – Selection of soil parametres. *The Geotechnics of Hard Soils-Soft Rocks*. (Ed. Evangelista & Picarelli), Balkema, 1441-1481.

[13] Leroueil, S., and Vaugan, P.R. (1990). The general and congruent effects of structure in natural soils and weak rocks. *Géotechnique 40*, 3, 467–488.

[14] Kavvadas, M., and Amorosi, A. (2000). A constitutive model for structured soils. *Géotechnique 50*, 3, 263-273.

[15] Rouainia, M., and Wood, M.D. (2000). A kinematic hardening model for natural clays with loss of structure. *Géotechnique 50*, 2, 153-164.

[16] Baudet, B.A. (2001). *Modelling effects of structure in soft natural clays*. PhD thesis. London: City University.

[17] Cotecchia, F. (1996). *The effects of structure on the properties of an Italian Pleistocene clay*. PhD Thesis, City University, London.

[18] Lambe, T.W., and Whitman, R.V. (1969). *Soil Mechanics*. New York: John Wiley & Sons Inc.

[19] Cotecchia, F., and Chandler, R.J. (2000). A general framework for the mechanical behaviour of a clays. *Géotechnique 50*, 4, 431-447.

[20] Rampello, S., and Silvestri, F. (1993). The stess-strain behaviour of natural and reconstituted samples of two overconsolidated clays. *Geotechnical Engineering of Hard Soils-Soft Rocks*, Athens, Greece, (Ed. Anagnostopoulos, A.G. et. al.), Balkema, 769-778.

[21] Jovičić, V., Coop, M., and Simpson, B. (2006). Interpretation and modelling of deformation characteristics of a stiff North Sea clay. *Can. geotech. journal 43*, 4, 341-354.

[22] Vukadin, V. (2004). *Development of a constitutive material model for soft rocks and hard soils*. PhD thesis. Ljubljana: University of Ljubljana.

[23] Vukadin, V., Likar, J., and Jovičić, V. (2005). Development of a conceptual material model for structured materials S_BRICK. *Acta Geotechnica Slovenica 2, 1*, 33-43.

[24] Simpson, B. (1992). Thirty-second Rankine Lecture: Retaining Structures: displacement and design. *Geotechnique 42*, 4, 541-576.

[25] Simpson, B. (2001). BRICK 17, *GEO suite for windows*. Published on: http://www.oasys-software.com/product/downloads/geo/brick_Nov01.pdf

3D NELINEARNA DINAMIČNA ANALIZA KAMNITE PREGRADE, KI TEMELJI NA IZIIS SOFTWARU

VIOLETA J. MIRCEVSKA, VLADIMIR BICKOVSKI in MIHAIL GAREVSKI

o avtorjih

Violeta J. Mircevksa
University "St. Cyril and Methodius",
Institute of Earthquake Engineering and Engineering Seismology
Salvador Aljende 73,
pp 101, 1000 Skopje, Makedonija
E-pošta: violeta@pluto.iziis.ukim.edu.mk

Vladimir Bickovski
University "St. Cyril and Methodius",
Institute of Earthquake Engineering and Engineering Seismology
Salvador Aljende 73,
pp 101, 1000 Skopje, Makedonija
E-pošta: bickovski@pluto.iziis.ukim.edu.mk

Mihail Garevski
University "St. Cyril and Methodius",
Institute of Earthquake Engineering and Engineering Seismology
Salvador Aljende 73,
pp 101, 1000 Skopje, Makedonija
E-pošta: garevski@pluto.iziis.ukim.edu.mk

izvleček

V tem prispevku je opisano 3D nelinearno dinamično obnašanje kamnite pregrade. Za kamnito maso je upoštevan material, ki zadovoljuje Mohr-Coulombov kriterij porušitve. Pregrada se nahaja v strmem, ozkem, ostrem kanjonu, v obliki črke 'V'. Obravnavan je koncept modela »brezmasnega kamnitega temelja«, pri čemer je določen del kamnine vključen v model. Kontaktna ploskev med kamnino in pregrado je modelirana s kontaktnimi elementi, ki omogočajo relativne premike med materialoma različne togosti. 3D matematičnega modela je bil izbran glede na topologijo terena. Nelinearni dinamični odziv temelji na direktni integracijski metodi linearnega pospeška, kis e izvaja 'korak za korakom' z uporabo metode Wilson-θ. Konvergentni postopek je v skladu z Newton-Raphsonovo metodo.
Najprej so bile določene začetne statične efektivne napetosti, ki so v stacionarnih pogojih filtracije skozi glinasto jedro. Analiza temelji na originalnem programu s končnimi elementi za statično in dinamično analizo kamnitih pregrad, kakor tudi na programu s končnimi elementi za reševanje stacionarnih filtracijskih procesov skozi glinasto jedro. Dinamični rezultat 3D modela pregrade je definiran za efekt harmoničnih indukcij. Dinamične analize v linearni in nelinearni domeni so bile izvedene zaradi primerjave rezultatov. Časovni poteki linearnih in nelinearnih odzivov so bili določeni za izbrane odseke in točke modela, natezne razpoke, plastične deformacije in napetostno deformacijske odnose. Določili smo tudi koeficient varnosti potencialnih drsnih površin. Ugotavljamo, da so 3D analize, kakor tudi nelinearno obravnavanje materialov vgrajenih v pregrado, nujne za pravilno oceno stabilnosti kamnitih pregrad izvedenih v ozkih kanjonih.

ključne besede

avtomatsko generiranje 3D modela, kamnita pregrada, nelinearna dinamična analiza, elasto plastični kriterij, natezna razpoka, cone z razpokami, plastične deformacije, stabilnost

A 3D NONLINEAR DYNAMIC ANALYSIS OF A ROCK-FILL DAM BASED ON IZIIS SOFTWARE

VIOLETA J. MIRCEVSKA, VLADIMIR BICKOVSKI and MIHAIL GAREVSKI

About the authors

Violeta J. Mircevska
University "St. Cyril and Methodius",
Institute of Earthquake Engineering and Engineering Seismology,
Salvador Aljende 73,
P.O. Box101, 1000 Skopje, Macedonia
E-mail: violeta@pluto.iziis.ukim.edu.mk

Vladimir Bickovski
University "St. Cyril and Methodius",
Institute of Earthquake Engineering and Engineering Seismology,
Salvador Aljende 73,
P.O. Box101, 1000 Skopje, Macedonia
E-mail: bickovski@pluto.iziis.ukim.edu.mk

Mihail Garevski
University "St. Cyril and Methodius",
Institute of Earthquake Engineering and Engineering Seismology,
Salvador Aljende 73,
P.O. Box101, 1000 Skopje, Macedonia
E-mail: garevski@pluto.iziis.ukim.edu.mk

Abstract

This paper treats the 3D nonlinear dynamic behavior of a rock-fill dam based on the Mohr-Coulomb failure criterion. The dam is situated in a steep, narrow, "V-shaped" rigid canyon. The concept of a massless rock foundation is treated, for which a certain part of the rock is included in the model. The dam-rock interface was modeled by contact elements, which allowed certain relative displacements between the two media of different stiffnesses. The generation of the 3D mathematical model was related to the topology of the terrain, and the nonlinear dynamic response was based on the "step-by-step" linear-acceleration direct-integration method, making use of the Wilson-θ method. The convergence process was in accordance with the Newton-Raphson method. First, the initial static effective stresses existing in the conditions of the established stationary filtration through the clayey core were defined. The analysis was based on an original FE program for the static and dynamic analyses of rock-fill dams, as well as a FE program for the solution of the stationary filtration process through the clayey core. The dynamic response of the 3D model of the dam was defined for the effect of harmonic excitations. Dynamic analyses in the linear and nonlinear domains were performed for the purpose of comparing the results. The time histories of the linear and nonlinear responses were defined for selected sections and nodes of the model, the tension cut-off zones, the plastic deformations, and the stress-shear strain relationships. The coefficient against the sliding of the potential sliding surfaces was also defined. It can be concluded that 3D analyses as well as a nonlinear material treatment of the soils built in the dam are imperative for a proper assessment of the stability of rock-fill dams situated in narrow canyons.

Keywords

automatic generation of 3D model, rock-fill dam, nonlinear dynamic analysis, elastic perfectly plastic criterion, tension cutoff, cracking zones, plastic deformations, stability

1 INTRODUCTION

This paper treats the 3D nonlinear dynamic response of a rock-fill dam with a central clayey core based on the application of the Mohr-Coulomb linear elasto-plastic criterion [4],[5]. The associated flow rule is accepted for the clay in the core, for which the failure criterion and the yielding surface are identical. In this case the shape of the yielding surface in the High-Westergaard's space is dependent only on the model's plasticity parameters, C and φ. The non-associated flow rule is accepted for the filters and the stone detritus, for which in addition to the yield function the plastic potential function is treated. The plastic potential is a function of the third plasticity parameter, the dilatancy angle ψ, used to control the inelastic volume increase as a result of the compressive stress increase after achieving the failure state.

The Mohr-Coulomb parameters can be evaluated by conventional laboratory tests, which makes their application easier. In fact, owing to its extreme simplicity and good accuracy, the Mohr-Coulomb linear elastic–perfectly plastic criterion [3],[4],[5] combined with the principle of tension cut-off [6] is used to predict the nonlinear behavior of the soils built in the dam, during the dynamic response. However, this failure criterion has two main shortcomings [5]. First, it assumes that the intermediate principal stress has no influence on the failure, which gives an unrealistic estimation of the shear strength under general loading conditions (except for triaxial compression conditions). This can, however, be overcome by the use of the SMP criterion [9]. The second disadvantage is that the meridians of the yielding surface are straight lines, which implies that the strength parameter φ does not change with the confining pressure, just like most of the other nonlinear methods for analyses [11],[12],[13],[14]. However, these two effects have an opposite impact to the shear strength: while with an increase in the confining pressure, the parameter φ decreases, and thus the shear strength decreases, the intermediate principal stress tends to increase the shear strength.

Very little has been done to reveal the dynamic behavior of rock-fill dams in typical 3D conditions, [16],[17],[18],[19],[20],[21], from the practical point of view. The analyses based on use of the QUAD-4 or FLUSH programs and their later modifications are of the shear-beam type, i.e., they do not define the residual displacements of the dam after the dynamic effect. During the dynamic effects, the developed tensile stresses can be sustained only by the clayey core of the rock-fill dams due to the cohesive properties of the clay. The development of fine cracks and the definition of the tension cut-off zones in the clayey core during the dynamic response of the dam are important for an evaluation of the dam's stability.

The contact elements are used to model more realistically the dam-rock interface, in this way preventing an unrealistic increase in the tensile stresses at the dam-rock interface and in the parts of the dam close to the support. The role of the contact elements interposed between the rock and the dam is to permit a smoother transition of the stresses in the zone of contact, allowing some differential movements in compliance with Coulomb's friction law and in accordance with the experimentally defined values of the frictional parameters C and φ at the dam-rock interface.

In the presented analysis the effect of the dam-foundation dynamic interaction is represented by the use of the most simple, conventional massless-foundation method (Wilson, 2002). Accordingly, only the effect of the foundation's flexibility is considered, while the inertia forces within the foundation's mass are neglected.

Due to the absence of any wave propagation the earthquake motion that is applied directly at the fixed boundaries is transmitted to the base of the dam without any changes. The massless concept requires the foundation's mass to be extended at least one dam height in the upstream, downstream and downward directions. The size of the massless foundation need not be very large, so long as it provides a reasonable estimate of the flexibility of the foundation rock and sufficient elimination of the boundary conditions' effect on the deformation, the stresses and the natural frequencies of the dam.

The distribution of stresses and strains in the dam body is directly affected by the profile of the canyon where the dam is situated. If a rock-fill dam is built in a narrow, ''V'-shaped" canyon, then only the sections in the central part act in plane-strain conditions. The closer the sections are to the abutments, the greater is the influence of the boundary conditions on the distribution of stresses and strains in these sections. This results in a deviation from plane-strain state conditions, followed by a decreased intensity of the spherical stress and hence a reduced shear resistance of the soil in these parts of the dam. Therefore, the behavior and the assessment of the stability of the central section based on a plain-strain analysis cannot be representative of the stability of the whole of the dam. The application of the 3D mathematical model that should be, from an engineering point of view, an appropriate and correct approximation of the real structure becomes a necessity. It is because of this that an original methodology and computer program for automatic generation was implemented, whereby the 3D model is connected with the contour lines of the terrain.

We have elaborated our own computer program, PROC3DN, for 3D static and dynamic analyses of earthfill dams and geotechnical structures, theoretically based on [1],[2], as well as on the application of the Mohr-Coulomb failure criterion [3],[4],[5].[6].

2 AUTOMATIC GENERATION OF THE 3D MODEL OF THE DAM

The automatic generation of 3D mathematical models requires a database on the topology of the terrain in the immediate vicinity of the dam's foundation, the projected position of the axis of the dam's crest at the base, Fig. 2, and the shape of the main central cross-section, Fig. 1.

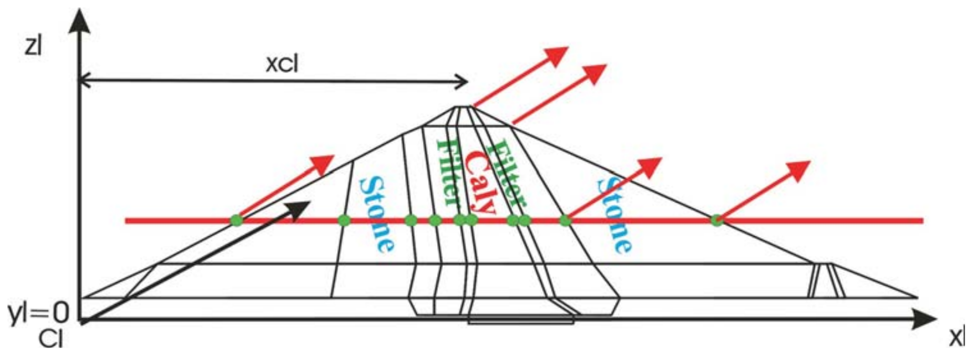

Figure 1. Main central cross-section of the dam.

The height of the dam is 127 m, which puts it in the category of high dams. The length of the dam along the crest axis is 300 m, the crest width is 10 m, and the maximum width of the base is 496 m. The clayey core has a width of 6 m at the crest and a width of 63 m at the foundation. The clayey core is founded on rock (schist). The inclinations of the upstream and downstream slopes are 1:2.2 and 1:2.0, respectively.

At each altitude the coordinates of the characteristic intersection points with the boundary lines of the plain model are defined (see Fig. 1). Drawn through these points are the straight lines parallel to the dam's crest axis. In this way the sections of the dam's body with the terrain at each altitude are obtained. A cumulative presentation of the selected horizontal cross-sections that are used for a definition of the 3D mathematical model is given in Fig. 2. The adopted 3D mathematical model, Fig. 3, has a total of 212 substructures in the dam body and 290 substructures in the rock's mass, Fig.5, 6250 external substructures' nodes, 2122 internal substructures' nodes and 2200 matrix band. The volume of the built-in clayey core is $0.338 \cdot 10^6$ m^3, while those of the filtration layers and the rock infill are $0.223 \cdot 10^6$ m^3 and $2.7 \cdot 10^6$ m^3, respectively. The dead weight of the entire structure is $G = 7.2 \cdot 10^7$ kN.

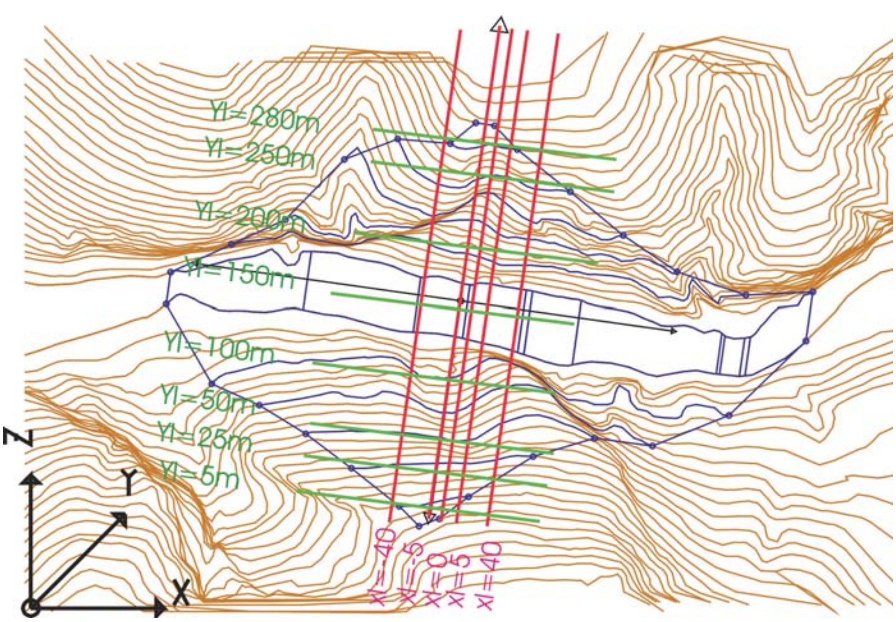

Figure 2. Plan view of the dam site with contour lines and an indication of the sections considered in the analysis.

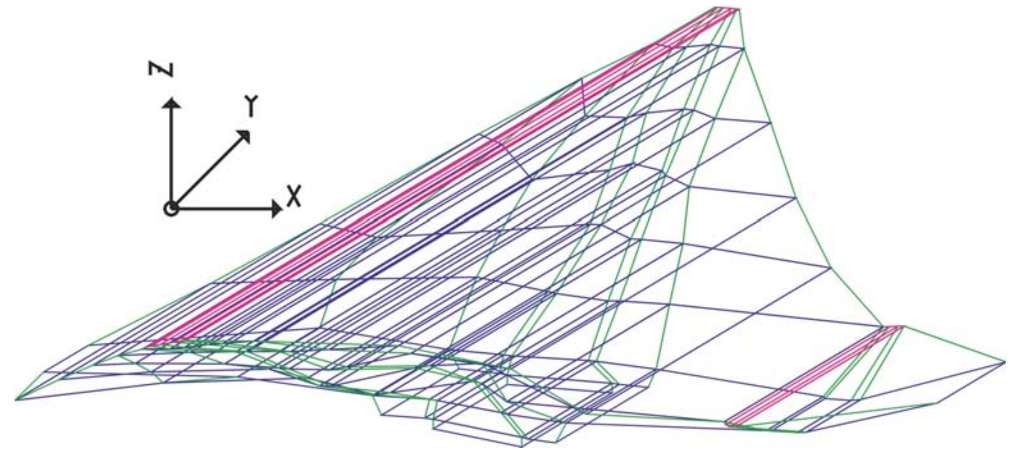

Figure 3. 3D model of the substructures adopted for the analysis.

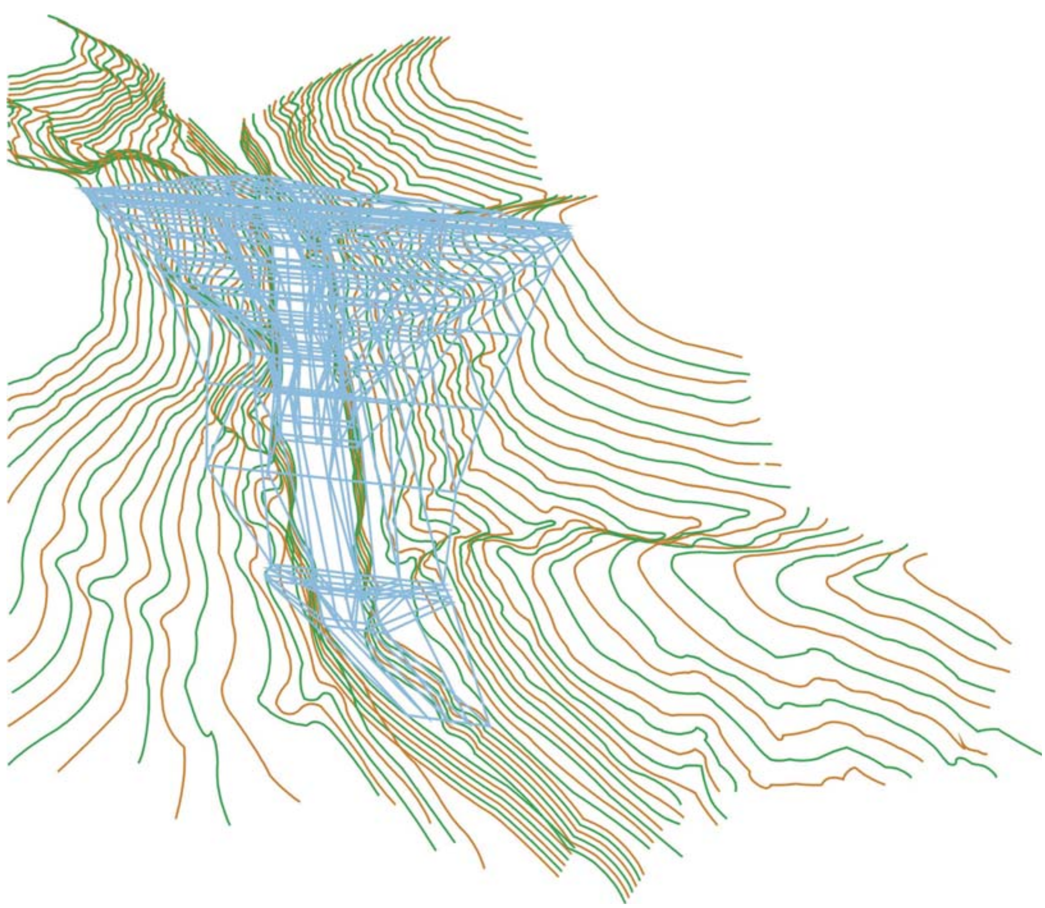

Figure 4. Perspective view of the dam and the terrain.

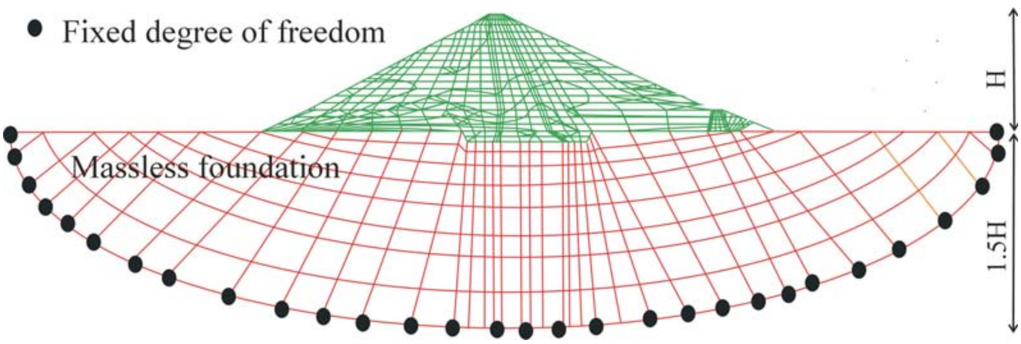

Figure 5. Rock massless model, section Yl=150 m.

3 DYNAMIC RESPONSE OF THE DAM

The dynamic response of the earth-fill dam is determined by applying the methods of modal analysis as well as by "step-by-step" direct integration, the linear acceleration method, and using linear and nonlinear analyses [7]. Within the frames of each finite element, the Newton–Raphson iterative procedure is applied in order to eliminate the vector of excessive stresses, i.e., the corresponding residual forces defined in accordance with the Mohr-Coulomb failure criterion. The main phases are as follows: solved within the frames of each i-th time step, and each iteration, is the incremental differential equation of dynamic equilibrium [8], with the following form:

$$M^{**}\Delta\ddot{U}_i + C^{**}\Delta\dot{U}_i + K^{**}\Delta U_i = \Delta P_i^{**} \qquad (1)$$

Applying the substructure technique, the differential equation of motion refers only to the external nodes of the model. Defined in this way are the incremental vectors of displacement, the velocity and the acceleration at the external nodes of the system. The matrices and vectors indicated by two stars refer to the external nodes of the substructures. The dynamic response at the end of each time step is defined by summing up the dynamic response from the beginning of the time step and the effect from the iterations performed in it.

$$U_n = U_0 + \sum_{i=1}^{n}\Delta Ui \qquad \dot{U}_n = \dot{U}_0 + \sum_{i=1}^{n}\Delta\dot{U}i$$
$$\ddot{U}_n = \ddot{U}_0 + \sum_{i=1}^{n}\Delta\ddot{U}i \qquad n = 1, iter \qquad (2)$$

where *iter* is the number of iterations within the frames of each time step, $U_0, \dot{U}_0, \ddot{U}_0$ are the initial vectors of displacement, velocity and acceleration, and $\Delta U_0, \Delta\dot{U}_0, \Delta\ddot{U}_0$ are the corresponding incremental vectors.

Using the incremental displacement vector, within each iteration we define the vector of incremental strains and the corresponding vector of incremental stresses for each finite element as follows:

$$\varepsilon = \varepsilon_0 + \sum_{i=1}^{n}\Delta\varepsilon_i \qquad \sigma = \sigma_0 + \sum_{i=1}^{n}\Delta\sigma_i \qquad n = 1, iter \qquad (3)$$

where ε_0, σ_0 are the initial vectors of the strains and stresses and $\Delta\varepsilon_0, \Delta\sigma_0$ are the corresponding incremental vectors.

At the end of each iteration the stress state is reviewed for each finite element. Only those finite elements for which the stress state is in the plasticity zone are selected, i.e., the stress point in the Haigh Westergaard's stress space lies beyond the failure surface, as defined by the Mohr-Coulomb criterion. For these finite elements we define the excessive stresses as the difference between the resulting and the ultimate stresses, which for a given spherical stress tensor and a given stress path lie on the yielding surface. For such defined excessive stresses there are the corresponding residual forces. Solving again the incremental differential equation for the dynamic equilibrium, only by considering the effect of the defined residual forces from the previous iteration, the new vectors of the incremental displacements, are the strains and the stresses obtained in the course of the next iteration. Since the residual forces are applied to a system with an unchanged stiffness matrix, excessive stresses exist during each iteration, but their intensities are decreased with each successive iteration, i.e., the iterative process converges. Successive iterations are made until the excessive stresses and the corresponding residual forces are higher than the tolerance of the iterative procedure. The tolerance used in the analysis was 0.01.

4 RESULTS AND DISCUSSION

A dynamic analysis was performed for the effect of a harmonic excitation with a frequency of ω_o= 5.2 rad/sec, a peak acceleration of A_o= 0.3 g and a duration of T = 20 sec. The harmonic excitation was applied only in the direction of the global X-axis of the system. The time step of the direct integration was Δt = 0.02 sec. The damping matrix had an explicit form, according to Rayleigh's damping concept. For the purpose of defining the Rayleigh coefficients, the first two mode shapes of the free vibrations with frequencies of ω_1 = 6.61 rad/sec and ω_2 = 8.97 rad/sec and critical modal dampings of ξ_1 = 10 % and ξ_2 = 15 % were adopted. The selected harmonic excitation with a frequency close to the first fundamental mode of free vibrations of the system had a dominant dynamic factor of participation in the system's response. For the same reasons, the dynamic factor of participation for the remaining frequencies must be lower, which is confirmed by the fact that the responses obtained with the modal analysis, in which only the first mode of the system was included, and the response obtained with the direct integration method (linear analysis), point to a good correlation.

The dynamic response obtained by means of the nonlinear analysis gave a different stress-strain state for the body of the dam. The dynamic response is presented through individual finite elements at selected cross-sections, Yl = 266 m, immediately next to the right support, and Yl = 150 m, representing the central part of the dam. Figures 6 and 7 present the time histories of the developed response for relative displacements as well as the histories of the developed plastic deformations in the three global directions and the time histories of the relative velocities and the absolute accelerations developed only in the global X direction, i.e., in the direction of the applied dynamic force.

The time histories of the relative displacements suggest that the system is out of a transient state of vibration and enters into a steady state after the first two-to-three periods of the system's response. Such a fast transition from a "transient" into a "steady-state" vibration state results from the small difference between the frequencies of the exciting force and the frequency of the first fundamental mode of free vibrations of the system. At the cross-section Yl = 150 m, representing the central part of the dam characterized by a greater flexibility, the transition from a "transient" into a "steady-state" vibration state is faster than for the cross-section Yl = 266 m, which is situated in the vicinity of the support.

The difference in the relative displacements between the linear and the nonlinear analyses (direct integration) for the cross-section Yl = 266 m, immediately next to the right support, in a finite element of the contact between the stone prism and the filtering layer, on the upstream side of the dam, is 35–40 %. The extreme current values of the plastic deformations are $U_{p,x}$ = 0.0205 m in the X direction, $U_{p,y}$ = -0.034 m in the Y direction, and $U_{p,z}$ = 0.028 m in the Z direction. The element tends to undergo plastic deformation in the X direction, i.e., in the direction of the excitation action, with a tendency for vertical displacement (settlement).

Comparing the displacement responses obtained by modal analysis and direct integration (linear analysis), the differences in all three directions, particularly in the global Y and Z directions, are evident. The reason is that the participation of only the first mode shape in the modal analysis is not sufficient to provide a more accurate response (a modal truncation problem).

The difference between the relative displacements obtained by the linear and nonlinear analyses (direct integration) for the cross-section Yl = 150 m, the central part of the dam, in a finite element close to the crest, amounts to 20 % in the X direction and 43–56 % in the Z and Y directions. The extreme current values of the plastic deformations amount to $U_{p,x}$ = -0.28 m in the X direction, $U_{p,y}$ = 0.098 m in the Y direction and $U_{p,z}$ = -0.12 m in the Z direction. The element has a tendency to be plastically deformed in the direction of excitation, with a tendency for vertical displacement (settlement).

Comparing the displacement response obtained with the modal analysis and the direct integration (linear analysis) at this cross-section, it is clear that there is very good agreement for the displacements in the global X direction. The central part of the dam, as the most flexible part of the structure, has the most intensive dynamic response, whereas the first fundamental mode of free vibrations of the system has a dominant effect on the response in the global X direction.

According to the nonlinear analysis, the dynamic amplification factor at the cross-section Yl = 266 m for the chosen finite element is DAF = 1.08, while for the finite element located at the dam's crest, it is DAF = 1.36 (not presented here). According to the nonlinear analysis, the dynamic amplification factor at the cross-section Yl = 150 m at the dam's crest is DAF = 4, while at 2/3 of the core's height, it is DAF = 2.4 (not presented here). The dynamic amplification factor of the dynamic effect obtained through nonlinear analysis is smaller than that obtained by linear analysis. The residual plastic deforma-

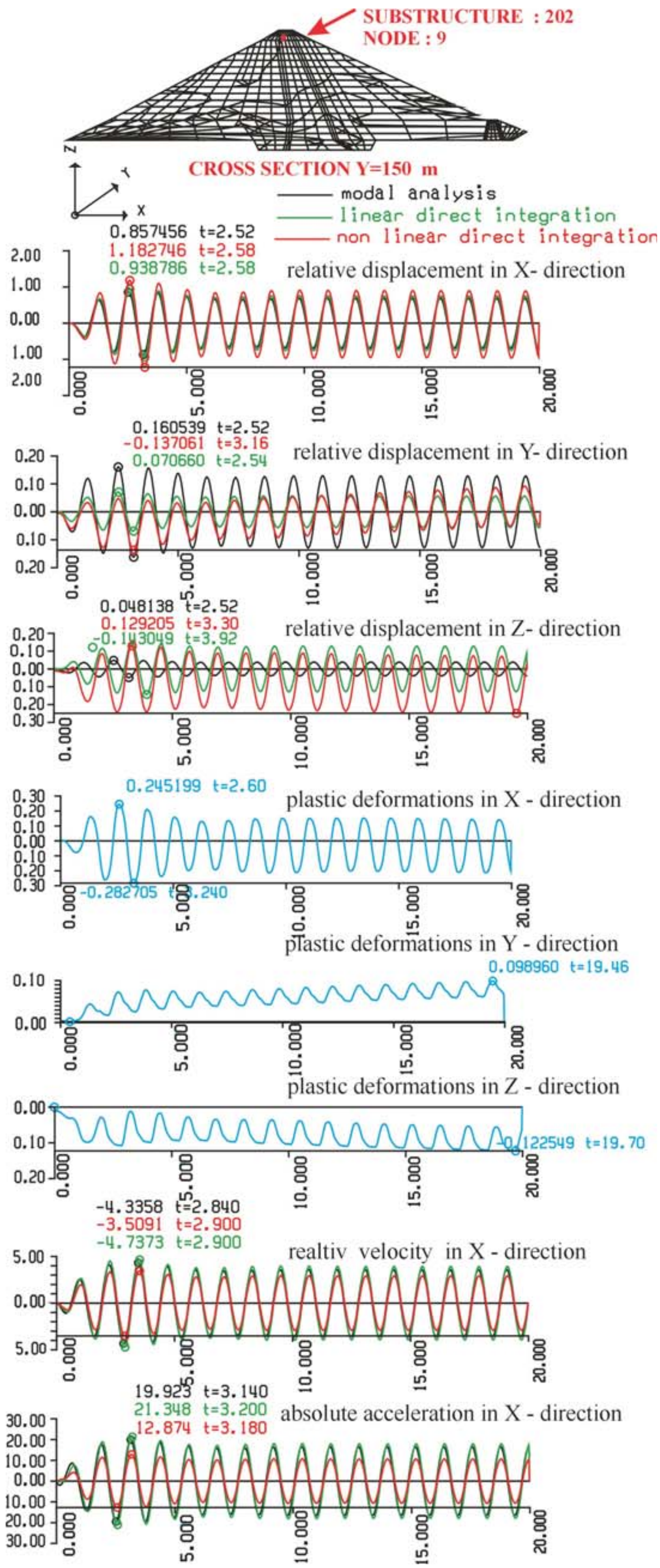

Figure 6. Time histories for a selected finite element as indicated for section Yl = 150 m.

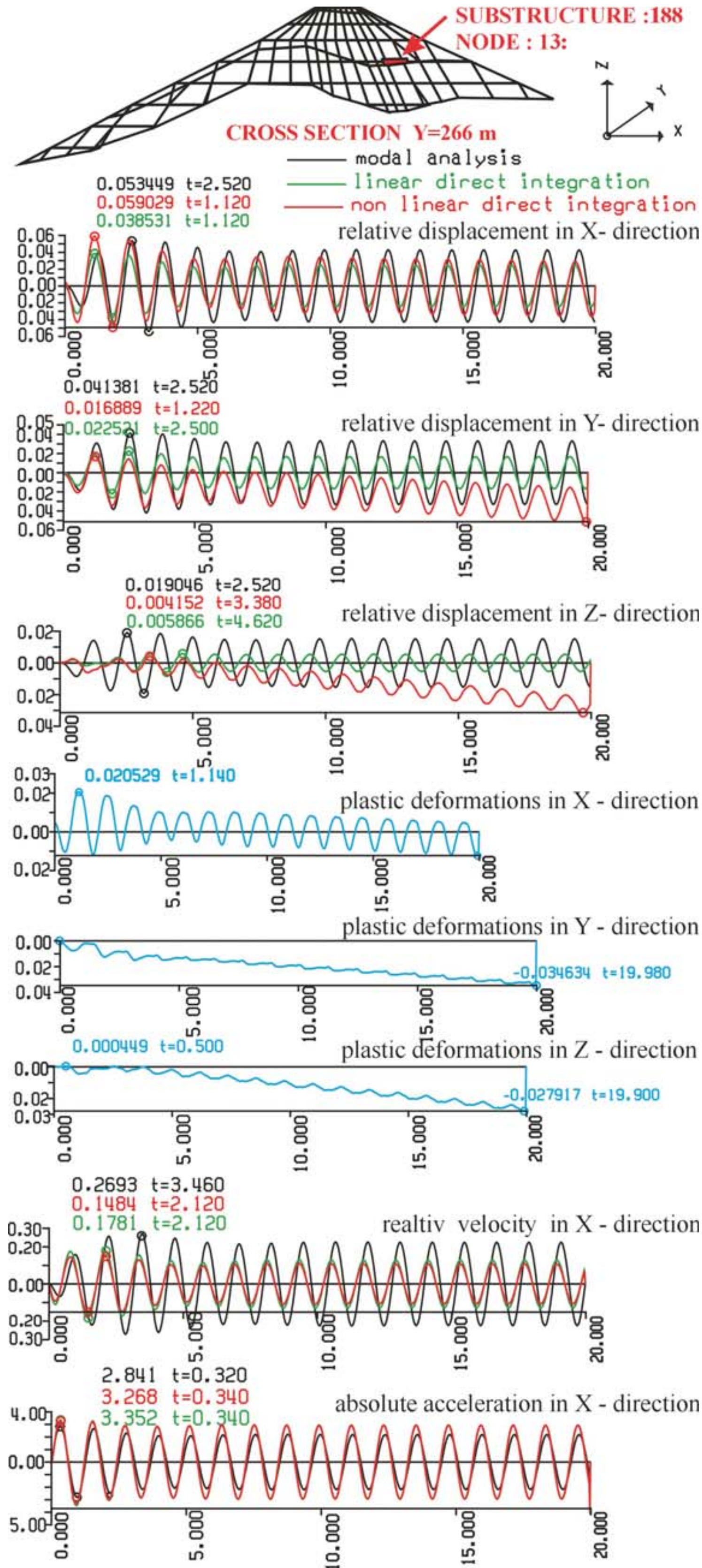

Figure 7. Time histories for a selected finite element as indicated for section Yl=226 m.

tions in the dam's body are obtained by superimposing the residual displacements in the course of the iterative processes within the frames of all the time steps. Figure 8 only shows the residual plastic deformations for the clayey core. From this we can conclude that after the effect of the harmonic excitation, the clayey core will be buckled along the dam crest, with the maximum plastic deformation in the X direction $U_{px,max}$ = -0.44 m and the maximum plastic deformation in the Z direction $U_{pz,max}$= -0.29 m. The residual plastic deformation in the Y direction, in the upper third of the core, shows a tendency to be compressed toward the central part $U_{py,max}$ = -0.16 m. Figure 9 and Fig. 10 show the plastic deformations at some chosen cross-sections of the dam. The residual plastic deformation of these cross-sections confirms the flexibility in the upper third of the core. Based on the residual plastic deformations we can conclude that there is compaction in the Z direction, i.e., settlement of the dam as a result of its nonlinear behavior during the dynamic response. Figures 11 and 12 show the time histories of the principal and component stresses for a selected finite element in the central cross-section Yl = 150 m.

A comparison has been made between the stresses obtained from the linear analysis by using the direct integration method and those obtained in the nonlinear analysis. As shown by the linear analysis, the principal stress, σ_1, is a tensile stress, which according to the Mohr-Coulomb failure criterion, cannot be sustained by the clay. The stress state, according to the nonlinear analysis, is transferred into the zone of pure compression. It is evident that there is a reduction of the component shear stresses down to the level of the allowable stresses, which are a function of the manifested spherical tensor of stresses and the stress path. The time histories of the principal and component stresses that refer to the finite elements located at the base show that the bottom of the dam is under compression, with high intensities of spherical compressive stresses and a weakly expressed nonlinearity (not presented here). Shown in Figures 13 and 14 are the component shear stress-strain relationships for chosen finite elements at the central cross-sections of the dam. The stresses and the shear strains have a lower intensity toward the supports and in the higher layers of the dam. Presented in Figs. 17 and 18 are snapshots of the nonlinear deformations for the selected sections of the dam, representing the time of manifestation of the widest zone of occurrence of cracks as a result of exceeding the allowable tensile stresses. The range of the manifested tensile strains is indicated by different colors. In the course of the dynamic response of the dam, the development of tensile strains (increases and decreases) is monitored and hence knowledge is acquired about the process of opening and closing the manifested cracks.

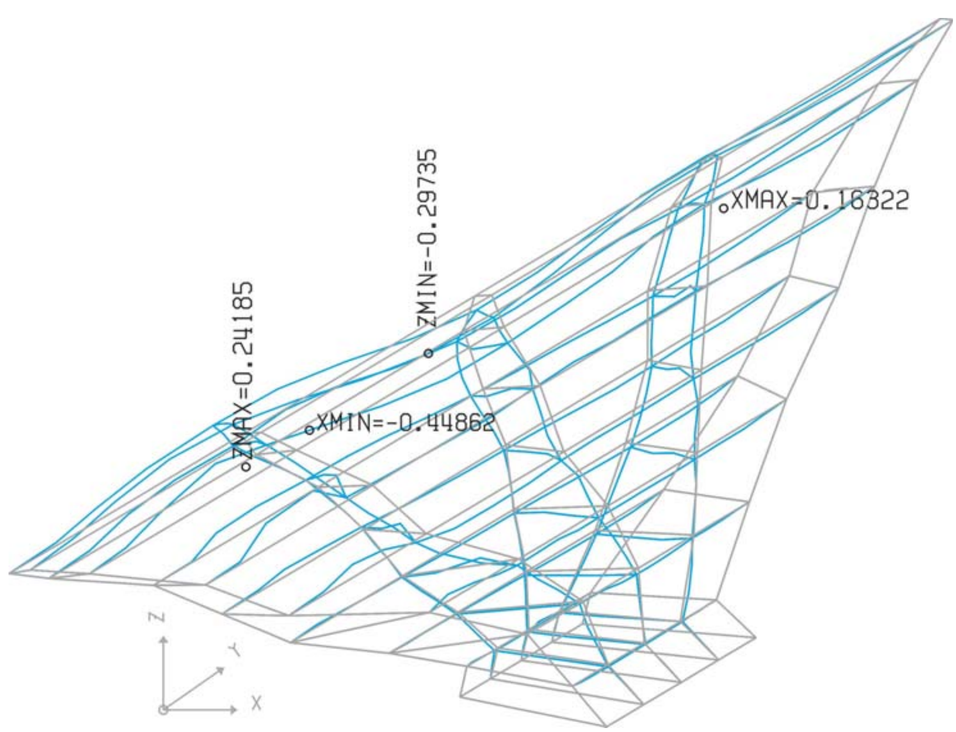

Figure 8. Plastic deformations of the clayey core.

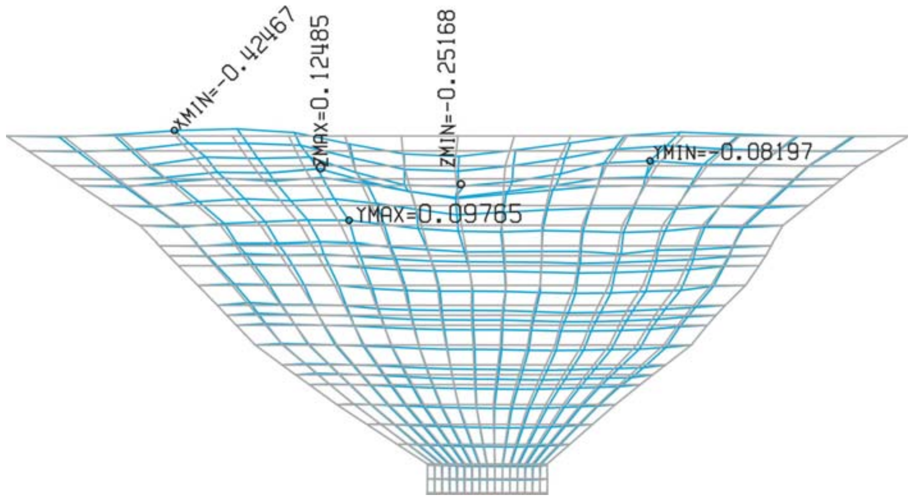

Figure 9. Plastic deformations in the longitudinal section Xl=0.

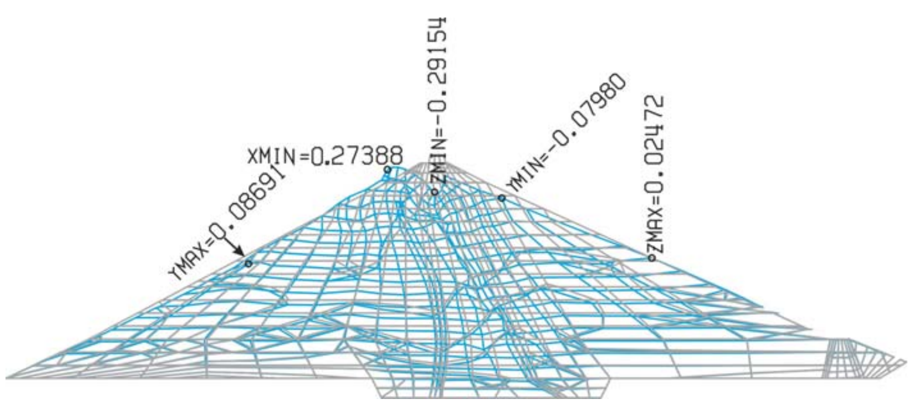

Figure 10. Plastic deformations in the central section Xl=150.

In earth-fill dams the potential sliding surfaces most frequently have the shape of a shell, so they should be defined by means of a parabola system composed of small triangles (planes), Fig. 15. The stress tensor is projected along the normal and the tangent of the elementary triangular surfaces, and with their integration the safety factor against sliding is defined. The time histories of the safety factor against sliding are defined on the basis of two performed analyses, i.e., the linear and nonlinear analyses, Fig. 16. The parameter PROB = 0.398 tells us that according to the linear analysis the potential sliding surface is unstable from 39 % of the total excitation time. According to the nonlinear analysis, the safety factor against sliding is higher than unity during the entire response time.

CONCLUSION

The profile of the canyon and the geometry of the dam structure have a predominant effect on the stress-strain state, whereby the application of a 3D mathematical model is necessary. The central part of the dam is characterized by a greater flexibility, so the transition from a transient state to a steady state of vibration is faster than with the cross-sections, which are in the vicinity of the abutments. The difference in the relative displacements between the linear analysis and the nonlinear analysis using the method of direct integration calculation for the X direction is approximately 20 % for the central part of the dam and 35–40 % for the sections toward the abutments. However, for the other two directions, this

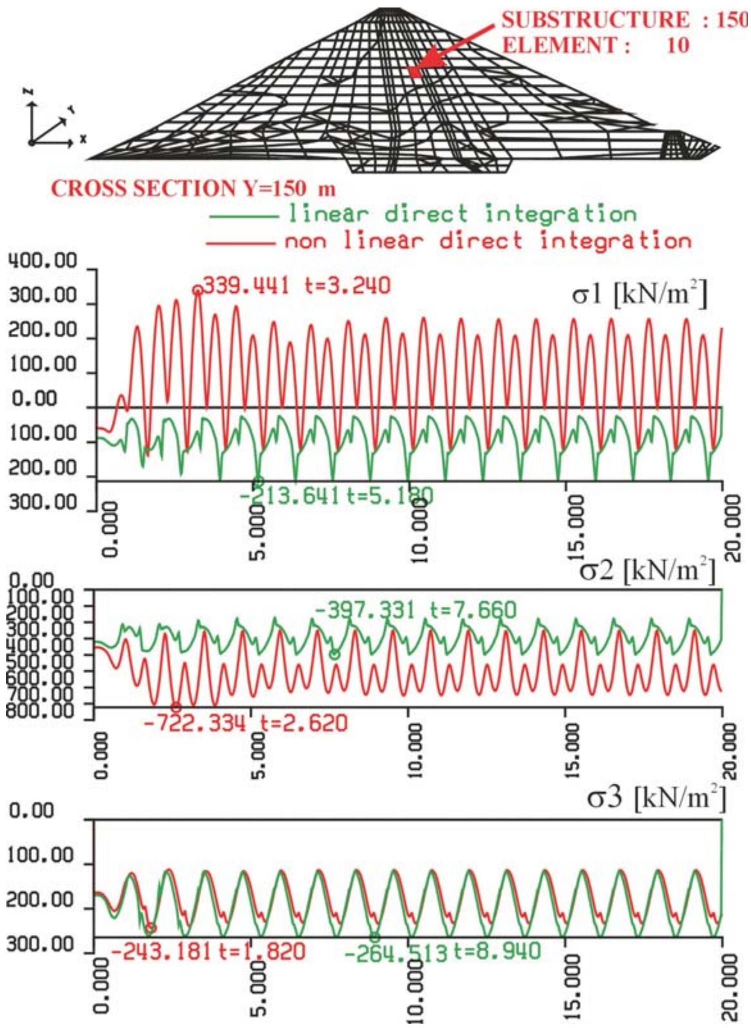

Figure 11. Time histories of the principal stresses for a selected FE for section Yl=150 m.

percentage is higher as a result of the development of larger plastic deformations, particularly in the Z direction.

The maximum value of the dynamic factor of amplification (DAF), according to the nonlinear analysis, occurs in the central part of the dam's crest, and the DAF is approximately equal to 4. However, it is smaller than the corresponding dynamic amplification factor obtained with the linear analysis. The dynamic amplification factor decreases toward the supports and with increasing depth. Under dynamic conditions the clayey core suffers plastic buckling deformations, which are particularly pronounced in the upper third of the core, because of the slender flexible core, i.e., the small dimensions in this zone. Based on the residual plastic deformations we can conclude that the settlement of the dam takes place as a result of the nonlinear dynamic response.

The component shear stresses obtained from the nonlinear analysis are lower than those obtained from the linear analysis. The reduction is down to the level of allowable octahedral shear stresses as a function of the existing spherical stress tensor. The stress state in the deepest zones of the dam is in the range of pure pressure, with a greater intensity of spherical stresses, which results in a slightly expressed nonlinearity. The shear strains are of the order of 10^{-3}, and the shear-stress/shear-strain diagrams clearly illustrate the elastic-plastic behavior of the soil media in accordance with the adopted constitutive law of nonlinearity.

According to the analysis, the time when the cracks occur can be recognized by the fact that in the time histories of all the principal stresses, the stresses are reduced to a value of $\sigma = 0$, at the same time.

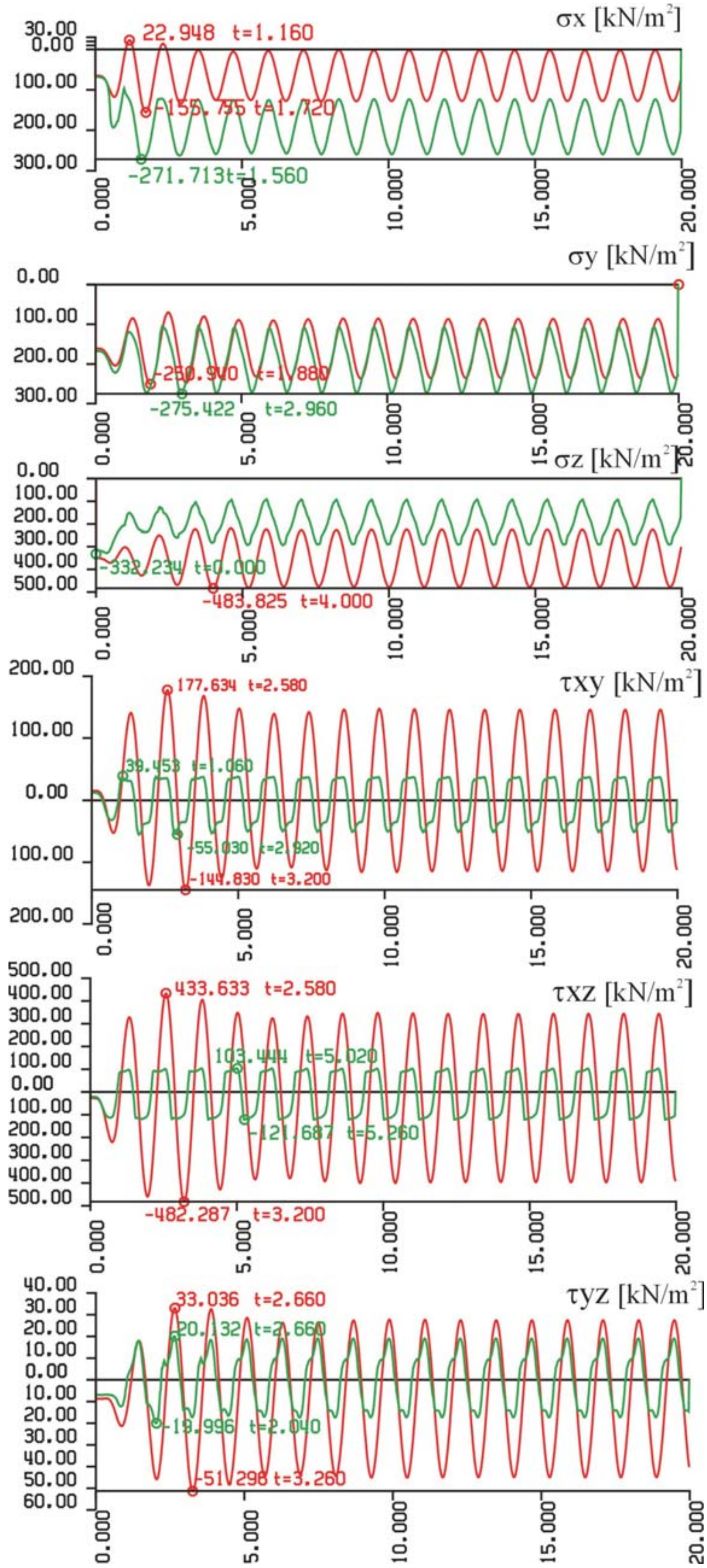

Figure 12. Time histories of the component stresses for a selected FE for section Yl=150 m.

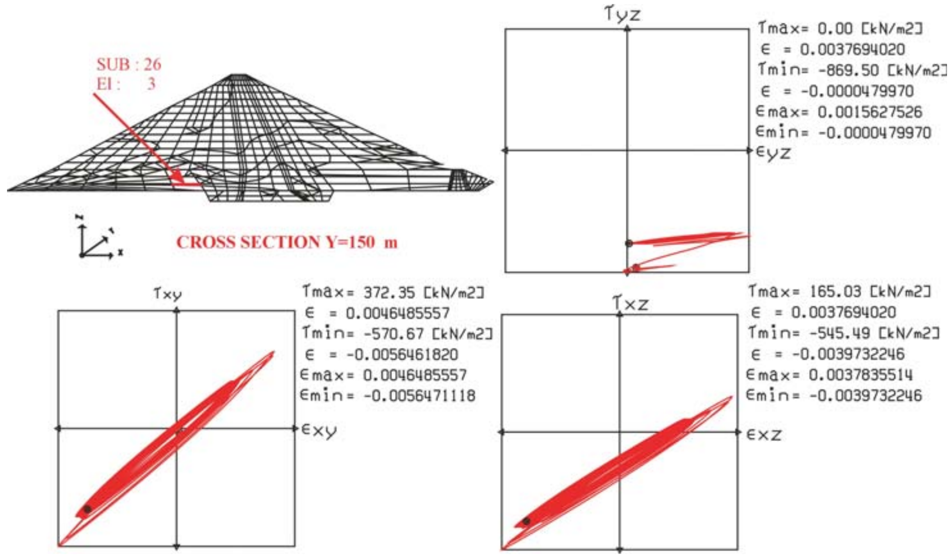

Figure 13. Shear stress-strain relationship for the chosen FE.

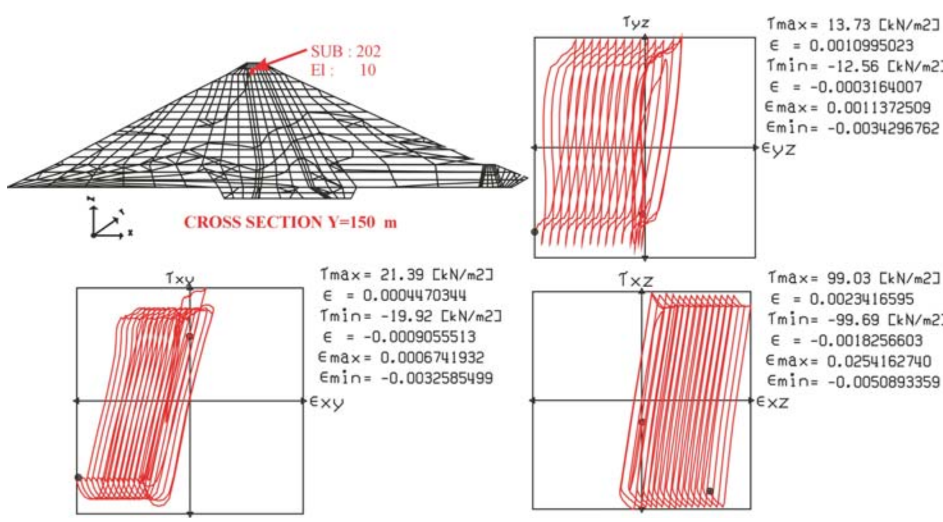

Figure 14. Shear stress-strain relationship for the chosen FE.

The mobilized strength in the analysis can achieve a value of less than or equal to unity. In the case when the element is in the zone of elastic behavior, the stress point is below the yield surface and the mobilized strength is less than unity. In the case when the element is in the zone of plastic behavior, the stress point lies on the yield surface and the mobilized strength is close to, or equal to, unity. The unit value of the mobilized strength provides information about those finite elements that exert plastic behavior. In this case any judgment about stability should be based on the resulting plastic deformations in the vicinity of such finite elements.

The safety factor against sliding defined by the linear analysis is lower than that defined by nonlinear analysis. This is due to the reduction of the active shear forces down to the level of the ultimate forces, in conditions of the existence of the ultimate plastic equilibrium.

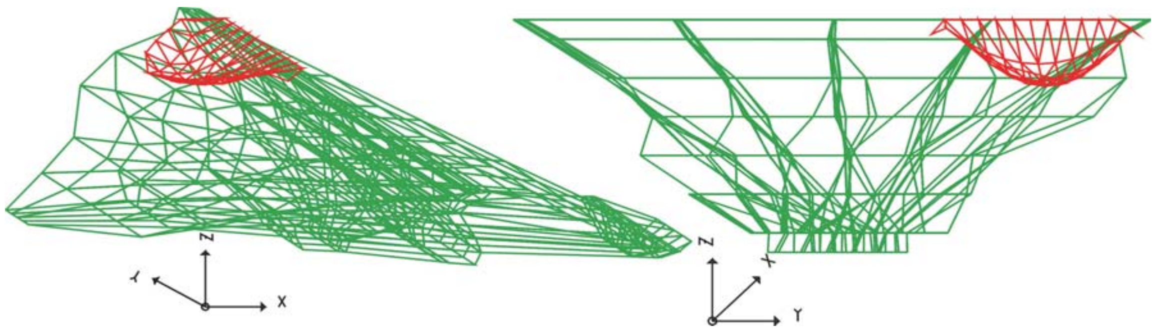

Figure 15. Position of the potential sliding surface in the dam.

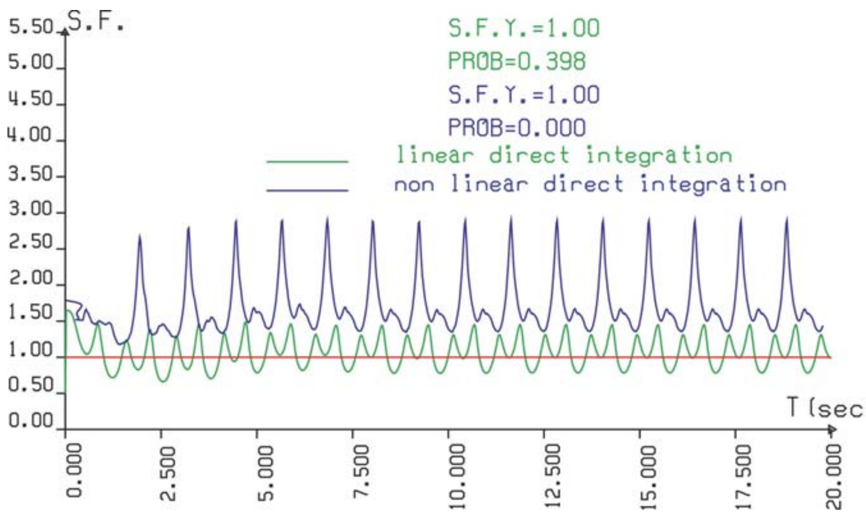

Figure 16. Time history of the safety coefficient against sliding.

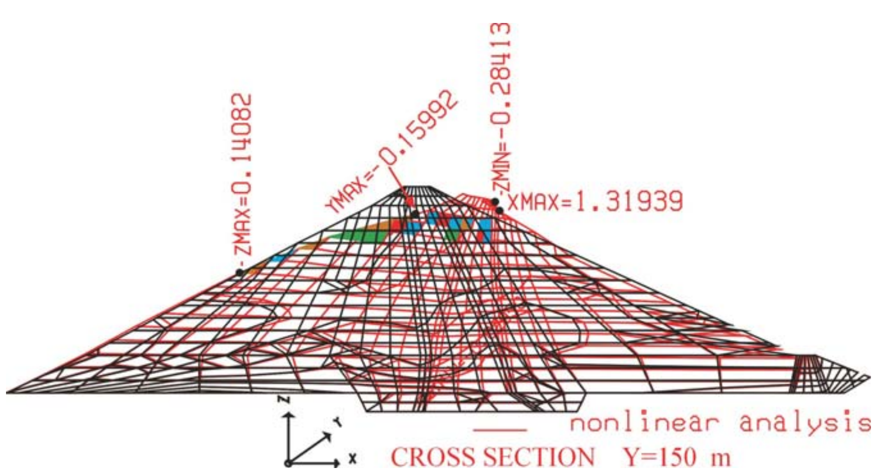

Figure 17. Snapshot T=2.58 sec. Extreme cracking zone in the section.

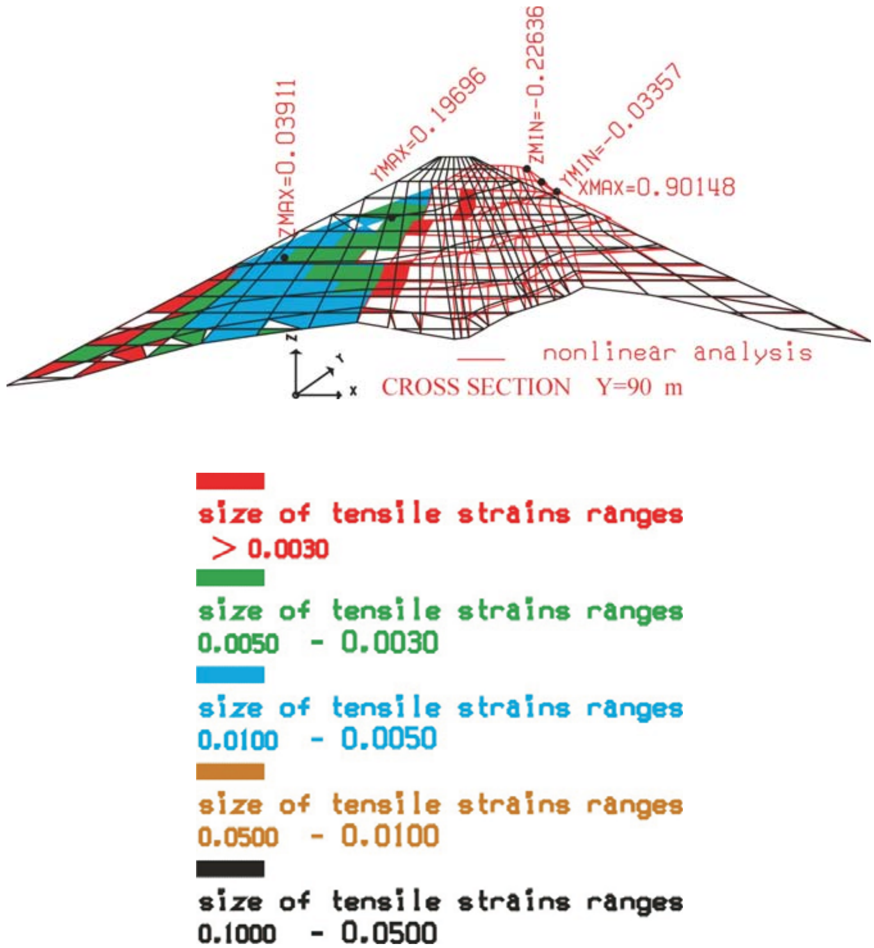

Figure 18. Snapshot T=2.66 sec. Extreme cracking zone in the section.

ACKNOWLEDGEMENT

The authors wish to express their gratitude to the Ministry of Education and Science of the Republic of Macedonia for its partial financial support of the research activities in the course of the creation of the computer program.

REFERENCES

[1] Bathe K.J. and Wilson, E.L. (1976). *Numerical Methods in Finite Element Analysis*. Prentice-Hall, Inc. Englewood cliffs, New Jersey.

[2] Bathe, K.J.(1982). *Finite Element Procedures in Engineering Analysis*. Prentice-Hall, Inc. Englewood cliffs, New Jersey.

[3] Duncan, J.M. and Chang, C.Y. (1970). Nonlinear Analysis of Stress and Strain in Soils. *Journal of Soil Mech. and Foundations Div. 96*, SM5, 1629-1653.

[4] Owen, D.R.J. and Hinton, E. (1980). *Finite Elements in Plasticity: Theory and Practice*. Pineridge Press, Swansea, U.K.

[5] Wai-Fan-Chen and Atef F. Saleeb (1982). *Constitutive Equations for Engineering Materials: Vol. 1 Elasticity and Modeling*. John Wiley&Sons.

[6] Wilson, E.L. and Clough, R.W. (1962). Dynamic Response of Step-by-step Matrix Analysis. *Proc. of the Symposium on the use of Computers in Civil Engineering*, Portugal.
[7] Clough, R.W. (1969). Analysis of Structural Vibrations and Dynamic Response. *Japan-U.S. Seminar on Matrix Methods of Structural Analysis and Design*, Japan.
[8] Paz, M. (1980). *Structural Dynamics, Theory and Computation*. Van Nostrand Reinhold Company, New York.
[9] Gazetas, G. and Dakoulas, P. (1992). Seismic Analysis and Design of Rockfill Dams: State of the Art. *Soil Dynamics and Earthquake Engineering 11*, 1, 27-61.
[10] Khoei, A.R., Azami, A.R., and.Haeri, S.M. (2004). Implementation of Plasticity Based in Dynamic Analysis of Earth and Rockfill Dams: A Comparison of Pastor-Zienkiewicz and Cap Models. *Computers and Geotechnics 31*, 5, 384-409.
[11] Idriss, I.M., Lysmer, J., Hwang, R., and Seed, H.B. (1983). Quad-4 a Computer Program for Evaluating the Seismic Response of Soil-Structure by Variable Damping Finite Element Procedures. *Report No. EERC 73-16. Univ. of California*, Berkeley.
[12] Gazetas, G. (1987). Seismic response of earth dams: some recent developments. *Soil Dynamics and Earthquake Engineering*, State of Art, 6, 1, 2–47.
[13] Prevost, J.H., Abdel - Ghaffar, A.M., and Lacy, S.J. (1985). Nonlinear dynamic analysis of earth dam: comparative study. *Journal of Geotech. Eng.* 111, 7, 882-897.
[14] Finn, W.D.L., Yogendrakumar, M.,Yoshida, N., and Yoshida, H. (1986). TARA - 3: A Program to Compute the Response of 2D Embankments and Soil-Structure Interaction Systems to Seismic : Loading. Univ. of British Columbia, Vancouver, Canada.
[15] Finn, W. D. L. (2000). State-of-the-art of geotechnical earthquake engineering practice. *Soil Dynamics and Earthquake Engineering 20*, 1-4, 1-15.
[16] Zienkiewicz, O.C., Leung, K.H., and Hintom, E. (1980). Earth Dam Analysis for Earthquakes: Numerical Solutions and Constitutive Relations for Non-linear (Damage) Analysis. *Design of Dams to Resist Earthquakes, ICE*, London, 141-156.
[17] Abdel-Ghaffar, A.M. and Elgamal, A.W.M. (1987). Elasto-plastic Seismic Response of 3-D Earth Dams: Theory and Application. Journal of Geotechnical Engineering 113, 11, 1293-1325.
[18] Dokoulas, P. (1990). Nonlinear Response of Dams Founded on Alluvial Deposit in Narrow Canyons. *JSDEE*, 9, 6, 301-312.
[19] Hayashi, M., Komada, H., and Fujiwara, Y. (1973). Three Dimensional Dynamic Response and Earthquake Resistant Design of Rock-fill Dam against Input Earthquake in Direction of Dam Axis. *Proceedings of the 5th World Conference on Earthquake Eng.*, Rome.
[20] Mejia, L.H., and Seed, H.B. (1983). Comparison of 2D and 3D Dynamic Analysis of Earth Dams. *Journal of Geotechnical Eng.* 109, 11, 1383-1398.

STOPNJA PROPADANJA TUNELOV PRAŠKEGA METROJA, KI TEMELJI NA OCENI MONITORINGA

IVAN VANÍČEK in MARTIN VANÍČEK

o avtorjih

Ivan Vaníček
Czech Technical University in Prague,
Geotechnical Department
Thakurova 7, 166 29 Praga 6, Češka Republika
E-pošta: vaniceki@fsv.cvut.cz

Martin Vaníček
Czech Technical University in Prague,
Geotechnical Department
Thakurova 7, 166 29 Praga 6, Češka Republika
E-pošta: vanicekm@mat.fsv.cvut.cz

izvleček

Razumevanje staranja objektov je z vidika ocene rizika teh objektov zelo pomembno. Geotehnični objekti imajo glede tega svoje posebnosti. Prispevek se osredotoča na tunele v praškem metroju z različnih vidikov – geologije, konstrukcijskih sistemov in vpliva poplavljanja. Izbrano mesto za izvedbo monitoringa predora je bilo eno najbolj prizadetih z velikim sistemom razpok. Monitoring tega mesta, ki je temeljil na makro in mikro pristopih, ni kazal posebnega propadanja. Vseeno je bil za kontrolo v daljšem časovnem obdobju nameščen in uporabljen brezžični sistem za zbiranje in prenašanje podatkov. Dosedanji rezultati tega monitorninga so pozitivni.

ključne besede

tunel, metro, propadanje, staranje, geologija, konstrukcija, kontrolno preverjanje, MEMS, geofizikalno, brezžični prenos podatkov, poplavljanje v metroju

THE DEGREE OF DETERIORATION OF THE TUNNELS OF THE PRAGUE METRO BASED ON A MONITORING ASSESSMENT

IVAN VANÍČEK and MARTIN VANÍČEK

About the authors

Ivan Vaníček
Czech Technical University in Prague,
Geotechnical Department
Thakurova 7, 166 29 PRAHA 6, Czech Republic
E-mail: vaniceki@fsv.cvut.cz

Martin Vaníček
Czech Technical University in Prague,
Geotechnical Department
Thakurova 7, 166 29 PRAHA 6, Czech Republic
E-mail: vanicekm@mat.fsv.cvut.cz

Abstract

Understanding the ageing of structures is a very important issue from the point of view of assessing the risk inherent in those structures. Geotechnical structures, of course, have their own specific risks. This paper is focused on the tunnels of the Prague Metro, looked at from various aspects, i.e., geology, construction systems, and the influence of flooding. The section of the tunnels that was selected for monitoring is one of the most affected, and has a large system of cracked segments. However, even for this affected section the monitoring systems, based on macro- and micro-approaches, showed no significant deterioration was taking place. Nevertheless, for long-term monitoring a wireless system for data collection and transfer was installed and implemented. The results so far have been very positive.

Keywords

tunnel, metro, deterioration, ageing, geology, construction, monitoring assessment, MEMS, geophysical, wireless data transfer, metro flooding

1 INTRODUCTION

Recently, the owners of infrastructures have started to become concerned about the life expectancy of engineering structures that were designed for lifetimes of about 100 years and are now beginning to approach such an age. This concern is very much connected with the risk of a sudden collapse of these structures and the consequences of such an occurrence. In this sense geotechnical structures have specific differences compared to other structures, like concrete, steel, timber, masonry, etc. Geotechnical structures include old dams and the protective embankments around settlements. As is evident from these examples, old earth structures have a much longer lifetime than other engineering structures. To simplify the issue we will not touch on the problem of pore-pressure development, which takes place shortly after the end of the construction of earth structures, rather we will consider the long-term behaviour, when the pore pressures are steady with respect to the stress-field changes, due to the construction of the earth structure.

Earth structures are increasing their strength and stability with time, as is clear from the age of the examples mentioned above. However, this is only true if the conditions for the internal and external erosion limit states are fulfilled. In most cases this improvement is given by the strengthening of the inter-particle connections, and in this improvement the composition of the liquid phase plays a significant role. Unfortunately, a change in the chemical composition of the liquid phase can significantly affect the potential risk of an earth-structure collapse. A classic example of such a negative change is the “quick clays” from Norway, where the fresh water washes out the salt that was present during the deposition of the clay layers on the sea bed.

A completely independent problem is associated with the weathering of the surfaces of geotechnical structures, such as the slopes of excavations or tunnels without linings. Here, the most significant role is played by the stress change due to unloading, which can initiate the opening of micro-cracks and start the process of physical weathering. In the case of foundation engineering we do not have any examples of the deterioration of the ground underneath shallow foundations or around deep foundations. The problems of the aging of geotechnical structures are therefore mainly becoming the same as the problems of ageing with other structures, e.g., concrete structures like foundations, retaining walls, and tunnel linings. In this paper we will concentrate on an example of the last of these, the deterioration of the tunnel lining of the Prague Metro. In our case the monitoring is not directed at determining the potential risk of collapse, rather it is to confirm that the tunnel is still in a stable state and to help us determine the appropriate moment to schedule minor repairs in order to significantly extend the expected lifetime of this underground structure. As an example, we can use the approach to this problem mentioned by Soga [1] (see Figure 1).

With underground structures there is always the problem of access, which is leading to the use of remote monitoring based on wireless technology.

2 BRIEF DESCRIPTION OF THE PRAGUE METRO

The design of traffic flow in Prague on two vertical levels started as early as 1898, when a Prague entrepreneur, Ladislav Rott, submitted the first proposal to build an underground railway to improve the traffic connections in the historic district of the city. In 1912–1941 a series of plans for new routes of the underground railway were developed; however, these plans were never implemented (see Figure 2). Starting in 1958, the design of an underground railway using a system of subsurface trams with a subsequent transition to metro trains began to be developed.

In 1967 the final decision to begin the construction of the Prague Metro was made. On 20 January 1969, driving operations on the first underground tunnel were launched, and on 9 May 1974 regular passenger operations began on the first line of the Prague Metro – line C, 6.57 km in length, and with 9 stations. One of the most recent metro sections put into operation was the

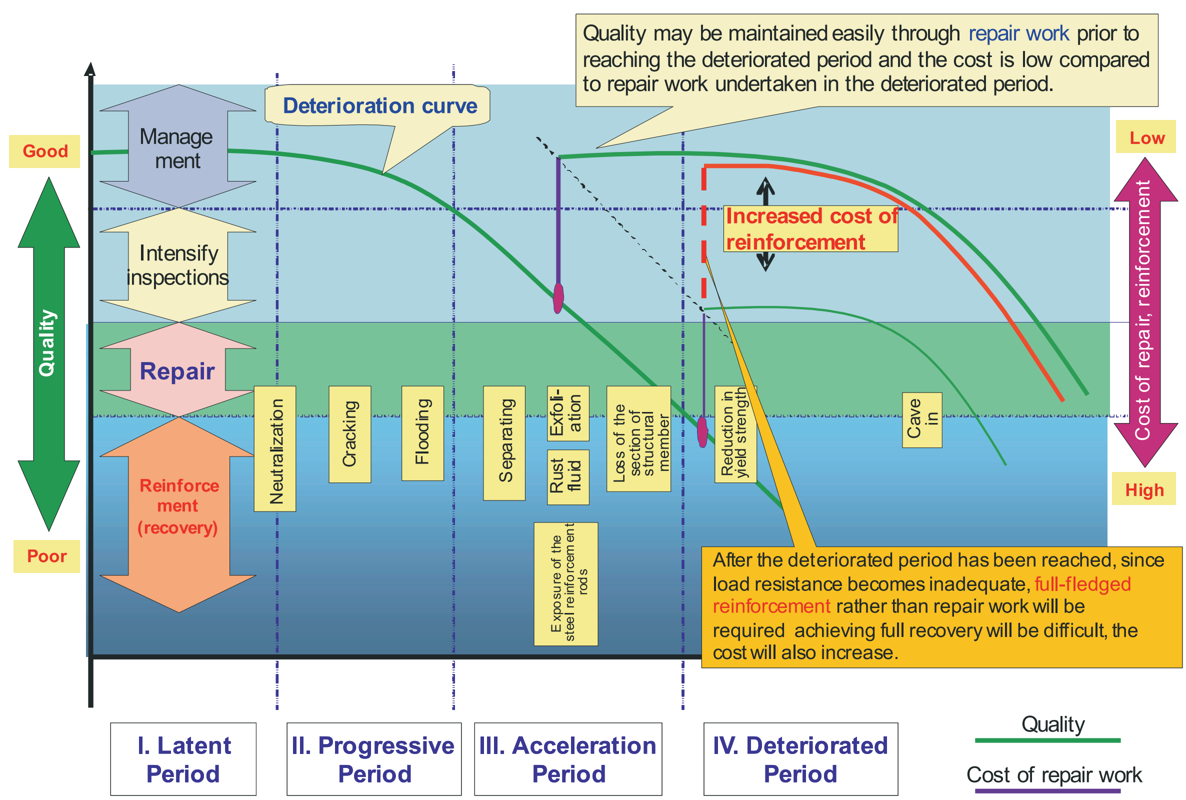

Figure 1. Life cycle of an ageing structure.

extension of line C as far as Ládví Station: two additional stations and a length of 3.981 km. The highlights of this section are the first double-track driven Metro tunnel (Figure 3) and Prague's first single-nave driven Kobylisy Station, which is also the deepest station on line C, being situated 31.5 m below ground.

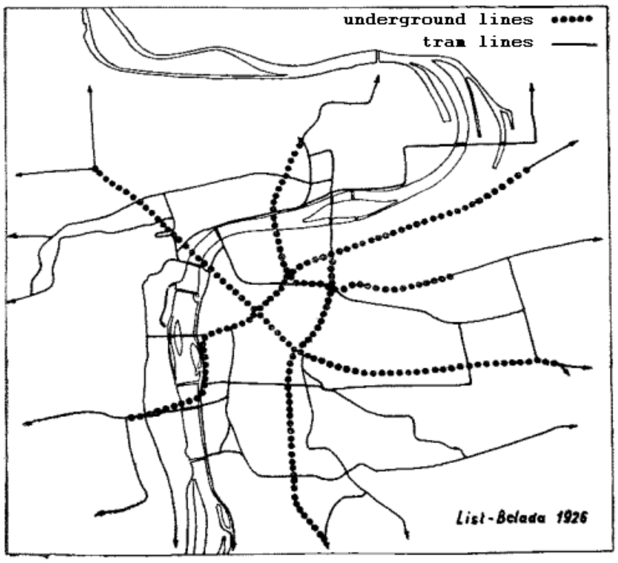

Figure 2. Plan of an underground railway network designed by Vladimír List and Bohumil Bellada in 1926.

The Prague Metro system presently (Jan 2008) operates 3 lines (A, B, C) with 54 stations and a total length of 54.7 km (see Figure 4 on next page). Line A has 13 stations and is 11.0 km long; line B is the longest, with 24 stations and a length of 25.7 km; and line C has 17 stations and is 18.0 km in length.

2.1 GEOLOGY

The area of interest in the vicinity of metro lines A, B and C is predominantly formed by sedimentary rocks from the early part of the Paleozoic era (during the Ordovician period), but also partly from the later part of the Proterozoic era, which are overlaid by soils of quarternary superficial deposits and made ground [2].

2.1.1 Bedrock

The tunnelled sections of the Prague Metro pass through a vast complex of sedimentary rocks of the Barrandien, from the late Proterozoic to the early Paleozoic eras, with the most numerous locations from various formations of the Central Bohemian Ordovician period. The entire succession of strata shows the predominance of clayey, silty-to-sandy shales and siltstones with different physical and mechanical properties and a varying degree of tectonic failure. The bedrock is also rich in sandstone-

Figure 3. Double-track metro tunnel on line C.

Figure 4. Present system of the Prague Metro's lines.

to-quartzite rock types, with the sporadic occurrence of subsurface forms of paleovolcanic activity. The whole area was intensely folded and tectonically deformed. One example is Můstek Station, in the city centre, the point of a prominent tectonic failure – the so-called Prague fault – where clayey-to-sandy shales of Šárka strata and quartzites and siliceous sandstones of Skalka strata are found. This area was subject to intensive tectonic failures, and the rocks are heavily fragmented into chips or cuts. The tunnelling operations here faced many difficulties.

2.1.2 Superficial deposits

Over the whole territory, the bedrock is overlaid by soils of superficial deposits. In the central part of the city, in the flood plains, these are mainly fluvial terrace deposits of the lowest Vltava River terrace benches, which are composed of sands and sandy gravels. Their thickness ranges from 6 to 12 m, and sporadically up to 18 m.

The overlying stratum of the terrace deposits contains Holocene alluvial plain deposits. Predominantly, they take the form of fine sandy, loamy and clayey sediments, at places with organic interlayers and separate horizons of re-deposited sandy gravels. The thickness of this alluvium is generally 1–3 m, and exceptionally up to 8 m.

Outside the flood plains, in the areas now occupied mainly by the outskirts of the city, there are eluvial, deluvial and deluvial-fluvial sediments, consisting predominantly of clayey-to-sandy loams, often with fragments of underlying rock.

A part of the territory is also covered by eolian deposits, reaching up to several metres in thickness, as well as loess and loess-like loams.

Close to the surface of the territory, man-made deposits are often found – backfill, made ground, and the remains of structures – with thicknesses of 1–5 m, and occasionally even greater.

2.1.3 Hydrogeological situation

The hydrogeological situation directly reflects the complex geological composition of the geology of Prague. There are groundwater horizons with distinctively different characteristics of the hydrogeological regime. In the sands and gravels of the lowest Vltava River terraces with considerable pore permeability, there is a continuous horizon of groundwater that can be called alluvial water. In other covering formations, groundwater of the pore type with an unconfined level is found. Another groundwater horizon is found in the bedrock of the predominantly Ordovician sedimentary rock mass. This is mostly a very poorly permeable-to-impermeable medium with fissure permeability. Here, the water also tends to show increased aggressiveness, mainly of the sulphate type.

2.2 CONSTRUCTION OF THE PRAGUE METRO

The tunnelling methods used during the construction of the Prague Metro had to respect the difficult geological conditions of Prague and minimize the impact on the structures on the surface, mainly in the historically valuable parts of the city. The rock was excavated mainly by blasting. The horizontal transport of the spoil was mostly by rail, and the vertical transport made use of winches in the access shafts.

The running tunnels were built using the following technologies:

a) The "Prague" ring tunnelling method with an erector (in the solid rocks),
b) The non-mechanized tunnelling shield (in the soft rocks and soils),
c) The mechanized tunnelling shield TCSB-3 (Soviet made),
d) The NATM method (from the 1980s),
e) The cut-and-cover technique,
f) The immersed tunnel (used for Vltava River crossing at Nádraží Holešovice)

2.2.1 The "Prague" ring tunnelling method

This method used an erector for the mechanical assembly of the lining from cast-iron or reinforced-concrete segments (Figure 5) in the blast-excavated tunnel. The prefabricated lining was activated against the rock mass by injection filling; the protection against water in the reinforced concrete segments was made by sealing injection, and in the cast-iron segments the calking of joints was used.

2.2.2 The non-mechanized tunnelling shield

The excavation of the tunnel made use of a shield with an Alpine roadheader (see Figure 6 on next page). This method also used mechanical assembling of the lining from cast-iron or reinforced-concrete segments. The activation of the tunnel lining and the water sealing of the tunnel was done in the same way as for the "Prague" ring tunnelling method.

2.2.3 The mechanized tunnelling shield TSCB-3

This shield had a full-profile cutting head for the tunnel excavation, and compressed concrete was used as the lining (see Figure 7 on next page). The tunnel was excavated by a tunnelling machine in full profile. The tunnel lining was created with concrete that was placed between the formwork and the excavated rock. The tunnelling

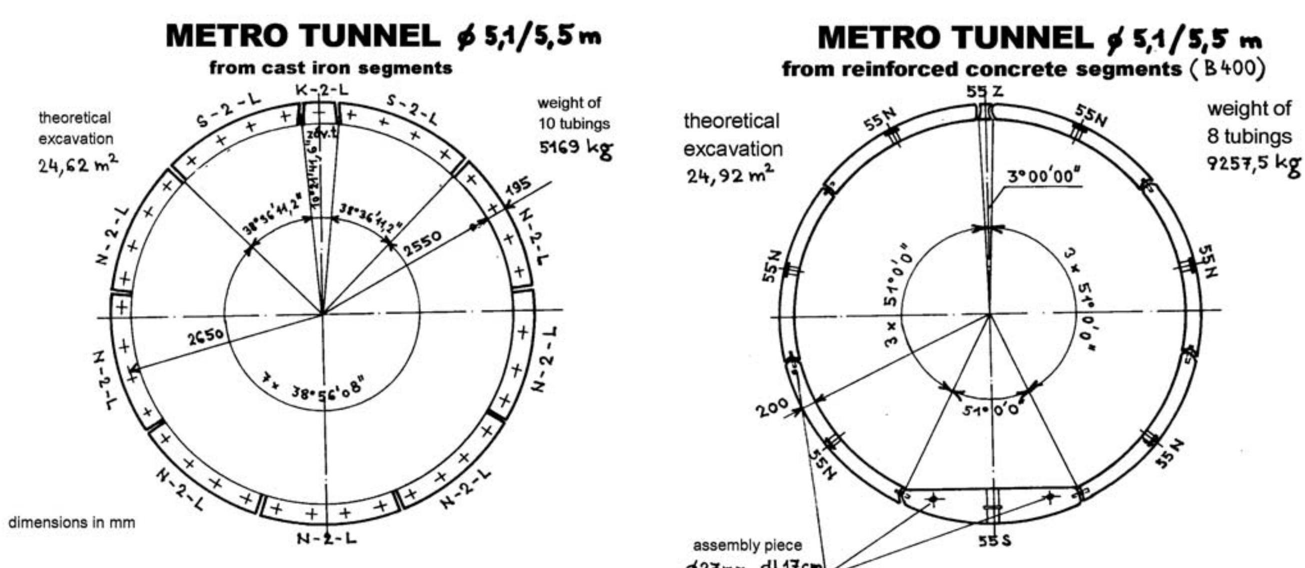

a) b)

Figure 5. Cross-section of the tunnel with a) cast-iron segment b) concrete segment [3].

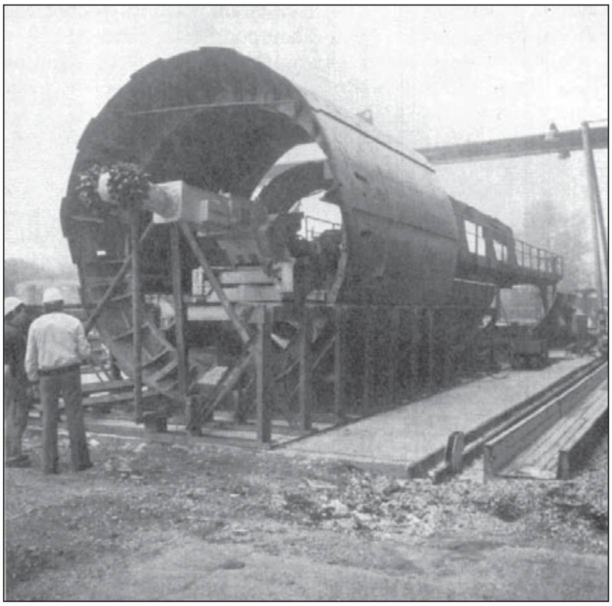

Figure 6. Open shield with roadheader.

machine (shield) was moved forward by pushing the pressing ring, using hydraulic jacks, against the just-concreted lining, which creates a highly compressed concrete tunnel lining.

2.2.4 The NATM method

This method was first used in the 1980s and is typical for a two-shell lining – the primary lining is made from shotcrete and the secondary lining is made from monolithic reinforced concrete, with a sealing in between (see Figure 8).

2.2.5 The immersed tunnel

The basic principle of this technique consists of constructing individual tubes in a dry dock, which was dug in the Troja bank at the location of future tunnels (see Figure 9) [7]. When the concrete structure of the tube was completed, the internal balance tanks and the

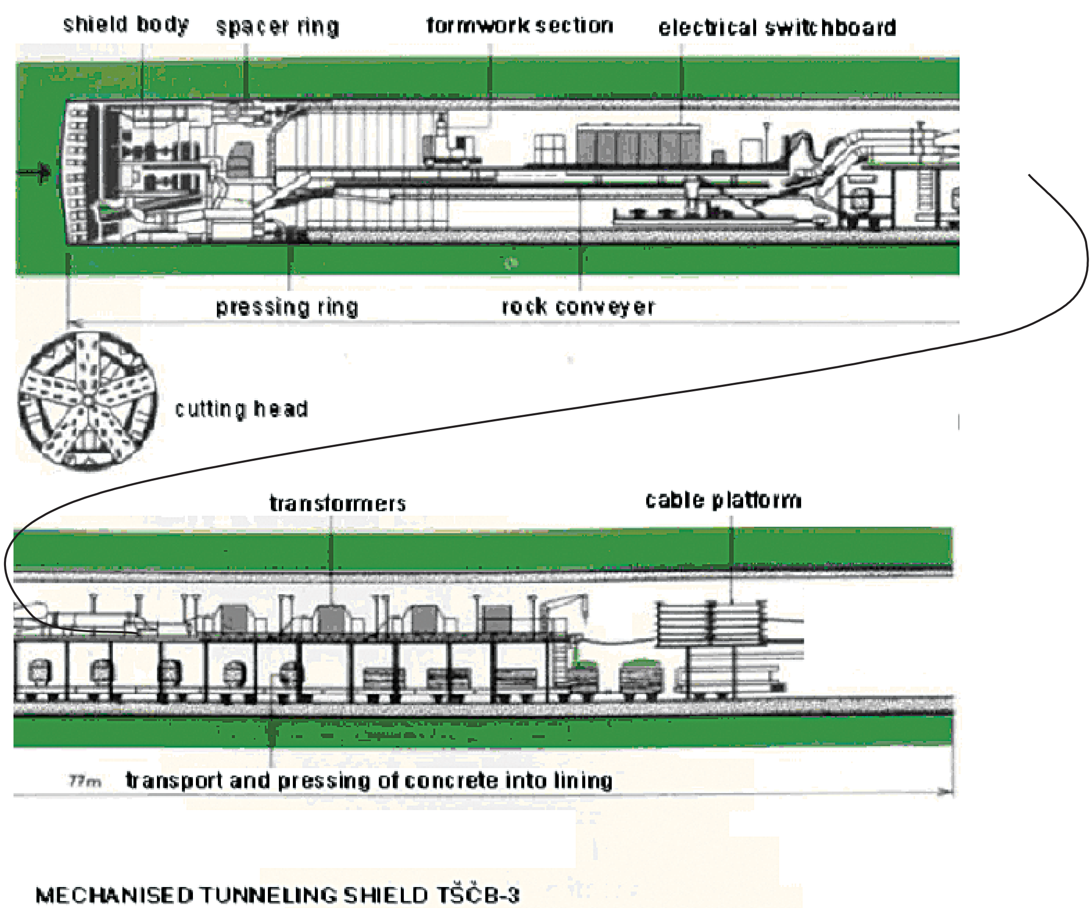

Figure 7. Cross-section of the mechanized tunnelling shield.

Figure 8. The building of the Kobylisy station.

Figure 9. Immersed tunnel – the concrete tube still in the dry dock.

steel bulkheads at both ends were installed. A suspension system was connected to the tubes in the form of anchoring elements cast into the tubes. After the installation of the tunnel outfit the dry dock was then flooded, allowing the shifting of an individual tube into its final position in a trench dug in the river bed. Two tow steel cables anchored on the opposite bank drew the tubes forward. The rear support of the tube, sliding along the track, carried the major part of the weight, and ensured the stability of the whole body. When the support in the Holešovice bank was reached, the tunnel position was stabilized, and then the tunnel was fixed to the river bed by anchoring.

2.2.6 Details of section Vltavská–Nádraží Holešovice

Both tunnel tubes were driven using the "Prague" ring method. During tunnelling an overbreak (approximately 50 m^3) developed under a railway-car repair shop, with a consequent depression in the surface. The hollow space was filled with concrete, but the construction was delayed for 6 weeks.

2.3 THE INFLUENCE OF THE FLOODING IN 2002 ON THE PRAGUE METRO

The first rainfall struck parts of the Czech Republic on 6–7 August 2002, affecting mainly Southern Bohemia, and to a minor extent West and Central Bohemia and Southern Moravia. The second rainfall came between 11 and 13 August 2002. This time the entire territory of Bohemia was struck, and on 13 August there was heavy rainfall mainly in Eastern Bohemia, including the Orlice Mountains and parts of Northern Moravia.

The August flood in the Czech Republic took a relatively unusual course, unprecedented in the past. During a relatively short time, two flood tides were generated.

The rise of the first flood wave on the Vltava River was, to a large extent, eliminated by the reservoirs of the Vltava River cascade, so that the flood flow recorded in Prague reached only a five-year high. At the same time, considerable saturation of the affected territory occurred during this first flood wave, leading to the exhaustion of its retention capacity. This is why the start of the second flood surge was followed by a rapid rise in the water levels on watercourses and in reservoirs. The subsequent flood on the Vltava River was the result of a collision between the flood wave from the Vltava River cascade and the flood wave from the Berounka River. The resulting flood wave on the Vltava River in Prague occurred on 14 August 2002 at 12:00, with a water level of 782 cm and a discharge of 5130 $m^3.s^{-1}$, which is a value corresponding approximately to a five-hundred-year flood. It was the most devastating natural disaster recorded in Prague since 1827 (see Figure 10).

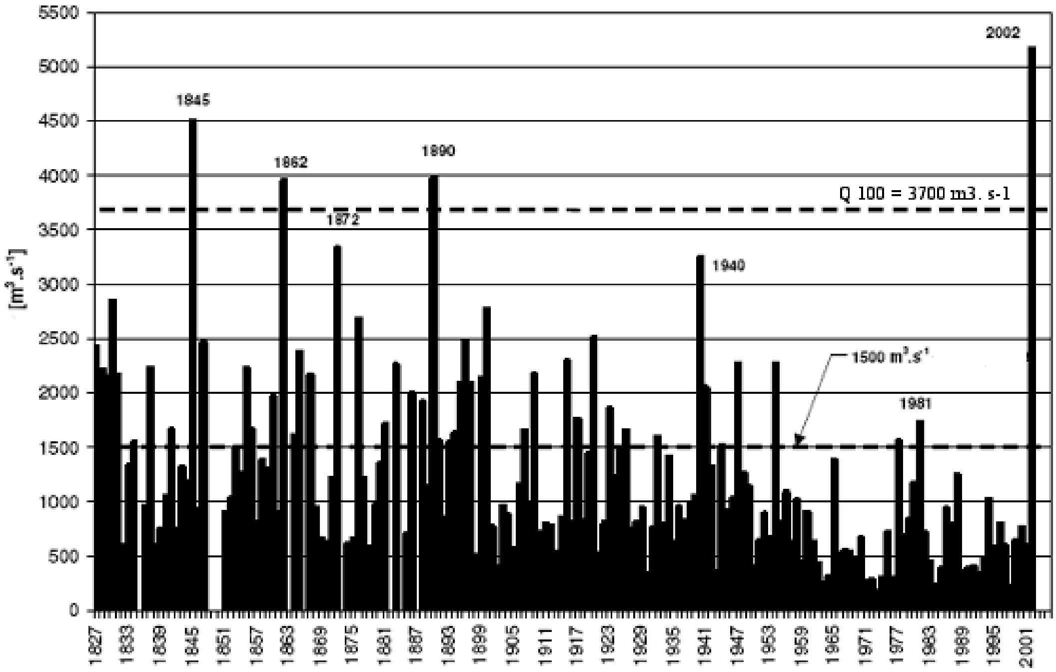

Figure 10. Floods on Vltava River, 1827–2002 [4].

The Prague Metro was flooded for approximately two days, from the evening hours of 13 August 2002 to the afternoon hours of 15 August 2002. The following sections of the Prague Metro were flooded:

Line A – for a length of about 3.8 km, including 4 stations (total operating length of 10.0 km, including 12 stations)

Line B – for a length of about 11.2 km, including 12 stations (total operating length of 25.7 km, including 24 stations)

Line C – for a length of about 2.3 km, including 3 stations (total operating length of 14.1 km, including 15 stations)

At that time (August 2002), the metro had a total of 51 stations, of which 19 were completely flooded (see Figure 11). The total volume of water in the stations and tunnels was estimated to be about 1.2 million m^3.

Figure 11. Submerged metro train in Florenc Station (after some of the water had been pumped out).

The conclusions from the inspections carried out after the events of the flooding, which were part of the investigation into the causes of the flooding, showed that the main structural systems of the metro were not affected by the flood [2]. The only affected systems were the non-structural ones, like floors, partition walls and facings. Also, there was some damage to the steel linings of the ventilation shafts and at localised points that suffered greater levels of water infiltration. During the walkovers the inspection teams also found some older faults, which had not been caused by the floods and which did not affect the serviceability or the stability of the running tunnels. The teams of experts stated that the metro system was, in general, safe for operation.

More details of the history, geology and construction systems of the Prague Metro have been described by Romancov [5].

This flooding accident clearly demonstrated the need for remote wireless monitoring, as the decision about the speed with which the water should be pumped out of the metro tunnels was connected with some uncertainties relating to the safety of the Prague Metro's underground structure.

3 MONITORING THE PRAGUE METRO

The research activity of monitoring the underground structures of the Prague Metro started in the frame of the European research project Micro-Measurement and Monitoring System for Ageing Underground Infrastructures (Underground M^3), with the Engineering Department of Cambridge University as the project leader. The experiences gained during the first monitoring stage from the Prague Metro will be used for metro systems in London, Barcelona and Madrid. As a result, representatives of these metro authorities were also involved in the project, because close cooperation is a necessity when monitoring these tunnels.

After a detailed visual control carried out on several kilometres of the Prague Metro's tunnels, the most appropriate places for locating the instrumentation were selected. Different methods for the monitoring measurements were proposed, agreed on, and are described in more detail below.

The tunnel lining of the Prague Metro is affected by cracking at different locations (see Figure 12). The tunnel section Vltavská–Holešovice at the chainage 18+725 km was selected for the pilot instrumentation as part of our monitoring project. The techniques selected for this pilot consist of traditional macro-scale measurements, geophysical measurements as well as wireless data collection and transfer [8].

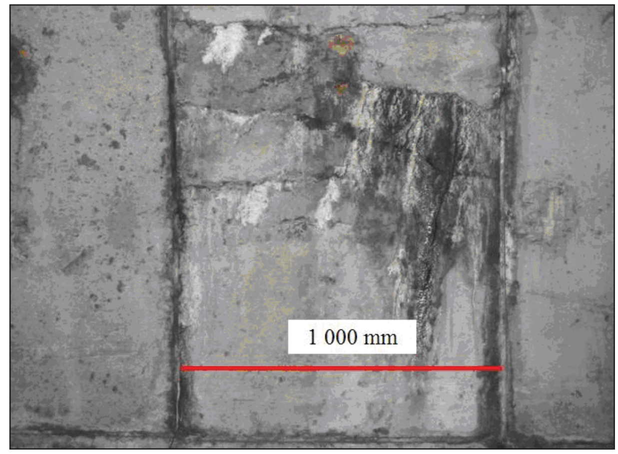

Figure 12. Set of cracks in the tunnel lining on line C.

3.1 MACRO-MONITORING

For the macro-scale measurements we determined the following requirements:

a) The monitoring of the overall deformation of the selected tunnel section should determine whether the development of the deformation is either important or negligible for the characterization of the tunnel lining's behaviour and for the numerical modelling of the stresses' distribution and the ageing of the lining.

b) The monitoring of the lining detail affected by the cracks should determine the crack activity and provide a basis for the cross comparison of the monitoring results on the "macro" and "micro" scales.

The macro-scale instrumentation was designed in two stages (see Figure 13 on next page). Standard methods of monitoring were used in the first stage of the instrumentation. The monitoring was based on convergence type measurements and the application of a portable tilt meter.

For the second stage, Geokon crack-meters were selected because of their long-term stability with respect to the requirements stated in point b), above.

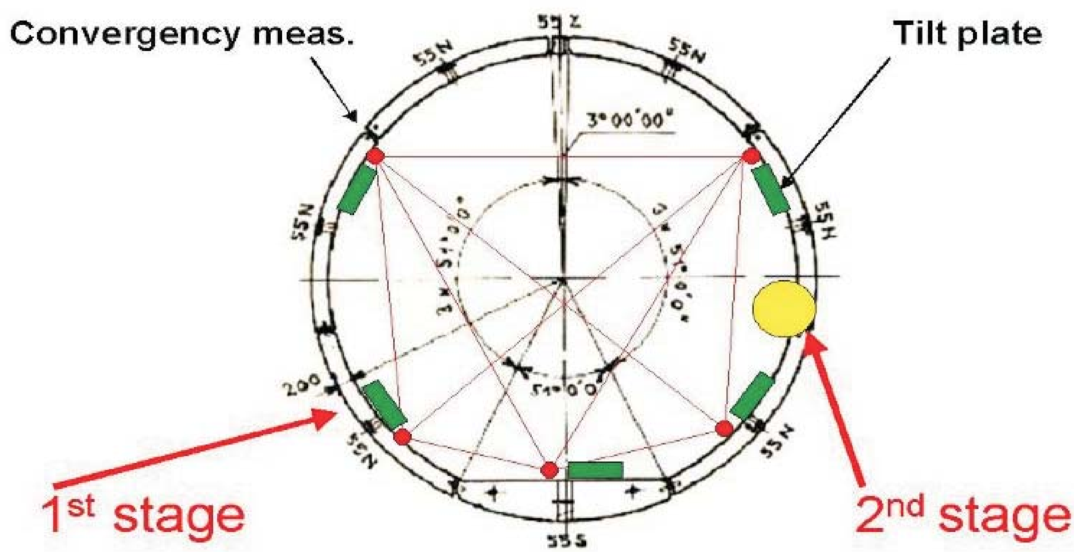

Figure 13. Typical section of the tunnel lining and the placement of bolts and plates (second stage = crack-meters).

To begin the strain monitoring, a segment with a "simple" crack was selected. The instrumentation for the overall deformation monitoring of the lining (stage 1) was completed at the end of 2006. The measurements indicate very small variations in the measured values, mainly due to seasonal variations rather than due to any deformations of the tunnel. The repeatability of the measuring equipment is better than 50μm for the convergence measurements, better than 40 arc seconds for the tilting, and better than 3 μm on the 300-mm base of the crack-meter.

3.2 GEOPHYSICAL MONITORING

3.2.1 In the tunnel

The geophysical systems for determining the structural condition using MEMS (micro-electro-mechanical systems) sensors that are now implemented in the Prague Metro use two different techniques. The first technique is seismic velocity sampling; this is based on measurements of the elastic wave velocity passing through the tunnel lining. The other technique is an analysis of the time-development frequency spectra of the structure's vibrations under traffic loads. For seismic velocity sampling we used MEMS accelerometers that are attached to fixed points on the lining in a 200 x 200 mm grid. Figure 14 shows a view of the final arrangement of the monitoring profile. The accelerometers measure the response to the other fixed points' excitation. The damping of the signal represents a potential gap or crack within the lining. In this way it is possible to determine the locations of cracked zones of different sizes. These measurements are carried out during night inspections at more or less regular intervals, and the changes in the responses are compared so potential micro-crack development can be detected. The disadvantage of this method is the need for physical access to the measuring location in order to take the measurements, because there is no automatic system for the excitation of the lining at the fixed points. As the fixed points on the measurement profile were installed in the region of visible cracks, we will be able to monitor the changes with time and hence the rate of deterioration of the structure.

An example of the successful use of this technique, for the location of weak zones in the old masonry tunnel lining of the sewerage system in Prague, was presented by Macháček and Barták [6].

The analysis of the time-development frequency spectra of the structure vibrations under traffic load uses geophones installed in the Prague Metro's lining measurement profile (see Figure 14). The geophones measure the development of changes in the frequency spectrum and the damping parameters of the tunnel lining with time. These measuring points are inaccessible while the tunnel is in operation, due to traffic loads;

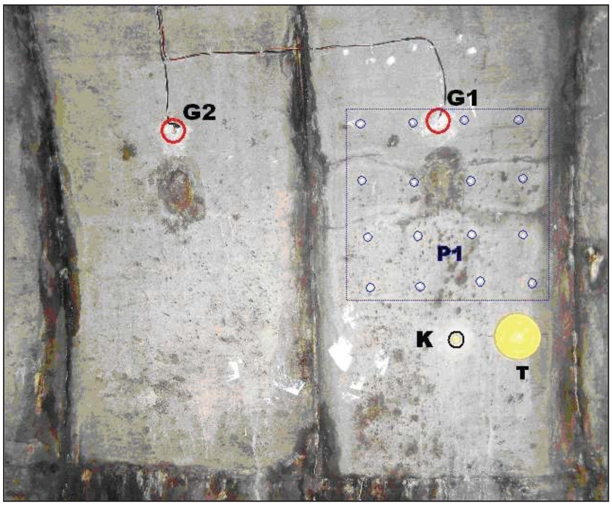

Figure 14. Final arrangement of the monitoring profile.

G1	=	monitoring geophone
G2	=	reference geophone
P1	=	field for seismic velocity sampling
K	=	convergence bolt
T	=	tiltmeter plate

therefore, a remote data-collection system is required. For the time being we are using long cables running from the measurement point to the station, where it is possible to gather the data instantaneously during the metro's operation using a high-sensitivity digital oscilloscope. Using this technique we want to obtain a direct relationship between the measured data and the deterioration status of the lining.

3.2.2 In the laboratory

In parallel with the monitoring in the Prague Metro's tunnel we also started to study the dynamic response accelerograms of a reinforced concrete slab in laboratory fatigue tests (see Figure 15).

We measured the acceleration of a single point movement at one-third of the span of the specimen's supports. Our main concern was the development of changes with time in the course of deformations, as there is no doubt that the specimen must gradually lose its elasticity with the increasing number of loading cycles it has undergone. As the laboratory test is currently only half way through, there is not yet enough data to process and determine the overall degree of deterioration of the slab. However, there are results from accelerometers that indicate some ageing of the tested member, and the results from the frequency spectra analysis indicate some fatigue development. At the time of writing there is no visible macroscopic failure whatsoever on the specimen.

3.3 WIRELESS MONITORING

Another part of the monitoring project is to deploy a wireless system for data collection and transfer from the tunnel to the monitoring office. The aim of the wireless system is to reduce the amount of wiring in the tunnels, in order to collect the data from monitoring points and also because the wires in the tunnels are affected by the strong electromagnetic fields that are present there. Another advantage is that the system is redundant, and so even if some points fail the system will continue to work. It is also possible to insert additional monitoring points if this will be required in the future.

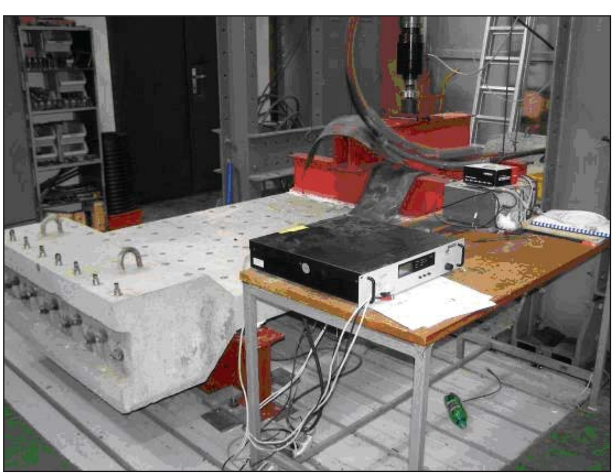

a)

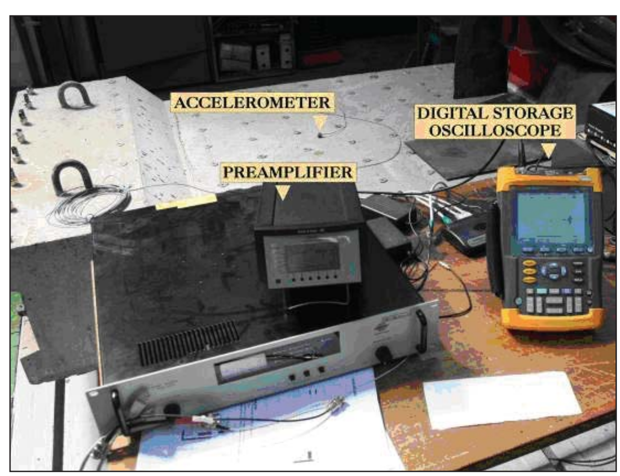

b)

Figure 15. The experimental arrangement (a) and the measuring line (b).

Up to now we have installed a pilot network of wireless points with temperature and light sensors in the vicinity of a metro station. The wireless monitoring points are configured around Intel motes working on a ZigBee platform (see Figure 16). This pilot installation serves several purposes, including being able to define the optimum distances between points to be able to guarantee the redundancy in the system for safe data collection at real locations. Another reason for the pilot is to determine if the system will interfere with wireless systems already being deployed in the Prague Metro for signalling purposes. We discovered during the initial stages that the optimum distance for the conditions in the Prague Metro's tunnels is about 15m, and that from the reliability point of view we should employ at least 2 to 3 motes in every profile along the tunnel.

Last, but not least, is the issue of how to wirelessly transfer the data from the tunnel to the monitoring office, in order that the data can be available in real time. The wireless monitoring system has a gateway in an embedded PC that is connected to the internet and hence to the monitoring office via a multi-protocol router. The router and the gateway are placed in a single box that is fixed to the tunnel lining. For the time being the transfer system is based on the mobile-phone GPRS platform, as the stations in Prague are covered by the mobile-phone signal and there is a plan to cover the tunnels in the near future. This system was not very stable at the beginning, mainly because we tried to find the longest possible distance from the station, where we could still achieve a good and reliable connection. We discovered – which should not have been a surprise – that the GSM signal is also affected by the electromagnetic fields in the running tunnels. For this reason we have chosen a location closer to the station and better antennas have been selected.

4 A BRIEF ASSESSMENT OF THE MOST UP-TO-DATE RESULTS

Our monitoring showed that even for a highly cracked lining the behaviour is very stable, as there we monitored mainly just the seasonal effects on the lining, more so than anything else. The geophysical measurements from the tunnel showed, in combination with the laboratory measurements, that the lining is in a stable state and is not approaching the acceleration period (see Figure 1). We can also say that the wireless approach to monitored data collection and transfer selected for the Prague Metro seems to be both reliable and useful.

Our experience leads us to believe that in the near future we will be able to achieve results on the micro-scale deformation measurements in the range of 10^{-4} mm and then be able to use those results for a comparison with numerical modelling using creep models and the theory of micro-crack development for concrete.

5 CONCLUSIONS

This paper is a reaction to the demands of infrastructure owners who want to determine the quality of their structures and the potential risks posed by the aging of those structures. Three different approaches to the evaluation of this problem, applied to the Prague Metro, are described in detail. Firstly, we have direct deformation measurements; secondly, we have geophysical methods of monitoring that utilise the vibration response to train passes and manual excitation, and, thirdly, we have wireless technology for data collection and transfer. The

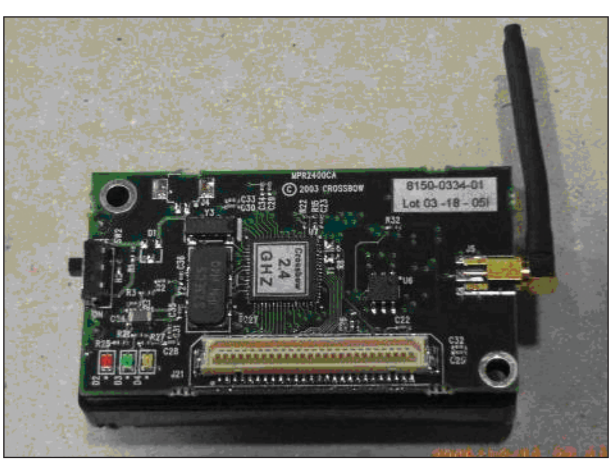

a)

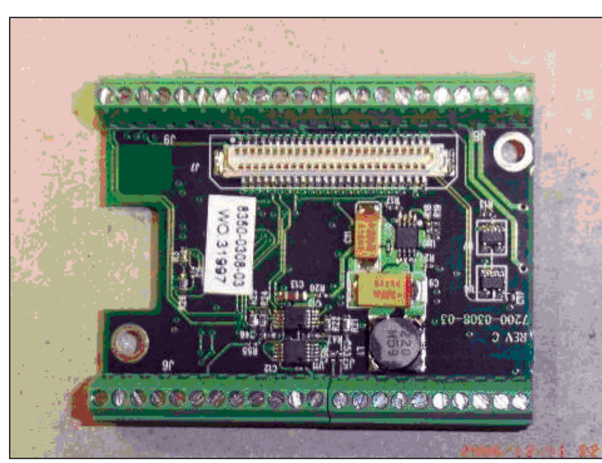

b)

Figure 16. Main board of the wireless mote (a) and the circuit board of the A/D converter.

latest results indicate that the Prague Metro's tunnel lining is in very good condition; nevertheless, some additional features should be added for subsequent long-term monitoring.

ACKNOWLEDGEMENT

The authors wish to express their gratitude to the Grant Agency of the Czech Republic for research project GA 103/06/1257 "Research of Ageing of Underground Infrastructures with the Help of Micro-measurements and Monitoring" for allowing us to prepare and present this paper.

REFERENCES

[1] Soga, K. et al (2005). Micro-Measurement and Monitoring System for Ageing Underground Infrastructures (Underground M^3). Project proposal, unpublished, Cambridge.

[2] Chamra, S. (2006). Flooding of the Prague metro during the August 2002 floods. IAEG2006 – *Engineering geology for tomorrow's cities*, Nottingham, Paper No 393, The Geological Society of London.

[3] Bucek, M. and Barták, J. (1989). Underground structures. Czech Technical University Press, Prague (in Czech).

[4] Czech Hydrometeorological Institute (2002), generally available data on web pages.

[5] Romancov, G. (2003). Geotechnical issues of metro construction in a historic built-up area (Experience gained during the preparations and the construction of the Prague metro in 1966-1985). *Proc. XIIIth ECSMGE*, Vaníček et al. (eds), ČGtS, Vol. 4, 246-264.

[6] Macháček, J. and Barták, J. (2003). Prague, Old Town Square: Sewerage Coupling Chamber. Application of geophysical methods in building structures diagnostics. *Proceedings of 9th European Meeting of Environmental and Engineering Geophysics*, Mareš and Pospíšil (eds), CAAG, P-016/1-5.

[7] Vítek, J.L. (2003). Launched metro tunnels under the Vltava River. *Proc. XIIIth ECSMGE*, Vaníček et al. (eds), ČGtS, Vol. 4, 295-312.

[8] Vaníček, M., Vaníček, I., Pruška, J., Bubeníček, M., Jirásko, D. and Soga, K. (2007). Prognosis of underground structures deterioration based on in-situ measurements. Proc. WTC 2007, *Underground space the 4th dimension of metropolises*. Barták et al (eds). Balkema, Vol. 2, 933-938.

DINAMIČNE LASTNOSTI POLŽARICE IZ LJUBLJANSKEGA BARJA

BOJAN ŽLENDER in LUDVIK TRAUNER

o avtorjih

Bojan Žlender
Univerza v Mariboru,
Fakulteta za gradbeništvo
Smetanova 17, 2000 Maribor, Slovenija
E-pošta: bojan.zlender@uni-mb.si

Ludvik Trauner
Univerza v Mariboru,
Fakulteta za gradbeništvo
Smetanova 17, 2000 Maribor, Slovenija
E-pošta: trauner@uni-mb.si

izvleček

Na vzorcih polžarice iz jugozahodne lokacije Ljubljanskega barja je bila izvedena raziskava njenih dinamičnih lastnosti. Izvedeni so bili ciklični triosni preizkusi. V preiskavi so bili spreminjani pogoji: začetna efektivna napetost (50, 100, 150 kPa), količnik por (2.1 do 1.2) in faktor ciklične obremenitve CSR (med 0.1 in 1). Med posameznim preizkusom so bile merjene časovne spremembe napetosti, deformacij in pornega vodnega tlaka.
Parametri fizikalnih lastnosti so podani kot funkcije zgoščenosti polžarice, torej volumenske deformacije, gostote, poroznosti ali vlažnosti. Kemični sestav delcev in mineralna sestava ter zrnatost polžarice se zaradi zgoščevanja ne spremenijo. Delež mikroorganizmov v polžarici je zelo majhen in ga lahko smatramo kot konstanto. Specifična površina je neodvisna od zgoščevanja. Nekateri parametri fizikalnih lastnosti polžarice (prostorninska teža, vlažnost, poroznost) se spreminjajo v odvisnosti od zgostitve, kar lahko izrazimo s splošno znanimi odnosi. Spremembe vodoprepustnosti, konsolidacije in stisljivosti so nelinearno odvisne od sprememb poroznosti, pri začetnem zgoščanju so spremembe očitne, z nadaljnim zgoščanjem se njihove spremembe manjšajo. Spremembe mehanskih parametrov kot so Youngov modul, Poissonov količnik in strižni kot, pa so pri pri začetnih spremembah poroznosti neizrazite in skoraj linearne, pri nadaljnem zgoščanju pa se njihove spremembe večajo. Vpliv zgoščanja na Poissonov količnik je skoraj linearen.
Polžarica je kljub židkosti in neugodnim fizikalnim lastnostim ter nizkim parametrom trdnosti dokaj odporna na pojav likvifakcije. Se pa že v začetnih ciklih obremenjevanja pojavijo velike specifične deformacije. Tudi porni vodni tlaki že po nekaj ciklih izrazito narastejo, vendar pri manjših vrednostih CSR praviloma ne dosežejo efektivne celične napetosti. Dušenje narašča eksponentno z deformacijo. Zaradi velikih deformacij pa praviloma že po nekaj ciklih doseže maksimalno vrednost in zatem upade na neko asimptotično vrednost. Maksimalna in asimptotična vrednost dušenja se s spremembo poroznosti polžarice minimalno spremenita. Na strižni modul vpliva zgoščevanje posredno, saj je le ta izražen kot funkcija strižne deformacije. Deformacija je manjša pri gostejšem materialu in večja z večanjem CSR. Za različne vrednosti začetne efektivne napetosti in poroznosti polžarice so določene deformacijske in porušne ovojnice tako, da so podane vrednosti CSR pri katerih je po nekem številu ciklov (npr. 10) dosežena določena deformacija. Kot mejna vrednost je izbrana dvojna amplituta osne deformacije velikosti 5%. Podobno so podane ovojnice za različna stanja pornega tlaka in za mejno stanje, ko razmerje naraščajočega pornega tlaka in efektivne celične napetosti doseže vrednost 1.
.

ključne besede

polžarica, ciklični triosni preizkus, poroznost, vodoprepustnost, konsolidacija, Youngov modul, strižni modul, koeficient dušenja, Poissonov količnik, strižni kot

THE DYNAMIC PROPERTIES OF THE SNAIL SOIL FROM THE LJUBLJANA MARSH

BOJAN ŽLENDER and LUDVIK TRAUNER

About the authors

Bojan Žlender
University of Maribor,
Faculty of Civil Engineering,
Smetanova 17, 2000 Maribor, Slovenia
E-mail: bojan.zlender@uni-mb.si

Ludvik Trauner
University of Maribor,
Faculty of Civil Engineering,
Smetanova 17, 2000 Maribor, Slovenia
E-mail: trauner@uni-mb.si

Abstract

A series of cyclic triaxial tests was performed on snail-soil samples with different porosities. The cyclic loading was performed with a Wykeham Farrance cyclic triaxial system. The investigation was based on a series of tests in which the following conditions were varied: the initial effective pressures (50, 100, and 150 kPa), the void ratio after consolidation (2.0–1.2) and the cyclic loading expressed by the cyclic stress ratio CSR (0.1–1.0). Measurements were made of the stress, the deformation and the pore-water pressure.

The results of the tests show that interdependency exists between the geomechanical characteristics and the porosity. These relationships can be expressed as functions of the density, the porosity or the water content. It is evident from the results that the changes in the coefficient of permeability, the coefficient of consolidation, and the coefficient of volume compressibility are non-linear with respect to the changes in the porosity. However, the changes at high porosity are much greater than the changes at low porosity, and the changes of the mechanical parameters, such as the Young's modulus, Poisson's ratio, and the friction angle, are indistinct and almost linear at lower changes of porosity, and after that become non-linear.

The initial void ratio e is extremely high and the snail soil is liquid after consolidation; a volume strain of ε_{vol} > 16 % is needed for the plastic limit state.

The chemical and mineral composition, the particle size distribution and the remains of micro-organisms in the snail soil are constants. In addition, the specific surface is independent of the porosity and the density or unit weight, the porosity and the volume strain are in the well-known correlation.

The performed cyclic triaxial tests show the dynamic characteristics of the snail soil and the influence of the porosity on the cyclic loading strength. The snail soil was recognized as a highly sensitive material. A large strain appears after the initial cycles. The pore pressure, increases already during the first cycle, to the hydrostatic part of the cyclic loading, or more (depending on CSR).

The damping ratio increases exponentially with strain, after some cycles it reach its maximum value, and after that it decreases to the asymptotic value. The reason for such behaviour is the large deformation. The maximum and asymptotic values of the damping ratio are a changed minimum with a void ratio. There is obviously no influence of the porosity on the damping ratio.

The shear modulus is described in relation to shear strain. The increasing of the pore pressure is independent of the porosity until it reaches some value of the pore-pressure ratio (>0.7). Similarly, the increasing of the shear strain becomes dependent on the void ratio until it reaches some particular value of the shear strain (>3%).

The deformation and failure lines for the different porosities are determined from the relationship between the shear stress and the effective stress at some shear strain, after 10 cycles.

The relationships between the shear stress and the effective stress at some value of the pore-pressure ratio are expressed in a similar way.

Two kinds of criteria were used to determine the triggering of liquefaction during the cyclic triaxial tests: first, when the pore pressure becomes equal to the effective confining pressure, and, second, when the axial strain reaches 5% of the double amplitude.

Keywords

snail soil, cyclic triaxial test, porosity, permeability, consolidation, Young's modulus, shear modulus, damping ratio, Poisson's ratio, friction angle

1 INTRODUCTION

The Ljubljana marsh is located in the south of Ljubljana, at an elevation of 287–290 m above sea level, and covers a surface of 163 km^2. It is a wide tectonic sink that was formed two million years ago by a gradual depression of the area. Consequently, the local rivers deposited huge amounts of sediments there, inundating the entire marsh basin at the same time. The geological structure of the Ljubljana marsh has been studied by numerous experts. The oldest geological documents go back to the middle of the 19th century, when the first geological map of this region was drawn. Later, several other studies were performed, and today the geological structure of the marsh is well investigated. The surface layer is composed of peat with a thickness of 1–9 m. The depth of the peat is nowadays significantly smaller than in the past, due to the intensive excavations in the first half of the 20th century. Below the peat layer, there is a layer of snail soil, with a thickness of a few metres at the borders to more than 10 m in the centre of the marsh. The snail-soil layer is distinctly porous, saturated with water, and of a low bearing capacity. There are clay and sandy-gravel layers below the snail-soil layer. A layer of rocks starts at a depth of some 10 m. Ground water is located immediately below the surface.

The first detailed investigation of the rheological properties of the snail soil was performed in the Laboratory of Soil Mechanics at the Faculty of Architecture, Geodesy and Civil Engineering of the University of Ljubljana [1]. A similar investigation was later repeated in the Laboratory of Soil Mechanics (LSM), Faculty of Civil Engineering of the University of Maribor [2].

Three years ago, within a research project [3], the investigation of snail soil was repeated and upgraded. An investigation of the mineralogical and physical characteristics, as well as of the geomechanical characteristics depending on the physical characteristics was made [4]. This article briefly presents the research performed and the influence of snail-soil density on the geomechanical characteristics. The density of the snail soil was increased by draining and consolidation. It is described by the volume deformation and higher density or by its porosity and water content. A short review of the snail-soil investigation in natural and different density states was made. The basic investigation and the tests with static and cyclic loading were performed. The results of the influence of snail-soil density on its physical properties and the static and dynamic strength parameters are presented. The parameters are presented as functions of the density, the porosity, the volume deformation and the water content.

2 THE CHARACTERISTICS OF SNAIL SOIL

A set of samples was taken from the southwest region of the Ljubljana marsh. The sampling took place in a region of 3 m x 3 m at a depth of 3 m. The ground was excavated to a depth of 2.5 m and a thin-walled tube sampler was forced into the ground. Samples with a diameter of 100 mm and a height of 300 mm were immediately packed after sampling and, except for the stress level; this prevents any change in the physical properties. The ground-water level was less than 1 m under the surface in the region of the sampling.

The visual appearance of the snail-soil samples was tested with a QUANTA 200 3D environmental scanning electron microscope at the Centre for Electron Microscopy at the University of Maribor. The electron microscope is equipped with a system of double jets, i.e., electronic and ionic. Photographs were taken of the wet samples, and different blow ups were made. Some photographs of dry samples, minerals in crystallized form, and the remains of micro-organisms in the snail soil were also developed.

The specific surface of the snail soil was determined at the Chemistry Institute, Ljubljana, using the five-point BET method. The experiment involved the adsorption of liquid nitrogen with 99.9% purity and a temperature of 77K. The measurements were performed using the automatic TriStar 3000 gas-adsorption analyzer, produced by the Micromeritics Instrument Corporation, Norcross, U.S.A. The results of the test showed that the snail soil has a specific surface $A_s = 5.03 \pm 0.03$ m^2/g.

The chemical composition of the snail soil (Fig. 1) was determined at the Centre for Electron Microscopy at the University of Maribor. Their SIRION scanning electron microscope is equipped with an Oxford INCA 350 energy-dispersive spectrometer (EDS).

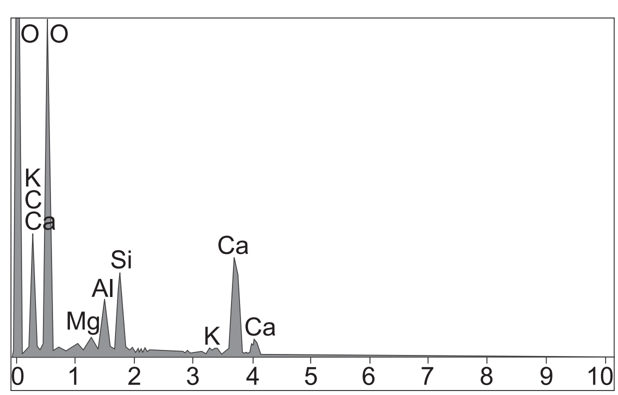

Figure 1. Chemical composition of the snail soil.

The mineral composition was determined in the Laboratory of the Geological Survey of Slovenia. The samples were scanned using the X-ray diffraction technique (XRD) with a Philips PW 3710 difractometer, a goniometer 1820, an automatic divergence slit and a curved graphite monochromator, operating at 40 kV, 30 mA with CuK_α radiation and a Ni filter. The snail soil was composed of 87% calcite, 7% kaolinite, 4% muscovite and 3% quartz.

The physical characteristics shown in Table 1 indicate that the snail soil is saturated in nature, highly porous and almost liquid.

Table 1. The physical characteristics of snail soil.

Soil property	Symbol	Unit	Value
Plastic limit	w_P	%	37
Liquid limit	w_L	%	60
Plasticity index	I_p	%	23
Consistency index	I_c	-	-0.65
Liquidity index	I_L	-	1.65
Density of solid	ρ_s	g/cm^3	2.70
Dry unit weight	γ_d	kN/m^3	0.88
Degree of saturation	S_r	%	100

The parameters shown in Table 1 are constants. With draining and consolidation the density (unit weight), water content and void ratio are changed. The initial values (in the natural state) are shown in Table 2.

Table 2. The natural physical properties of snail soil.

Soil property	Symbol	Unit	Value
Water content	w_0	%	75
Unit weight	γ_0	kN/m^3	15.5
Void ratio	e_0	-	2.1

The grain size distribution of the snail-soil sample was determined using a Fritsch Laser Particle Sizer Analysette 22 at the Laboratory of the Geological Survey of Slovenia. The results of the grain size measurement analysis show that this snail soil falls within the range of 90% silt with respect to its granulometrical structure. The amount of clay particles is less than 10%, and there are almost no sandy particles in the snail soil.

The investigation of the compressibility was performed in the LSM. The triaxial consolidation tests were performed at different effective stresses σ_0'. The consolidation parameters of the natural snail soil are given in Table 3. The values of the consolidation parameters change with a lower porosity, and the parameters can be expressed as functions of the porosity.

Table 3. Consolidation parameters of natural snail soil.

Soil property	Symbol	Unit	Value
Consolidation coefficient	c_v	m^2/year	2.8
Coefficient of volume compressibility	m_v	kPa^{-1}	$1.0–1.5 \cdot 10^{-3}$
Coefficient of soil permeability	k	m/s	$2 \cdot 10^{-9}$
Secondary compression ratio	C_α	-	0.002

The strength parameters were determined in a series of triaxial tests. The parameters of the natural snail soil are given in Table 4. The values of the parameters can also change with a lower porosity, and they can be expressed as functions of the porosity.

Table 4. The strength parameters of natural snail soil.

Soil property	Symbol	Unit	Value
Cohesion	c	kPa	0
Friction angle	φ	°	21
Compression modulus	M_c	kPa	700-1000
Poisson's ratio	ν	-	0.4

3 EXPERIMENTATION

The following tests were performed:

- Basic investigations: visual appearance, remains of micro-organisms, specific surface, chemical and mineral composition, and physical characteristics of snail soil.
- Standard oedometer tests.
- Direct shear tests.
- Static triaxial tests: consolidated drained and undrained shear tests were performed using the Wykeham Farrance triaxial testing device.

The following strength parameters were calculated: the coefficient of permeability k, the coefficient of consolidation c_v, the coefficient of volume compressibility m_v, the compression modulus M_c, the Young's modulus E, the shear modulus G, and the Poisson's ratio ν.

The cyclic loading was performed on a Wykeham Farrance cyclic triaxial system. The basic set-up comprises:

- a load frame, capacity 100 kN;
- a triaxial pressure cell for specimens;
- a hydraulic press with electro-mechanical equipment;
- automatic hydraulic equipment and connections;
- measuring and recording equipment;
- a control and data-acquisition system;
- computer hardware and software;
- de-air watering apparatus, reservoir for de-aired water, compressor, and air-dryer.

The tests were performed under undrained conditions ($\nu = 0.5$) for a particular confining stress σ_0'. The tested specimens were solid cylinders, 7.0 cm in diameter and 14.0 cm in height. A total of sixty-two cyclic triaxial tests were performed. The investigation was based on a series of tests in which the following conditions were varied:

- the void ratio after consolidation … $e_c = 2.0–1.2$
- the initial effective pressures … $\sigma_0' = \sigma'_{3c} = 50, 100, 150$ kPa
- the cyclic loading (deviator stress) … σ_d (t)
- the cyclic stress ratio … CSR = 0.1–1.0

The following pressures were measured during the test:

- the cell pressure … σ_{3c} (kPa)
- the back pressure … u_b (kPa)
- the pore water pressure … u_w (kPa)
- the axial stress in compression … σ_z (kPa)

Measurements of the axial and volume deformations ε_z (%), ε_r (%), ε_v (%) were also taken. In the undrained tests $\varepsilon_v = 0$.

Two kinds of criteria were used to determine the liquefaction triggering during the cyclic triaxial tests: the pore pressure becoming equal to the effective confining pressure, and the axial strain reaching 5% of the double amplitude.

The following steps were observed during the testing: the preparation of the sample, the procedure for the apparatus, the performance of the test, and the interpretation of the obtained results. The investigation included drained and undrained stress-oriented three-axial tests according to the following phases: saturation, consolidation, and static loading.

In the first phase the saturation was tested by determining the coefficient $B = d_u/d_\sigma > 0.96$. This was a relatively short-term phase because of the saturation in the natural state.

The saturated sample was consolidated at the selected effective isotropic consolidation stress σ'_{3c} . The effective isotropic consolidation stress is expressed as the difference in the cell pressure σ_{3c} and the back pressure u_b.

Static loading was performed so that the sample was loaded with the selected compression $d\sigma_{3c}$ or the axial stress $\sigma_a = \sigma_z$.

The following dynamic strength parameters were calculated: the Young's modulus E, the shear modulus G, and the damping ratio ζ. An investigation of the influence of density (in effect, porosity) on the increase in strain and pore pressure was performed.

4 BASIC CHARACTERISTICS

The geomechanical properties of snail soils with different porosities were determined. The snail soil was saturated and treated as a two-phase material (particles and pore water). The chemical and mineral compositions were constant with density, only the volume of water in the pores was changed. The particle size distribution and remains of micro-organisms in snail soil are also constants. In contrast, the specific surface is independent of porosity.

The visual appearance of the snail-soil samples was only tested in the natural state and after static loading.

The parameters of the physical characteristics (Table 1) are constants. The density ρ or the unit weight γ, the void ratio e and the volume strain ε_{vol} are in the well-known correlation. The initial void ratio e_0 is extremely high and the snail soil is at the liquid limit state.

5 STATIC LOADING BEHAVIOUR

The results of previous investigations [4] have shown the relationship between the permeability coefficient k and void ratio e_c. This relationship can be expressed as follows:

$$k(e) = 4 \cdot 10^{-11} \cdot e_c^{5,50} \qquad (1)$$

Equation (1) is similar to Eq. (2), which was previously proposed by Dolinar and Žnidaršič for fine-grained soils [5].

$$k(e) = \alpha \cdot e^{\beta} \qquad (2)$$

In Eq. (2) α and β are soil-dependent coefficients.

We can express in a similar way the relationships for the coefficient of consolidation c_v vs. the void ratio e_c. We obtained the expression for the coefficient of consolidation c_v (m^2/s):

$$c_v(e) = 3 \cdot 10^{-8} \cdot e_c^{1,46} \qquad (3)$$

The relationship of the coefficient of volume compressibility m_v (kPa^{-1}) vs. the void ratio e_c is expressed in a similar way.

$$m_v(e) = 9 \cdot 10^{-5} \cdot e_c^{3,5} \qquad (4)$$

An insufficient number of tests were performed to determine the relationship between the strength parameters and the void ratio, and therefore the results were unreliable. The strength did not increase substantially with the decreasing porosity, in fact a greater difference can only be seen for the larger changes of porosity. The relationship between the Young's modulus E (kPa) and the void ratio e_c can be expressed as:

$$E(e) = 7700 \cdot e_c^{-3,15} \qquad (5)$$

The ratio between the Poisson's ratio ν and the void ratio e_c is almost linear. The value of the Poisson's ratio is $\nu = 0.4$ at a void ratio of $e_c = 2.0$, and it decreases to a value $\nu = 0.37$ at the plastic limit (the void ratio $e = 1.6$).

The same is true for the shear properties. We can see that they increase almost linearly for smaller changes of the void ratio. The relationship between the friction angle φ (°) and the void ratio e_c is expressed as:

$$\varphi(e) = 39,58 \cdot e_c^{-0,92} \qquad (6)$$

6 CYCLIC LOADING BEHAVIOUR

The saturated specimens were consolidated to a particular effective isotropic consolidation stress σ'_0, expressed as the difference between the cell pressure σ_0 and the back pressure u_b.

The cyclic loading in the undrained conditions was performed with a particular frequency f and an axial cyclic stress σ_d. The axial loading σ_d is a deviator component of the stress, and it has a sinusoidal form with respect to time. The cyclic stress ratio CSR is expressed as:

$$CSR = \frac{\sigma_d}{2\sigma_0}, \qquad (7)$$

The initial void ratio e_0 and the void ratio after each consolidation e_c were calculated as:

$$e_0 = \frac{\gamma_s}{\gamma_d} - 1 \; ; \quad e_c = e_0 - \frac{\Delta V}{V_0}\frac{\gamma_s}{\gamma_d} \qquad (8)$$

where V_0 is the initial volume of the specimen, ΔV is the volume change, and γ_s, and γ_d are the unit weight and the dry unit weight.

The mechanism of the generation of pore-water pressure due to the cyclic loading in the undrained conditions was used [6]. Due to a particular number of cyclic loadings, a change in the void ratio Δe of the soil occurs if full drainage is allowed. However, if drainage is prevented, the void ratio will remain as an initial effective stress σ'_0, and will be reduced with an increase in the pore-water pressure Δu. If the number of cycles and the load level is large enough, the magnitude of Δu can become equal to σ'_0 and, in such a case, the soil will liquefy.

The axial strain $\varepsilon_1 = \Delta H / H$ is expressed as a sum

$$\varepsilon_1 = \varepsilon_{1,r} + \varepsilon_{1,p} \quad (9)$$

where ε_r is the recovery part of strain and ε_p is the permanent part of the strain. The recovery part of the strain is calculated as a half of the double amplitude axial strain $\varepsilon_{da}(t)$:

$$\varepsilon_{1,r}(t) = \frac{\varepsilon_{1,\max}(N(t)) - \varepsilon_{1,\min}(N(t))}{2} = \frac{\varepsilon_{da}(t)}{2} \qquad (10)$$

where $N(t)$ is the cycle number at the time t, and $\varepsilon_{1,max}(N(t))$ and $\varepsilon_{1,min}(N(t))$ are the maximum and minimum values of the deformation. The increase of the double amplitude axial strain depends on the initial effective stress, the porosity and the cyclic loading. Fig. 2 (see next page) shows typical relationships for the double amplitude axial strain ε_{da} vs. the number of cycles N.

The permanent part of the strain is calculated as a medium value between $\varepsilon_{1,max}$ and $\varepsilon_{1,min}$ for every cycle. The test result shows a constant and almost zero value of $\varepsilon_{1,p}(t)$.

$$\varepsilon_{1,p}(t) = \frac{\varepsilon_{1,\max}(N(t)) + \varepsilon_{1,\min}(N(t))}{2} \approx 0 \qquad (11)$$

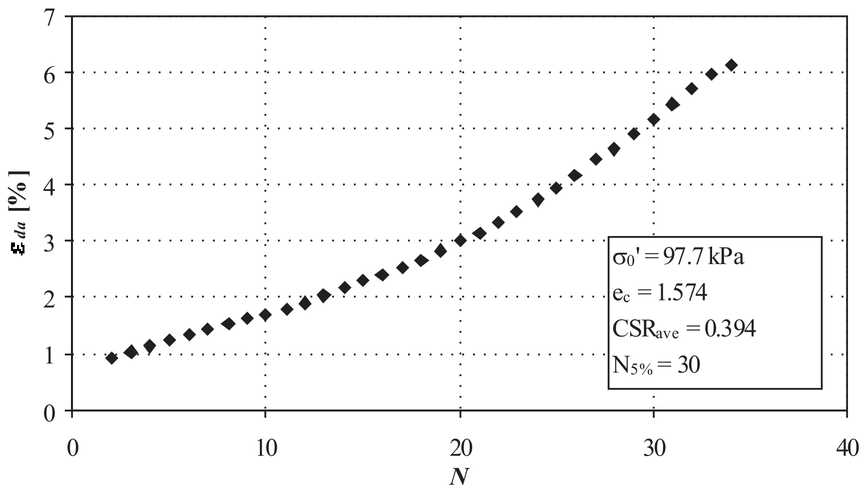

Figure 2. Double amplitude axial strain ε_{da} vs. the number of cycles N.

The undrained test is made with the volume strain $\varepsilon_v(t) = 0$ and the Poisson's ratio $\nu = 0.5$. The relationships between the cyclic stress σ_d and the shear strain γ can be expressed with a hysteresis loop (Fig. 3)

The damping ratio ξ is derived from the given hysteresis loop and is defined as the ratio between the dissipated energy and the energy used in the deformation. It can be calculated from the ratio between the areas ΔW and W.

$$\xi = \frac{\Delta W}{2\pi W} \qquad (12)$$

where ΔW is the area of the cyclic loop and W is the area of the triangle O – σ_d – γ. The deviator stress σ_d is constant and the shear strain γ increases with the number of cycles. The dissipated energy ΔW can be calculated for each cycle as:

$$\Delta W = \frac{1}{2}\sum_{t=0}^{T}\left(\sigma_d\left(t - t_{\sigma_d} + \Delta t\right) + \sigma_d\left(t - t_{\sigma_d}\right)\right)\left(d\varepsilon\ (t + \Delta t) - d\varepsilon(t)\right) \quad (13)$$

where t is the time, $t_{\sigma d}$ is the time at the maximum deviator stress σ_d, Δt is the time increment and T is a period (T = 1s).

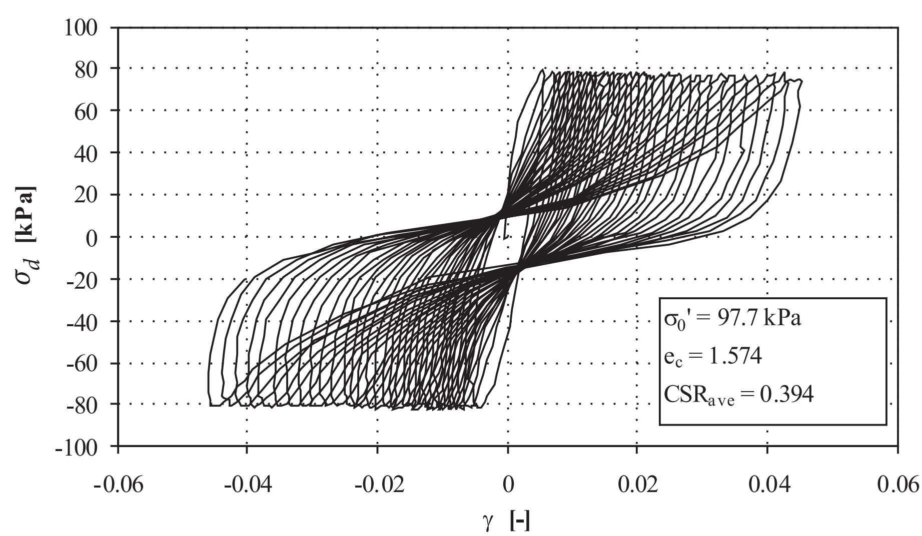

Figure 3. Deviator stress σ_d vs. shear strain γ.

The cyclic loading $\sigma_d\,(t)$ has a sinusoidal form in each test. The axial strain ε_1 has a sinusoidal form in the first cycles, and after that the part of the plastic strain $\Delta\varepsilon_{1,pl}/\varepsilon_1$ increases with the number of cycles *N*; it depends on the cyclic stress ratio *CSR* and the void ratio *e*. Fig. 4 shows the part of plastic strain $\Delta\varepsilon_{1,pl}/\varepsilon_1$ after 10 cycles, for the void ratio *e* = 1.6 and for different cyclic stress ratios (*CSRs*).

The increasing of the pore pressure (Fig. 5) can also be separated into the recovery and permanent parts of the pore pressure [7]. It can, for instance, be expressed with the pore-pressure ratio r_u, as the relationship between the pore-pressure change Δu and the effective isotropic consolidation stress σ'_0.

$$r_u = \frac{\Delta u}{\sigma_0{}'} \qquad (14)$$

Due to ground shaking during an earthquake, a cyclic shear stress is imposed on the soil element. A laboratory test to study the liquefaction problem must be designed in a manner so as to simulate the condition of a constant normal stress and a cyclic shear stress on a plane of the soil specimen. As the actual triaxial tests can be conducted by applying a cyclic load in the axial direction only, corrected cyclic pore-pressure ratios $r_{u,corr}$ are used.

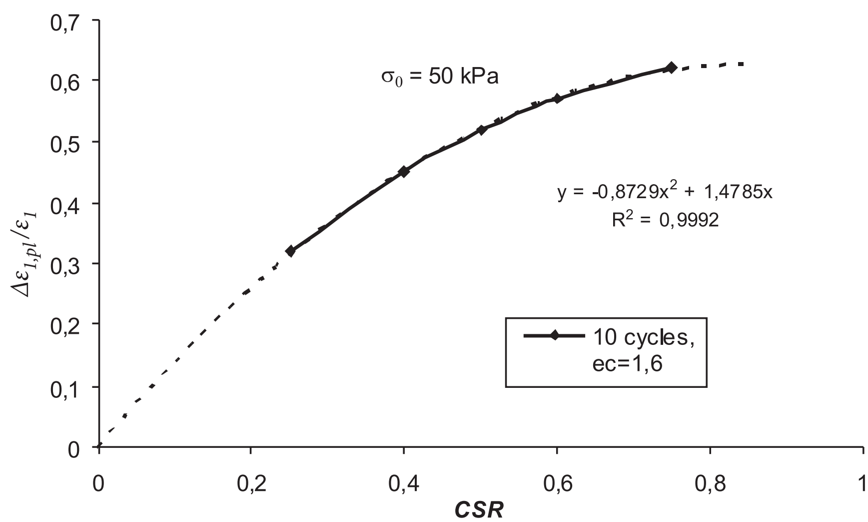

Figure 4. Plastic strain $\Delta\varepsilon_{1,pl}/\varepsilon_1$ vs. the cyclic stress ratio (*CSR*).

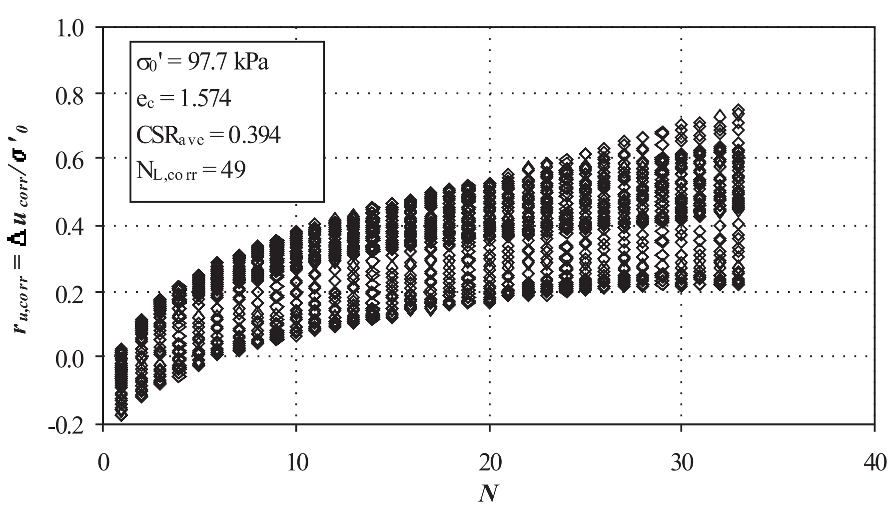

Figure 5. Corrected pore-pressure ratio $r_{u,corr}$ vs. the number of cycles *N*.

The corrected cyclic pore-pressure ratio $r_{u,corr}$ is expressed as:

$$r_{u,corr} = \frac{\Delta u_w - \frac{\sigma_a}{2}}{\sigma'_0} = r_u - CSR \qquad (15)$$

The total change of the pore-pressure ratio r_u is:

$$\begin{aligned} r_u(t) &= r_{u,pov}(t) + r_{u,nepov}(t) \\ r_{u,r}(t) &= \frac{r_{u,\max}(N(t)) - r_{u,\min}(N(t))}{2} \\ r_{u,p}(t) &= \frac{r_{u,\max}(N(t)) + r_{u,\min}(N(t))}{2} \end{aligned} \qquad (16)$$

where $r_{u,r}$ is the recovery part of the pore-pressure ratio and $r_{u,p}$ is the permanent part of the pore-pressure ratio. The ratios $r_{u,max}$ and $r_{u,min}$ are the maximum and minimum measured values of r_u in the cycle $N(t)$.

The recovery part of the pore pressure is a consequence of the transfer of pressure to the pore water and it is present as long as the cyclic loading continues. The permanent part of the pore pressure is a consequence of the volume change and the removal of particles because of the cyclic shear stress. The permanent part of the pore-pressure ratio $r_{u,p}$ increases with the number of cycles N and it is dependent on the cyclic stress ratio CSR and the void ratio e_c. The recovery part of the pore pressure, already during the first cycle, increases the hydrostatic part of the cyclic loading to $u(N = 1) \geq \sigma_d/3$ or more (depending on the CSR).

The strain and the pore-pressure increases correlate well and depend on the initial stress σ'_0, the cyclic stress ratio (CSR) and the void ratio e_c. Fig. 6 shows the relationship for the corrected cyclic pore-pressure ratio $r_{u,corr}$ vs. the shear strain γ.

Fig. 7 shows the number of cycles N for the various void ratios e_c needed to reach some value of the pore-pressure ratio r_u and for constant values of the cyclic stress ratio (CSR) and the initial effective stress σ'_0. It is evident that increasing the pore pressure is independent of the void ratio e_c until it reaches some value of the pore-pressure ratio ($r_u > 0.7$).

The relationship between the number of cycles N and the void ratio e_c in order to reach some value of the shear strain γ is similar. Fig. 8 shows such a relationship for the constant values of the cyclic stress ratio $CSR = 0.39$ and the initial effective stress $\sigma'_0 = 100$ kPa. The increase of the shear strain becomes dependent on the void ratio when it reaches some value of the shear strain ($\gamma > 0.3$).

The damping ratio ξ in stress-controlled tests shows an initial increasing of the curve with the increasing strain deformation and the number of cycles. The shape of the curve (Fig. 9) shows an exponential increase with the increase of the shear strain, up to a strain of about 0.5%. With greater strains, the damping ratio is constant and after that the values exponentially fall and appear to reach an asymptotic value. This phenomenon is due to the loss of shear strength because of the effective stress approaching zero and the material being about to liquefy. Similar behaviour for the damping ratio ξ has been observed in lacustrine carbonate silt from the

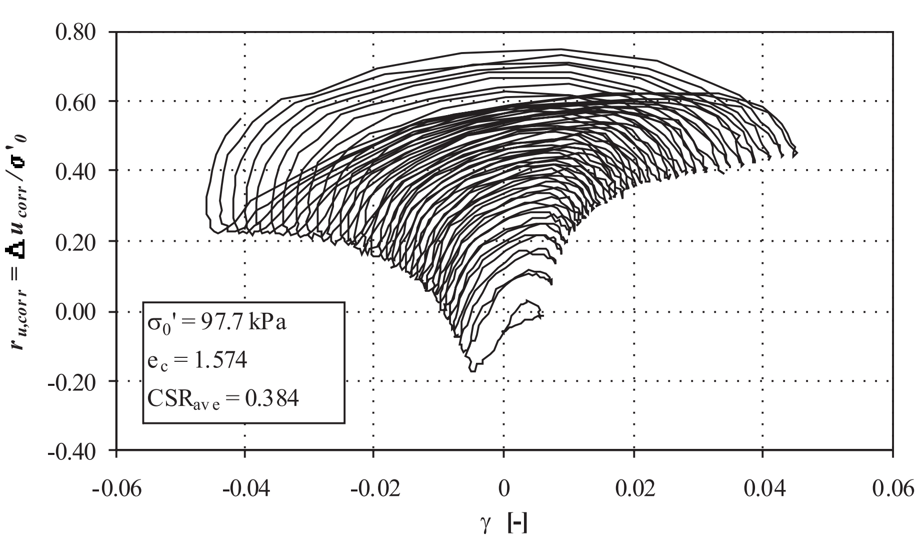

Figure 6. Pore-pressure ratio $r_{u,corr}$ vs. shear strain γ.

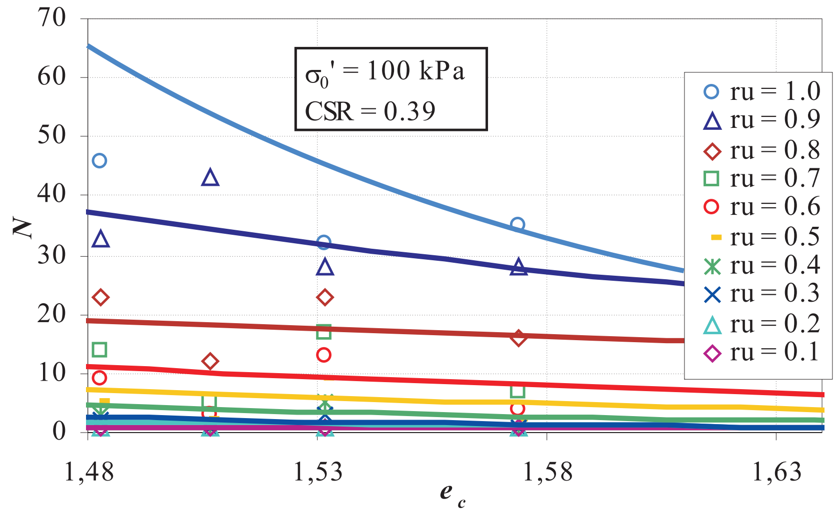

Figure 7. Number of cycles N_{ru} vs. the void ratio *e*.

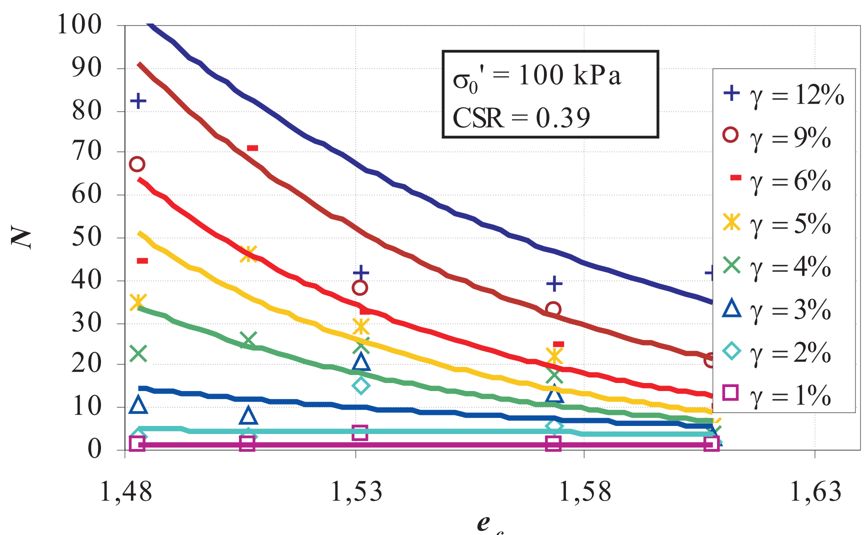

Figure 8. Number of cycles N_γ vs. the void ratio *e*.

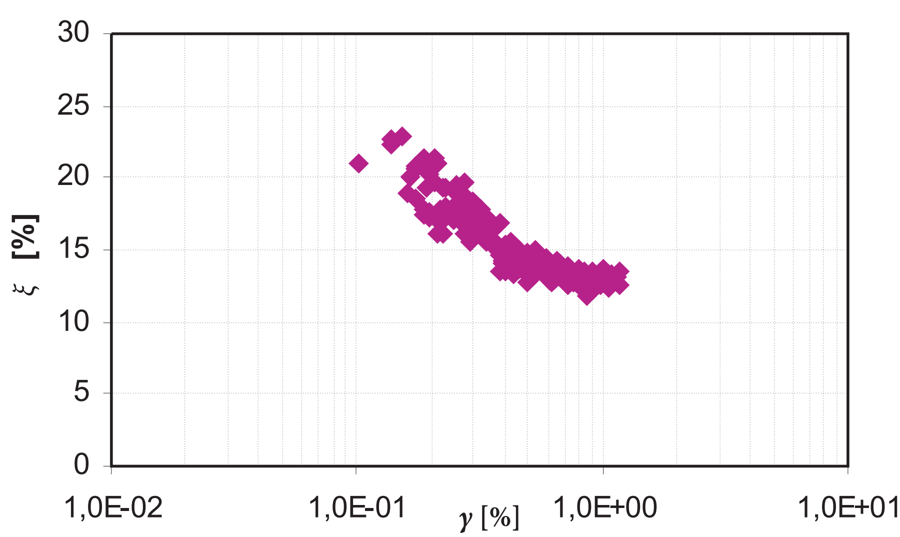

Figure 9. Damping ratio ξ vs. the shear strain γ.

Julian Alps [8]. The strain and the maximum value of ξ are different, but the shapes of the curve describing the phenomenon are similar.

Figure 10 shows the maximum and the asymptotic values of the damping ratio ξ for the different initial effective stress conditions σ'_0 and the void ratio e_c. It is evident that the porosity does not influence the damping ratio ξ during larger strains.

The shear modulus G and the Young's modulus E are described in relation to the shear strain γ and to the axial strain ε_1. The impact of the initial effective stress on the shear modulus across a large strain range is shown in Fig. 11.

Fig. 12 shows the relationship between the shear modulus G and the void ratio e_c after 10 cycles and for different cyclic stress ratios (*CSRs)* and for an initial effective stress σ'_0 = 50 kPa. It is evident that porosity influences the shear modulus, but only for higher values of the cyclic stress ratio (*CSR*).

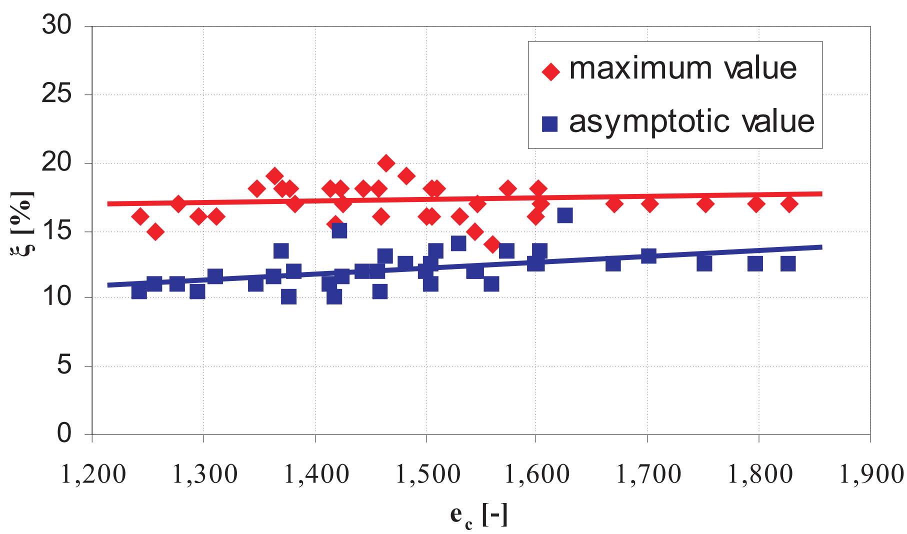

Figure 10. The range of limit values for damping ratio ζ with respect to the void ratio etio e.

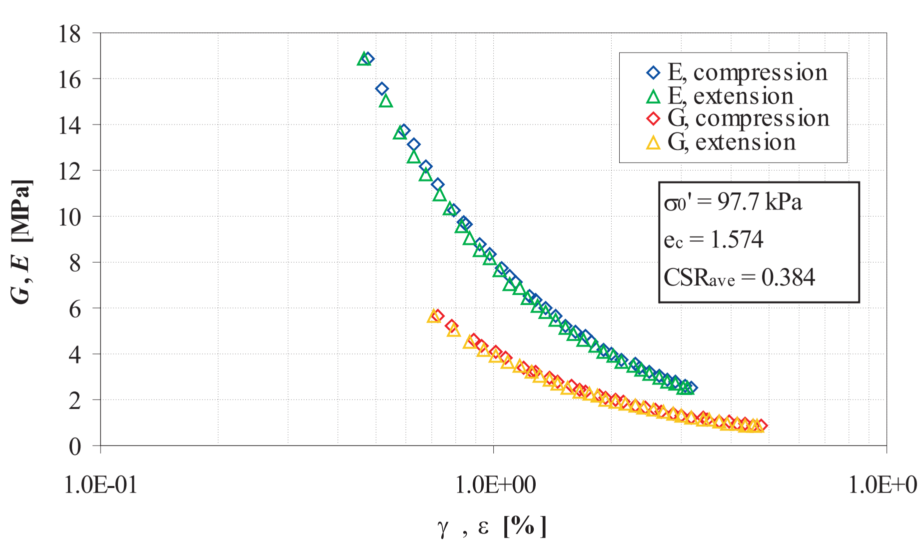

Figure 11. Young's modulus E vs. the axial strain ε_1, and shear modulus G vs. the shear strain γ.

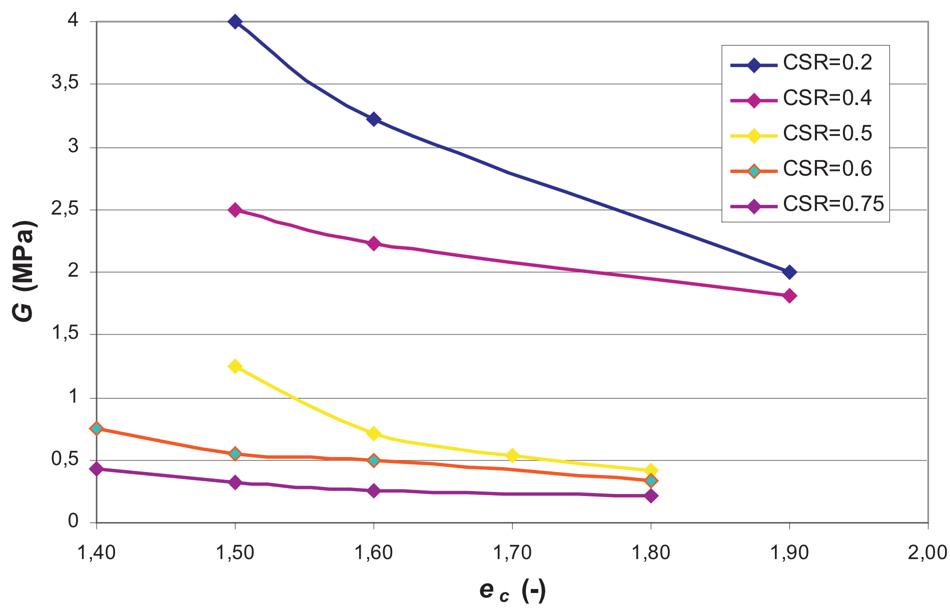

Figure 12. Shear modulus *G* versus the void ratio e_c at an initial effective stress σ_0' = 50 kPa and for various cyclic stress ratios (*CSRs*), after 10 cycles.

The axial and shear strain γ increase with the number of cycles *N* depending on the initial effective stress σ'_0 and the cyclic stress σ_d (or the cyclic stress ratio *CSR*). The cyclic stress σ_d, the cyclic stress ratio *CSR* and the shear modulus *G* can be expressed for each initial effective stress σ'_0 and for a selected value of the shear strain γ. Fig. 13 shows the relationship between the cyclic stress ratio *CSR* and the void ratio e_c for a shear strain γ after 10 cycles and for different initial effective stresses σ'_0.

Fig. 14 shows the similar relationship between shear stress τ and the effective stress σ'_0 = 50 kPa for the shear strain γ = 7.5% after 10 cycles. It is expressed for different initial effective stresses σ'_0 and for different void ratios e_c. It is evident that the relation $\tau - \sigma'_0$ is linear and expresses the failure lines of the snail soil for different void ratios e_c. The relationship shear stress τ vs. effective stress σ'_0 for smaller values of shear strain γ is similar and represents the deformation lines.

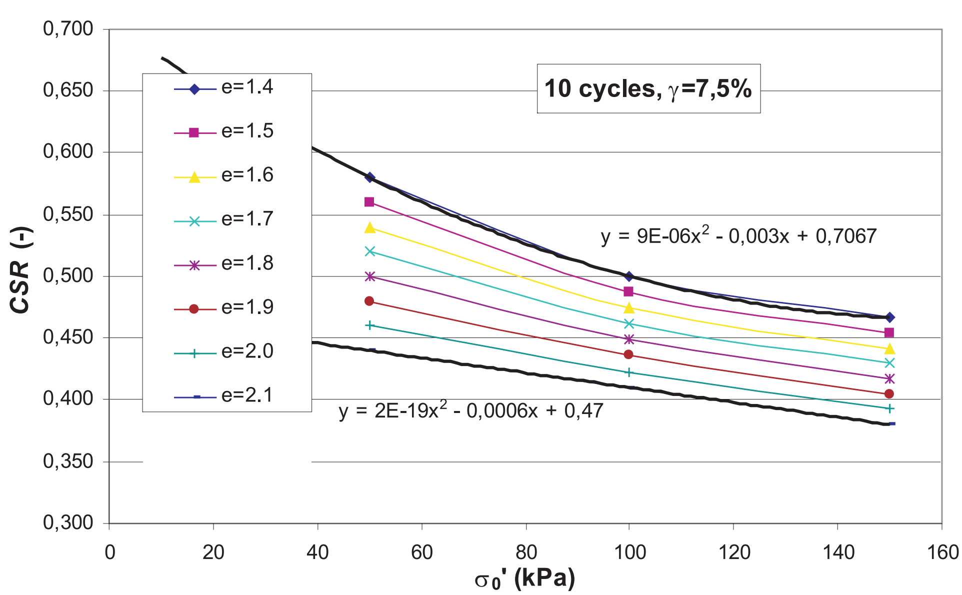

Figure 13. Cyclic stress ratio *CSR* versus the void ratio e_c for a shear strain γ = 7.5 % after 10 cycles.

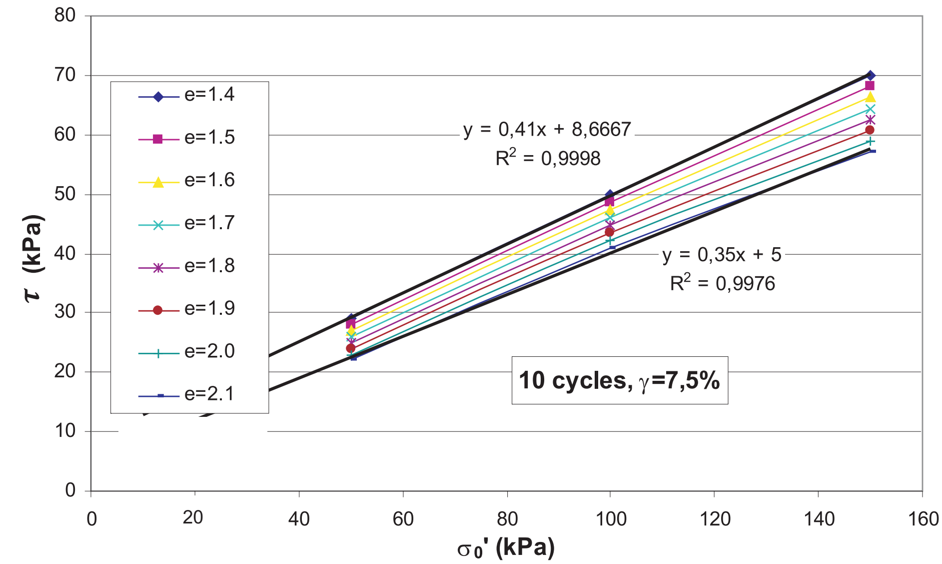

Figure 14. Shear stress τ versus the effective stress σ'_0 = 50 kPa for a shear strain γ = 7.5 %.

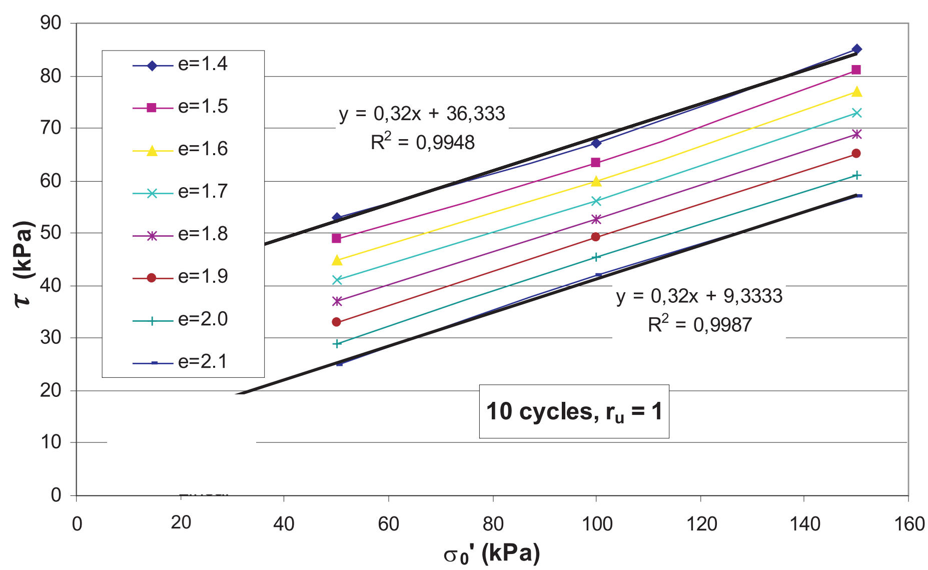

Figure 15. Shear stress τ versus the effective stress σ'_0 = 50 kPa at a pore-pressure ratio r_u = 1.

Fig. 15 shows the relationship between the shear stress τ and the effective stress σ'_0 for a pore-pressure ratio r_u = 1 and for various void ratios e_c, after 10 cycles. Such a relationship is also linear (except for small values of the effective stress $\sigma'_0 < 20$ kPa and the express failure lines of the snail soil at various void ratios e_c using the pore-pressure criteria).

The relationships between the shear stress τ and the effective stress σ'_0 for values of the pore-pressure ratio $r_u < 1$ are expressed similarly.

By comparing both criteria, it is clear that the snail soil is a highly sensitive material. For low values of the effective stress σ'_0 (under the surface) the large strain results in failure; however, at higher values of the effective stress σ'_0 (deeper under the surface) failure arises as a consequence of a high pore pressure.

7 CONCLUSIONS

The geomechanical characteristics of snail soil were investigated for their dependence on the physical characteristics. A series of tests with different porosities was performed. The test results show that the geomechanical characteristics depend on the porosity. It is evident from the results that the changes in the coefficient of permeability, the coefficient of consolidation, and the coefficient of volume compressibility are non-linear with respect to the changes in the porosity. The initial changes (at high porosity) are higher than the changes at low porosity.

The changes of the mechanical parameters, such as the Young's modulus, the Poisson's ratio, and the friction angle are indistinct and almost linear for smaller changes of porosity, but become non-linear for larger changes of porosity.

The snail soil was recognized as being a highly sensitive material. A large strain appears after the initial cycles.

The pore pressure increased even during the first cycle to the hydrostatic part of cyclic loading, or higher (depending on the *CSR*).

The damping ratio increased exponentially with the strain, and after some cycles reached its maximum value, and after that decreased to an asymptotic value. The reason for such behaviour is the large plastic deformation. The maximum and asymptotic values of the damping ratio are changed only minimally with the void ratio. There is clearly no influence of the porosity on the damping ratio.

The shear modulus G and the Young's modulus E are described in relation to the shear strain γ and to the axial strain ε_1. The porosity influences the shear modulus only at higher values of the cyclic stress ratio (*CSR*).

The increase of the pore pressure is independent of the void ratio e_c until it reaches some value of the pore pressure ratio ($r_u > 0.7$). Similarly, the increase of the shear strain becomes dependent on the void ratio until it reaches some value of the shear strain ($\gamma > 0.3$).

The deformation and failure lines are determined from the relationship between the shear stress τ and the effective stress σ'_0 at some shear strain γ after 10 cycles. The limit value of the shear strain is $\gamma = 7.5\%$.

The relationships between the shear stress τ and the effective stress σ'_0 for values of the pore-pressure ratio $r_u < 1$ are expressed similarly. Such a relationship is linear (except for small values of the effective stress $\sigma'_0 < 20$ kPa and express pore-pressure lines of snail soil at different void ratios e_c using pore-pressure criteria and a failure line when the pore pressure ratio $r_u = 1$).

ACKNOWLEDGMENTS

This research is part of a three-year research project financed by the Slovenian Ministry of Higher Education, Science and Technology. The financial support of the company Prevent and the Slovenian Road Operator, DARS, is also gratefully acknowledged.

REFERENCES

[1] Trauner, L. (1982). *Applicability of theory of elasticity for foundation design*. Doctoral thesis, University of Ljubljana, Ljubljana.
[2] Trauner, L. et al. (1982). Structure soil interaction, *Research report*, University of Maribor, 67, Maribor.
[3] Žlender, B. et al. (2007). Cyclic triaxial tests of soil, *Research report*, University of Maribor, Maribor.
[4] Žlender, B., Trauner, L. (2006). The influence of porosity on geomechanical characteristics of snail soil in the Ljubljana marsh. *Acta Geotechnica Slovenica*, Vol. 3, No. 1, 34-42.
[5] Dolinar, B. and Žnidaršič, M. (2007). Evaluation of permeability of saturated clays based on their physical properties. *Geologija* 50, 2 487-495.
[6] Das, B.M. (1993). Principles of soil dynamics, *PWS-KENT Publishing Company*, 397-453.
[7] Lenart, S. (2005). *Numerical model for calculation pore pressure in soils with high liquefaction potential*. Doctoral thesis. University of Ljubljana.
[8] Žlender, B. and Lenart, S. (2005). Cyclic liquefaction potential of lacustrine carbonate silt from Julian Alps. *Acta Geotechnica Slovenica*, Vol. 2, No. 1, 22-31.

NAVODILA AVTORJEM

Članki so objavljeni v angleškem jeziku s prevodom izvlečka v slovenski jezik.

VSEBINA ČLANKA

Članek naj bo napisan v naslednji obliki:

- Naslov, ki primerno opisuje vsebino članka in ne presega 80 znakov.
- Izvleček, ki naj bo skrajšana oblika članka in naj ne presega 250 besed. Izvleček mora vsebovati osnove, jedro in cilje raziskave, uporabljeno metodologijo dela, povzetek izidov in osnovne sklepe.
- Uvod, v katerem naj bo pregled novejšega stanja in zadostne informacije za razumevanje ter pregled izidov dela, predstavljenih v članku.
- Teorija.
- Eksperimentalni del, ki naj vsebuje podatke o postavitvi preiskusa in metode, uporabljene pri pridobitvi izidov.
- Izidi, ki naj bodo jasno prikazani, po potrebi v obliki slik in preglednic.
- Razprava, v kateri naj bodo prikazane povezave in posplošitve, uporabljene za pridobitev izidov. Prikazana naj bo tudi pomembnost izidov in primerjava s poprej objavljenimi deli.
- Sklepi, v katerih naj bo prikazan en ali več sklepov, ki izhajajo iz izidov in razprave.
- Literatura, ki mora biti v besedilu oštevilčena zaporedno in označena z oglatimi oklepaji [1] ter na koncu članka zbrana v seznamu literature.

OBLIKA ČLANKA

Besedilo naj bo pisano na listih formata A4, z dvojnim presledkom med vrstami in s 3.0 cm širokim robom, da je dovolj prostora za popravke lektorjev. Najbolje je, da pripravite besedilo v urejevalniku Microsoft Word. Hkrati dostavite odtis članka na papirju, vključno z vsemi slikami in preglednicami ter identično kopijo v elektronski obliki.

Enačbe naj bodo v besedilu postavljene v ločene vrstice in na desnem robu označene s tekočo številko v okroglih oklepajih.

ENOTE IN OKRAJŠAVE

V besedilu, preglednicah in slikah uporabljajte le standardne označbe in okrajšave SI. Simbole fizikalnih veličin v besedilu pišite poševno (npr. v, T itn.). Simbole enot, ki sestojijo iz črk, pa pokončno (npr. Pa, m itn.).

Vse okrajšave naj bodo, ko se prvič pojavijo, izpisane v celoti.

SLIKE

Slike morajo biti zaporedno oštevilčene in označene, v besedilu in podnaslovu, kot sl. 1, sl. 2 itn. Posnete naj bodo v kateremkoli od razširjenih formatov, npr. BMP, JPG, GIF. Za pripravo diagramov in risb priporočamo CDR format (CorelDraw), saj so slike v njem vektorske in jih lahko pri končni obdelavi preprosto povečujemo ali pomanjšujemo.

Pri označevanju osi v diagramih, kadar je le mogoče, uporabite označbe veličin (npr. v, T). V diagramih z več krivuljami mora biti vsaka krivulja označena. Pomen oznake mora biti razložen v podnapisu slike.

Za vse slike po fotografskih posnetkih je treba priložiti izvirne fotografije ali kakovostno narejen posnetek.

PREGLEDNICE

Preglednice morajo biti zaporedno oštevilčene in označene, v besedilu in podnaslovu, kot preglednica 1, preglednica 2 itn. V preglednicah ne uporabljajte izpisanih imen veličin, ampak samo ustrezne simbole. K fizikalnim količinam, npr. t (pisano poševno), pripišite enote (pisano pokončno) v novo vrsto brez oklepajev.

Vse opombe naj bodo označene z uporabo dvignjene številke[1].

SEZNAM LITERATURE

Vsa literatura mora biti navedena v seznamu na koncu članka v prikazani obliki po vrsti za revije, zbornike in knjige:

[1] Feng, T. W. (2000). Fall-cone penetration and water content ralationship of clays. *Geotechnique 50*, No. 2, 181-187.

[2] Ortolan, Ž. and Mihalinec, Z. (1998). Plasticity index-Indicator of shear strength and a major axis of geotechnical modelling. *Proceedings of the Elev-*

enth Danube-European conference on soil mechanics and geotechnical engineering, Poreč, 25 –29 May 1998.
[3] Toporišič, J. (1994). *Slovenski pravopis*. 2nd.ed., DZS, Ljubljana.

PODATKI O AVTORJIH

Članku priložite tudi podatke o avtorjih: imena, nazive, popolne poštne naslove, številke telefona in faksa, naslove elektronske pošte. Navedite kontaktno osebo.

SPREJEM ČLANKOV IN AVTORSKE PRAVICE

Uredništvo si pridržuje pravico do odločanja o sprejemu članka za objavo, strokovno oceno mednarodnih recenzentov in morebitnem predlogu za krajšanje ali izpopolnitev ter terminološke in jezikovne korekture.

Avtor mora predložiti pisno izjavo, da je besedilo njegovo izvirno delo in ni bilo v dani obliki še nikjer objavljeno. Z objavo preidejo avtorske pravice na revijo ACTA GEOTECHNICA SLOVENICA. Pri morebitnih kasnejših objavah mora biti AGS navedena kot vir.

Rokopisi člankov ostanejo v arhivu AGS.

Vsa nadaljnja pojasnila daje:

Uredništvo
ACTA GEOTECHNICA SLOVENICA
Univerza v Mariboru
Fakulteta za gradbeništvo
Smetanova ulica 17
2000 Maribor
Slovenija
E-pošta: ags@uni-mb.si

INSTRUCTIONS FOR AUTHORS

The papers are published in English with a translation of the abstract into Slovene.

FORMAT OF THE PAPER

The paper should have the following structure:

- A Title that adequately describes the content of the paper and should not exceed 80 characters;
- An Abstract, which should be viewed as a mini version of the paper and should not exceed 250 words. The Abstract should state the principal objectives and the scope of the investigation and the methodology employed, it should also summarise the results and state the principal conclusions;
- An Introduction, which should provide a review of recent literature and sufficient background information to allow the results of the paper to be understood and evaluated;
- A Theoretical section;
- An Experimental section, which should provide details of the experimental set-up and the methods used for obtaining the results;
- A Results section, which should clearly and concisely present the data using figures and tables where appropriate;
- A Discussion section, which should describe the relationships shown and the generalisations made possible by the results and discuss the significance of the results, making comparisons with previously published work;
- Conclusions, which should present one or more conclusions that have been drawn from the results and subsequent discussion;
- References, which must be numbered consecutively in the text using square brackets [1] and collected together in a reference list at the end of the paper.

LAYOUT OF THE TEXT

The text should be written in A4 format, with double spacing and margins of 3 cm, to provide editors with space to write in their corrections. Microsoft Word for Windows is the preferred format for submission. One hard copy, including all figures, tables and illustrations and an identical electronic version of the manuscript must be submitted simultaneously.

Equations should be on a separate line in the main body of the text and marked on the right-hand side of the page with numbers in round brackets.

UNITS AND ABBREVIATIONS

Only standard SI symbols and abbreviations should be used in the text, tables and figures. Symbols for physical quantities in the text should be written in Italics (e.g. *v*, *T*, etc.). Symbols for units that consist of letters should be in plain text (e.g. Pa, m, etc.).

All abbreviations should be spelt out in full on first appearance.

FIGURES

Figures must be cited in consecutive numerical order in the text and referred to in both the text and the caption as Fig. 1, Fig. 2, etc. Figures may be saved in any common format, e.g. BMP, JPG, GIF. However, the use of CDR format (CorelDraw) is recommended for graphs and line drawings, since vector images can be easily reduced or enlarged during final processing of the paper.

When labelling axes, physical quantities (e.g. *v*, *T*) should be used whenever possible. Multi-curve graphs should have individual curves marked with a symbol; the meaning of the symbol should be explained in the figure caption.

Good quality black-and-white photographs or scanned images should be supplied for illustrations.

TABLES

Tables must be cited in consecutive numerical order in the text and referred to in both the text and the caption as Table 1, Table 2, etc. The use of names for quantities in tables should be avoided if possible: corresponding symbols are preferred. In addition to the physical quantity, e.g. *t* (in Italics), units (normal text), should be added on a new line without brackets.

Any footnotes should be indicated by the use of the superscript[1].

LIST OF REFERENCES

References should be collected at the end of the paper in the following styles for journals, proceedings and books, respectively:

[1] Feng, T. W. (2000). Fall-cone penetration and water content ralationship of clays. *Geotechnique 50*, No. 2, 181-187.
[2] Ortolan, Ž. and Mihalinec, Z. (1998). Plasticity index-Indicator of shear strength and a major axis of geotechnical modelling. *Proceedings of the Eleventh Danube-European conference on soil mechanics and geotechnical engineering*, Poreč, 25 –29 May 1998.
[3] Toporišič, J. (1994). *Slovenski pravopis*. 2nd.ed., DZS, Ljubljana.

AUTHOR INFORMATION

The following information about the authors should be enclosed with the paper: names, complete postal addresses, telephone and fax numbers and E-mail addresses. Indicate the corresponding person.

ACCEPTANCE OF PAPERS AND COPYRIGHT

The Editorial Committee of the Slovenian Geotechnical Review reserves the right to decide whether a paper is acceptable for publication, to obtain peer reviews for submitted papers, and if necessary, to require changes in the content, length or language.

Authors must also enclose a written statement that the paper is original unpublished work, and not under consideration for publication elsewhere. On publication, copyright for the paper shall pass to the ACTA GEOTECHNICA SLOVENICA. The AGS must be stated as a source in all later publication.

Papers will be kept in the archives of the AGS.

For further information contact:

Editorial Board
ACTA GEOTECHNICA SLOVENICA
University of Maribor
Faculty of Civil Engineering
Smetanova ulica 17
2000 Maribor
Slovenia
E-mail: ags@uni-mb.si

NAMEN REVIJE

Namen revije ACTA GEOTECHNICA SLOVENICA je objavljanje kakovostnih teoretičnih člankov z novih pomembnih področij geomehanike in geotehnike, ki bodo dolgoročno vplivali na temeljne in praktične vidike teh področij.

ACTA GEOTECHNICA SLOVENICA objavlja članke s področij: mehanika zemljin in kamnin, inženirska geologija, okoljska geotehnika, geosintetika, geotehnične konstrukcije, numerične in analitične metode, računalniško modeliranje, optimizacija geotehničnih konstrukcij, terenske in laboratorijske preiskave.

Revija redno izhaja dvakrat letno.

AVTORSKE PRAVICE

ODGOVORNOST

Revija ne prevzame nobene odgovornosti za poškodbe in/ali škodo na osebah in na lastnini na podlagi odgovornosti za izdelke, zaradi malomarnosti ali drugače, ali zaradi uporabe kakršnekoli metode, izdelka, navodil ali zamisli, ki so opisani v njej.

AIMS AND SCOPE

ACTA GEOTECHNICA SLOVENICA aims to play an important role in publishing high-quality, theoretical papers from important and emerging areas that will have a lasting impact on fundamental and practical aspects of geomechanics and geotechnical engineering.

ACTA GEOTECHNICA SLOVENICA publishes papers from the following areas: soil and rock mechanics, engineering geology, environmental geotechnics, geosynthetic, geotechnical structures, numerical and analytical methods, computer modelling, optimization of geotechnical structures, field and laboratory testing.

The journal is published twice a year.

COPYRIGHT

RESPONSIBILITY

No responsibility is assumed by the publisher for any injury and/or damage to persons or property as a matter of product liability, negligence or otherwise, or from any use or operation of any methods, products, instructions or ideas contained in the material herein.